NASA
Technical
Paper
3009

AVSCOM
TR-90-B-005

July 1990

Aerodynamic Characteristics of Two Rotorcraft Airfoils Designed for Application to the Inboard Region of a Main Rotor Blade

Kevin W. Noonan

APPLICATION TO THE [illegible] OF A MAIN
[illegible] (NASA) [illegible] COLUMBIA unclas
41/02 0274767

US A
AVIA
SYST
AVIAT

NASA
Technical
Paper
3009

AVSCOM
TR-90-B-005

1990

Aerodynamic Characteristics of Two Rotorcraft Airfoils Designed for Application to the Inboard Region of a Main Rotor Blade

Kevin W. Noonan
Aerostructures Directorate
USAARTA-AVSCOM
Langley Research Center
Hampton, Virginia

National Aeronautics and
Space Administration
Office of Management
Scientific and Technical
Information Division

Summary

A wind-tunnel investigation has been conducted to determine the two-dimensional aerodynamic characteristics of two new rotorcraft airfoils designed specifically for application to the inboard region (stations $\leq$85 percent radius) of a helicopter main rotor blade. The two new airfoils, the RC(4)-10 and RC(5)-10, and a baseline airfoil, the VR-7 which is currently in use, were all investigated in the Langley 6- by 28-Inch Transonic Tunnel at Mach numbers from about 0.34 to 0.84 and at respective chord Reynolds numbers from about 4.7×10^6 to 9.3×10^6. The VR-7 airfoil had a trailing-edge tab that is deflected upward 4.6°. In addition, the RC(4)-10 airfoil was investigated in the Langley Low-Turbulence Pressure Tunnel at Mach numbers from 0.10 to 0.44 and at Reynolds numbers from 1.4×10^6 to 5.4×10^6, respectively. Some of the experimental data for the two new airfoils were compared with two different theories.

The results of this investigation indicate that both of the new airfoils offer advantages over the baseline airfoil. Of the three airfoils investigated in the 6- by 28-Inch Transonic Tunnel, the RC(4)-10 airfoil had the highest maximum lift coefficients at Mach numbers M from 0.34 to about 0.42. The maximum lift coefficients of the RC(4)-10 were 1.57 at $M = 0.34$ and 1.42 at $M = 0.42$, whereas those of the baseline airfoil were 1.47 at $M = 0.34$ and 1.38 at $M = 0.42$. The highest maximum lift coefficient measured for the RC(4)-10 in the Low-Turbulence Pressure Tunnel was 1.74 at $M = 0.20$. The drag-divergence Mach number of the RC(5)-10 airfoil was higher than that of the baseline airfoil for lift coefficients from 0 to 0.3, whereas the drag-divergence Mach number of the RC(4)-10 airfoil was higher than that of the baseline airfoil for lift coefficients from 0.1 to 0.3. The drag-divergence Mach number at zero lift coefficient was 0.79 for the RC(5)-10, 0.74 for the RC(4)-10, and 0.75 for the baseline airfoil. In general, both new airfoils had lower drag coefficients and pitching-moment coefficients (nearly zero) than the baseline airfoil for Mach numbers up to 0.63.

Introduction

The U.S. Army and NASA have an ongoing program to improve the performance and efficiency of helicopters via the development of advanced airfoil sections for helicopter main rotor blades, and significant results have been achieved to date (refs. 1–4). The performance requirements for the next generation of military helicopters include both higher forward flight speeds and more maneuverability requiring higher lift loads on the retreating rotor blade. This additional loading can be accommodated by increases in the airfoil-section maximum lift coefficients and/or an increase in the blade solidity. Since a higher solidity typically results in greater blade weight and drag, improving the airfoil-section lift capability is the more efficient approach. As pointed out in reference 5 (et al.), the attainment of higher airfoil-section lift is always in conflict with the need for high drag-divergence Mach number characteristics and low pitching-moment characteristics. For these reasons, an effort was undertaken to design airfoil sections with improved maximum lift characteristics applicable to the rotor blade inboard region (stations $\leq$85 percent radius) where some compromise in the drag-divergence Mach number could be made.

An experimental investigation was conducted in the Langley 6- by 28-Inch Transonic Tunnel (6×28TT) to determine the two-dimensional aerodynamic characteristics of two new rotorcraft (RC) airfoils, the RC(4)-10 and RC(5)-10, at Mach numbers from about 0.34 to 0.84 and at chord Reynolds numbers from about 4.7×10^6 to 9.3×10^6, respectively. A baseline airfoil, the VR-7, was tested in the same facility at the same conditions to ensure the best evaluation of the performance of the new airfoils. The VR-7 was selected as the baseline since it was currently in use on modern full-scale rotors (ref. 6) and a wind-tunnel model of it was also available. The RC(4)-10 airfoil was also investigated in the Langley Low-Turbulence Pressure Tunnel (LTPT) at Mach numbers from 0.10 to 0.44 (the facility limit) so that data at Mach numbers below that obtainable in the 6- by 28-Inch Transonic Tunnel could be measured. In addition, maximum lift coefficients not degraded by sidewall boundary-layer effects (ref. 7) could be measured in the Low-Turbulence Pressure Tunnel.

The lift and pitching-moment coefficients were determined from measurements of airfoil surface static pressures, and the drag coefficients were determined from measurements of wake total and static pressures. Some comparisons of the experimental data for the new airfoils and the predictions of a transonic, viscous theory were made. Some comparisons were also made between the data for the new airfoils and the predictions of a subcritical, viscous theory.

Symbols

The units used for the physical quantities in this paper are given in U.S. Customary Units. The measurements and calculations were also made in U.S. Customary Units.

c	airfoil chord, in.
c_d	section profile-drag coefficient, $\sum_{\text{Wake}} c_d' \frac{\Delta h}{c}$

c'_d	point-drag coefficient (refs. 16 and 18)
$c_{d,o}$	section profile-drag coefficient at zero lift
c_l	section lift coefficient from integration of airfoil surface pressure coefficients
c_m	section pitching-moment coefficient about quarter-chord from integration of airfoil surface pressure coefficients
$c_{m,o}$	section pitching-moment coefficient at zero lift
C_p	static-pressure coefficient, $(p_l - p_\infty)/q_\infty$
d	section drag force, lb
h	height of wake-survey probe tubes from given reference plane, in.
l	section lift force, lb
l/d	ratio of section lift force to section drag force
M	Mach number
M_{dd}	Mach number for drag divergence, $(dc_d/dM) = 0.1$
p	static pressure, psi
q	dynamic pressure, $\frac{1}{2}\rho V^2$, psf
R	Reynolds number based on airfoil chord and free-stream conditions
t	airfoil thickness, in.
V	velocity, ft/sec
x	airfoil abscissa, in.
z_c	ordinate of airfoil camber line, in.
α	angle of attack, angle between airfoil chord and airstream direction, deg
Δ	incremental change in parameter
ρ	density, slugs/ft^3

Subscripts:

c	wind-tunnel corrections applied
l	local
max	maximum
sep	boundary-layer separation occurred
sonic	Mach number equal to 1
∞	free stream

Abbreviations:

AOA	angle of attack
BLC	boundary-layer control
LTPT	Low-Turbulence Pressure Tunnel
6×28TT	6- by 28-Inch Transonic Tunnel

Airfoil Designation

The new airfoils were designated the RC(4)-10 and RC(5)-10 to be consistent with the form established in reference 4 for rotorcraft airfoils (the RC(3)-series). Thus, the "RC(4)" and "RC(5)" indicate a member of the fourth and fifth series of rotorcraft airfoils, respectively, and the "10" indicates that both airfoils have a maximum thickness of 10 percent chord. A difference in the series number indicates that as a minimum, the camber line or the thickness distribution is different between the airfoils.

Airfoil Design

In general, the desired characteristics for an airfoil to be used in the inboard region of a main rotor blade are (1) very high maximum lift coefficients at Mach numbers from about 0.30 to 0.50 for increased blade loading on the retreating side of the rotor disk, (2) pitching-moment coefficients nearly equal to zero for as wide a range of lift coefficient/Mach number conditions as possible for low pitch-link loads and blade torsion loads, and (3) moderate drag-divergence Mach numbers at lift coefficients from about 0 to 0.30 for reduced power requirements on the advancing side of the rotor disk. The specific design goals for the two airfoils of the present investigation were the following:

(1) $c_{l,\max} > 1.4$ at $M = 0.40$ and $R \approx 5.0 \times 10^6$

(2) $c_{l,\max} > 1.2$ at $M = 0.50$ and $R \approx 6.0 \times 10^6$

(3) $M_{\mathrm{dd}} > 0.70$ at $c_l = 0$ with $c_m < -0.015$

(4) $(t/c)_{\max} = 0.10$

Major emphasis was placed on attaining the first two design goals while maintaining a nearly zero pitching-moment level for a wide range of lift coefficient/Mach number conditions. How well the third design goal was met (or exceeded) would determine how far out on the rotor blade the new airfoil could

be applied. The maximum thickness of the new airfoil was restricted to 10 percent chord for two reasons. First, the experimental performance of an 11- or 12-percent-thick member of the same airfoil family could be extrapolated from that of the 10-percent-thick airfoil if needed, i.e., if the experimental $c_{l,\max}$ values of a 10-percent-thick section turned out to be below the design goals. Second, a lower drag level at almost all operating conditions would be attained if a 10-percent-thick section could be designed to meet the $c_{l,\max}$ design goal instead of the typical 12-percent-thick inboard rotor airfoil. These design goals represent an improvement relative to a good baseline airfoil like the VR-7, which is 12 percent thick. A maximum lift coefficient of 1.40 at $M = 0.40$ is about the same level as that reported in reference 8 for the VR-7 with a 5-percent tab deflected $-3.1°$; however, the zero-lift pitching-moment coefficient of the VR-7 with this tab was between -0.007 and -0.025 for Mach numbers from 0.30 to 0.74. The drag-divergence design goal represents an improvement relative to the VR-7 with respect to the allowable pitching-moment coefficient at that condition. The VR-7 had a value of M_{dd} at zero lift of about 0.74, but with a corresponding pitching-moment coefficient of -0.025.

The airfoil design process was the same as that successfully used for other rotor airfoils (ref. 2). This approach involved combining an arbitrary camber line and thickness distribution to result in an airfoil shape that was subsequently evaluated with a transonic analysis code (ref. 9). An iteration process of modifying the airfoil shape by changing the camber line and/or thickness distribution and of evaluating the new airfoil was used to converge on the design goals. The transonic analysis code does not adjust the airfoil pressure distribution to account for separated flow when boundary-layer separation is predicted, and thus it could not predict the maximum lift coefficient of an airfoil.

The approach was to try to develop an airfoil shape that achieved the maximum lift coefficient goals with the indicated upper-surface boundary-layer separation point at or aft of the 95-percent-chord station. Correlation of the analysis-code results with experimental data on existing airfoils had indicated that the prediction of the upper-surface boundary-layer separation point was generally conservative; i.e., the theory generally predicted the separation to occur earlier than indicated by the test data. If the predicted lift coefficient of an airfoil was close to the $c_{l,\max}$ design goal and the predicted boundary-layer separation point was not forward of $x/c = 0.95$, then that airfoil would be expected to attain the design $c_{l,\max}$ experimentally.

Models and Wind Tunnels

Models

The airfoil profiles are shown in figure 1 and the airfoil thickness and camber distributions are shown in figure 2. The maximum thickness of the RC(4)-10 and RC(5)-10 airfoils is 10 percent chord and is located at the 38-percent-chord station, whereas that of the baseline VR-7 airfoil is 12 percent chord and is located at the 32.5-percent-chord station. The thickness distribution of the RC(4)-10 is greater than that of the RC(5)-10 from the airfoil leading edge to about the 30-percent-chord station, and this difference is the only one between these two airfoils. The maximum positive camber of the two new airfoils is 1.75 percent chord and is located at the 35-percent-chord station, and both airfoils have a leading-edge droop of about 1 percent chord. As in earlier RC-series airfoils, the camber line aft of about 95 percent chord is slightly reflexed to minimize pitching-moment coefficients. The maximum camber of the baseline VR-7 is 3.1 percent chord and is located at the 32.5-percent-chord station. The VR-7 camber line aft of the 95-percent-chord station is significantly reflexed (trailing-edge tab deflected upward 4.6°) to reduce nose-down pitching-moment coefficients. The design coordinates for the RC(4)-10, RC(5)-10, and VR-7 airfoils are given in tables I, II, and III, respectively. The design concept for the new airfoils is described in reference 10.

6×28TT models. The three airfoil models are of identical construction and each was machined from a heat-treated stainless steel block with a finished span of 6.010 in. and a chord of 6.000 in. Each model has a total of 45 orifices: one on the leading edge, 22 on the upper surface, and 22 on the lower surface. The upper- and lower-surface orifices are located in single chordwise rows on respective surfaces, and the rows are positioned 12.6 percent span on opposite sides of the midspan (tables IV, V, and VI). Channels were milled in the airfoil surface and tubes were placed in the channels and then covered with an epoxy filler material. The orifices were then drilled from the metal side of the model to the embedded tubes to minimize surface irregularities near the orifices. The orifices have a diameter of 0.020 in. and were drilled perpendicular to the local surface contour. The surface of each model was polished by hand until it was judged to be aerodynamically smooth.

LTPT model. The RC(4)-10 airfoil model was machined from a heat-treated aluminum block and has a span of 36.000 in. and a chord of 23.760 in. The model has 72 static-pressure orifices: one on the leading edge, one in the trailing edge, 42 on the

upper surface, and 28 on the lower surface. Twenty-eight of the upper-surface orifices are located in several chordwise rows that are between the midspan and a station 10.2 percent span to one side of the midspan. The remaining 14 upper-surface orifices are located in two spanwise rows of 7 each, the first row being 5 percent chord from the leading edge and the second being at the 80-percent-chord station. The 28 lower-surface orifices are located in chordwise rows in a mirror image of the upper-surface chordwise orifices (table VII). Channels were milled in the airfoil surface and tubes were placed in the channels. One end of each tube was turned upward at an angle approximately normal to the local airfoil surface contour, and a steel rod was inserted into each tube before the tubes were covered with an epoxy filler material. After the filler cured, the steel rods were removed creating orifices that were 0.020 in. in diameter. The surface of the model was polished by hand until it was judged to be aerodynamically smooth.

Wind Tunnels

A sketch of the model and wake-survey probe installation in the 6×28TT is shown in figure 3, and a detailed sketch of the 6×28TT wake-survey probe is shown in figure 4. The LTPT model-support system and survey apparatus are illustrated in figures 5 and 6, respectively. Details of the LTPT wake-survey probe are shown in figure 7.

6×28TT description. The Langley 6- by 28-Inch Transonic Tunnel (6×28TT) is a blowdown wind tunnel with a slotted floor and ceiling (5.0 percent openness ratio) and is generally operated at stagnation pressures from about 30 to 90 psia and at Mach numbers from 0.35 to 0.90 (refs. 11 and 12). The slot geometry is described in detail in reference 13. The Mach number is controlled by hydraulically actuated choker doors located downstream of the test section. The airfoil model spans the 6.010-in. width of the tunnel (fig. 3) and is rigidly attached by mounting tangs to circular end plates that are driven by a hydraulic actuator to position the airfoil at the desired angle of attack. A run sequence usually consists of an angle-of-attack sweep at a constant Mach number and Reynolds number.

LTPT description. The Langley Low-Turbulence Pressure Tunnel (LTPT) is a single-return, closed-throat tunnel that can be operated at stagnation pressures from near vacuum to 10 atm (refs. 14 and 15). The minimum unit Reynolds number is about 1.2×10^4 per foot at a Mach number of 0.05, and the maximum unit Reynolds number is about 1.5×10^7 per foot at a Mach number of 0.23. The maximum Mach number obtainable with an empty test section is about 0.46 at a stagnation pressure of about 1 atm. The test section is 3 ft wide, 7.5 ft high, and 7.5 ft long, and the tunnel sidewalls have an outward total divergence of about 0.0038 in/in. to allow for the growth of the tunnel sidewall boundary layer. The airfoil model spans the width of the tunnel between two end plates that are connected to inner drums that are themselves held in place by an outer drum and yoke-arm support system (fig. 5). The yoke-arm support system is mounted to a force balance that is connected to the tunnel through a balance platform. The model angle of attack is controlled by a motorized pitch mechanism that rotates the bearing-mounted inner drums. A multipath labyrinth seal is used to minimize air leakage from the test section into the outer tunnel plenum. A run sequence normally consists of an angle-of-attack sweep at a constant Mach number and Reynolds number.

LTPT sidewall boundary-layer control system. The LTPT is equipped with a sidewall boundary-layer control system to ensure the two-dimensionality of the flow for high-lift airfoil testing, principally multielement airfoils (ref. 15). The sidewall boundary-layer control is accomplished by the blowing of high-pressure air tangential to the model end plate at up to five locations on each model end plate. The high-pressure air is supplied to blowing boxes with tangential blowing slots, and the boxes were designed to provide uniform tangential flow at the slot exit. A pair of end plates with two blowing boxes on each one was used for the test of the RC(4)-10 airfoil. The slot exit for one blowing box was at the leading edge of the airfoil, and the slot exit for the second box was at about the 75-percent-chord station.

Apparatus

6×28TT Wake-Survey Probe

A traversing wake-survey probe is cantilevered from one tunnel sidewall to measure the profile drag of the airfoils (fig. 3). The vertical sweep rate of the probe was about 1.0 in/sec, consistent with previous investigations. The probe was located 1.67 chords (based on a 6.000-in-chord model) downstream of the airfoil trailing edge and had a maximum vertical travel of about ±11.0 in. from the tunnel centerline. Data are measured with four stainless steel total pressure tubes having an outside diameter of 0.060 in. and an inside diameter of 0.040 in., and the tubes are spaced 0.375 in. apart laterally as shown in figure 4.

LTPT Wake-Survey Apparatus

A remote-controlled survey arm was used to traverse the rake head through the wake of the airfoil to determine the airfoil profile drag. A sketch of this survey apparatus is shown in figure 6. The arm is composed of three movable components, each of which has a position control device: a main boom, an offset boom, and a forward-pivoting rake head. The main boom is mounted on the strut and can be rotated in the vertical plane about the pivot point by the linear actuator. The offset boom can be rotated about the main boom by the roll actuator, which allows survey positions to be made at distances up to 12 in. from the tunnel centerline. The forward-pivoting rake head is mounted at the end of the offset boom and may be rotated in the vertical plane by the internally mounted pitch-adjustment mechanism. The position and rate of movement of the survey apparatus are controlled by a microprocessor. For this investigation, the tips of the rake-head total pressure tubes were located 1.2 chords downstream of the airfoil trailing edge. A survey rate of about 0.10 in/sec was used to determine the airfoil drag.

The details of the wake-survey rake are shown in figure 7. The rake is composed of seven total pressure probes, two standard-type static pressure probes, two disk-type static pressure probes, and two claw-type flow-angularity probes. The total pressure probes consist of stainless steel tubing having an outside diameter of 0.063 in. and an inside diameter of 0.043 in. with the ends of the tubing flattened to a 0.020-in. opening in the vertical direction. The standard-type static pressure probes consist of tubing having a 0.125-in. outside diameter and a 0.061-in. inside diameter with hemispherical ends. Each standard-type probe has eight flush orifices drilled 45° apart and located eight tube diameters from the tip of the tube. The disk-type probe is 0.437 in. in diameter and has a single orifice of 0.018 in. drilled through the center of the disk that connects with an internal passage extending to the outer edge of the disk. The flow-angularity probes are located near the ends of the rake and are used to align the rake with the airfoil wake.

Instrumentation

All measurements made during the test programs in both wind tunnels were obtained with the use of the same high-speed, computer-controlled, digital data acquisition system and were recorded by the same high-speed tape recording unit (ref. 11). In the 6×28TT, the airfoil surface static pressures and the airfoil wake pressures were measured with individual variable-capacitance-type pressure transducers. The free-stream stagnation and static reference pressures were also measured with the same type of pressure transducers. The geometric angle of attack was determined from the output of a digital shaft encoder attached to a pinion engaging a rack on one model-support end plate.

In the LTPT, the airfoil surface pressures and wake pressures were measured by the use of an automatic pressure-scanning system and the variable-capacitance-type pressure transducers. Precision quartz pressure transducers were used to measure the tunnel stagnation and static reference pressures. The geometric angle of attack was measured by using a digital shaft encoder in a setup similar to that of the 6×28TT.

Repeatability

The overall precision of the data was determined by examination of the repeatability of the data. The 6×28TT repeat points for the three airfoils were measured at a nominally zero geometric angle of attack, and those points considered to be valid repeat points differed by no more than 0.05°. An examination of these 26 repeat points measured at Mach numbers up to 0.73 (below M_{dd} for these airfoils) indicated that the average of the differences between 26 pairs of data points was 0.00036 in drag coefficient (that is, $(1/26)\sum|c_{d,2}-c_{d,1}|$), 0.0035 in lift coefficient, and 0.0002 in pitching-moment coefficient. The LTPT repeat points were measured at angles of attack nominally from −3° to 6°. The six repeat points differed by 0.04° or less in angle of attack and spanned the range of test Mach numbers. The average of the differences between these six pairs of data points was 0.00005 in drag coefficient, 0.0032 in lift coefficient, and 0.0001 in pitching-moment coefficient.

Methods and Corrections

Methods

6×28TT. For each airfoil with a smooth model surface, data were taken for an angle-of-attack sweep at stagnation pressures of 60 psia at Mach numbers from about 0.34 to 0.84 to obtain Reynolds numbers typical of full-scale main rotor blades. For the RC(4)-10 model, additional data were taken at stagnation pressures from about 48 to 36 psia at Mach numbers from 0.34 to 0.49, respectively, to investigate the sensitivity of the maximum lift coefficients to changes in Reynolds number. At the lower test Mach numbers, the geometric angle of attack ranged from about −3° to 16° with 2° increments between the lower angles and 1° increments between angles approaching the stall angle. This range of angle of attack was decreased with increasing Mach number.

Section lift and pitching-moment coefficients were calculated from the airfoil surface pressures by a trapezoidal integration of the pressure coefficients. The pressure coefficient at the most rearward orifice on each surface was applied from that station to the airfoil trailing edge in the integration. Each of the pressure coefficients represents the average of five measurements obtained in a 1.0-sec interval.

The point-drag coefficients were calculated (ref. 16) from the measured wake pressures, and a trapezoidal integration of the point-drag coefficients was used to calculate the drag coefficient. The static pressures used in the point-drag calculation were measured with tunnel sidewall orifices located at the same longitudinal tunnel station as the tips of the tubes on the wake-survey probe. The drag coefficients represent the average of the measurements made with the four total pressure tubes on the wake-survey probe in one sweep through the wake of an airfoil.

LTPT. With a smooth model surface, data were taken for an angle-of-attack sweep at Mach numbers from 0.10 to 0.44 and stagnation pressures from about 14.7 to 43 psia to obtain Reynolds numbers typical of full-scale rotor blades. The angle of attack varied from $-3°$ to $19°$ at the lowest Mach number, and the range of angle of attack was reduced with increasing Mach number. One run was made with a 0.10-in-wide strip of No. 100 carborundum grit applied to the upper and lower model surfaces at the 5-percent-chord station to investigate the effects of fixing transition on the aerodynamic characteristics. The grit was sparsely applied and the size was selected according to the method of reference 17.

At the beginning of the test program, tufts were placed on the upper surface of the RC(4)-10 model and end plates and they were then observed during an angle-of-attack sweep through the stall angle at $M = 0.10$ and $R = 1.4 \times 10^6$ without any sidewall blowing. The tuft pattern indicated no premature separation of the sidewall boundary layer without sidewall blowing. The tufts were then observed at an angle of attack that was $3°$ less than the stall angle with sidewall blowing turned on. (This angle of attack was selected because there was separation on the model and the tufts could be observed for some time before many of them were torn off.) The tuft pattern was not noticeably different from that observed at the same angle of attack with the blowing turned off. As a result, the test was initiated without using any sidewall boundary-layer control. The effect of sidewall blowing on the measured lift coefficients was later determined at $M = 0.39$ and $R = 4.9 \times 10^6$. The difference between the lift coefficients with blowing on and off was less than 0.01 for angles of attack up to about $11°$. The difference in $c_{l,\max}$ with blowing on and off was less than 0.01 for measurements made during the same run, and it was 0.03 for measurements made in different runs (fig. 8). These small differences further confirmed that there was no need for sidewall blowing with this particular airfoil.

Section lift and pitching-moment coefficients were calculated from the airfoil surface pressures by a trapezoidal integration of the pressure coefficients. Section profile-drag coefficients were calculated by the method of reference 18 from measurements of the wake static and total pressures made with a wake-survey rake.

Corrections

6×28TT data. The corrections for lift interference, which have been applied to the angles of attack, were obtained from references 13 and 19. The maximum correction for the angle of attack is about $1.9°$. No correction for blockage was made since the 6×28TT slot geometry was designed to yield a flow that was relatively blockage free (ref. 13). Although a similarity-rule type of correction for tunnel sidewall boundary-layer effects has been reported for cases of fully attached flow on the airfoil model (ref. 20), the state of the art does not presently permit a general correction applicable to the entire range of the lift, drag, and pitching-moment curves important to rotorcraft airfoils, i.e., one which applies with or without separated flow on the model. Additionally, the existing 6×28TT data base of two-dimensional airfoil data is extensive and does not include corrections for sidewall boundary-layer effects. For these reasons, no correction for tunnel sidewall boundary-layer influences has been made to the data presented herein, and the emphasis is placed on a comparison of the performance of the two new airfoils with that of the baseline airfoil, the VR-7.

LTPT data. Corrections for solid and wake blockage were applied to the free-stream dynamic pressure, and corrections for the effects of floor and ceiling constraint on streamline curvature were applied to lift, pitching moment, and angle of attack (ref. 18). The corrections to the lift and drag coefficients are about 2 percent and 1 percent, respectively, of the measured coefficients. The maximum correction for the angle of attack is about $0.25°$.

Presentation of Results

The results of this investigation have been reduced to coefficient form and are presented as follows:

Results	Airfoil	Facility	Figure
Experimental results			
Basic aerodynamic characteristics: c_l against α_c; c_m and c_d against c_l; l/d against α_c	RC(4)-10	6×28TT	9
	RC(5)-10	6×28TT	10
	VR-7	6×28TT	11
Basic aerodynamic characteristics	RC(4)-10	LTPT	12
Comparison of facilities	RC(4)-10	LTPT and 6×28TT	13
Effect of fixing transition	RC(4)-10	LTPT	14
$c_{l,\max}$ against M	RC(4)-10	6×28TT	15
	RC(5)-10	6×28TT	15
	VR-7	6×28TT	15
	RC(4)-10	LTPT and 6×28TT	16
$c_{m,o}$ against M	RC(4)-10	6×28TT	17
	RC(5)-10	6×28TT	17
	VR-7	6×28TT	17
Comparison of M_{dd}	RC(4)-10	6×28TT	18
	RC(5)-10	6×28TT	18
	VR-7	6×28TT	18
Comparison of experiment and theory			
Basic aerodynamic characteristics: c_l against α; c_l against c_m and c_d	RC(4)-10	LTPT	19
	RC(4)-10	6×28TT	20
	RC(5)-10	6×28TT	21
$c_{m,o}$ against M	RC(4)-10	6×28TT	22
	RC(5)-10	6×28TT	22
$c_{d,o}$ against M	RC(4)-10	6×28TT	23
	RC(5)-10	6×28TT	23
Experimental pressure distributions			
C_p against x/c	RC(4)-10	6×28TT	24
	RC(5)-10	6×28TT	25
	RC(4)-10	LTPT	26

Discussion of Results

Lift

The lift coefficients for Mach numbers from 0.34 to 0.84 measured in the 6×28TT are presented as a function of angle of attack in figures 9(a), 10(a), and 11(a) for the RC(4)-10, RC(5)-10, and VR-7 airfoils, respectively. The lift coefficients of the RC(4)-10 airfoil measured in the LTPT for Mach numbers from 0.10 to 0.44 are presented in figure 12(a).

Reduction of $c_{l,\max}$ in 6×28TT. The results of a previous investigation of rotorcraft airfoils in the Langley 6- by 28-Inch Transonic Tunnel (ref. 7) have shown that the measured maximum normal-force coefficient (or $c_{l,\max}$) is reduced by tunnel-wall boundary-layer influences. This reduction is characteristic of two-dimensional wind tunnels without proper sidewall boundary-layer control and is the result of initial flow separation beginning at the tunnel-wall/airfoil juncture instead of in the centerspan of the model. The flow separates first at the tunnel-wall/airfoil juncture because the tunnel-wall boundary layer is thicker than the airfoil boundary layer but the same adverse pressure gradient is imposed on the wall by the airfoil.

Quantifying this degradation with confidence is possible for the RC(4)-10 airfoil since this

configuration was tested in both the 6×28TT and LTPT, in which more realistic two-dimensional maximum lift coefficients can be measured. The $c_{l,\max}$ data presented in figure 16 for the RC(4)-10 indicate that the 6×28TT data are lower by 0.09 at $M = 0.34$, but the difference in the data between the two facilities is approximately zero at $M = 0.39$ and 0.44. The 6×28TT airfoil data are unexpectedly higher than the LTPT data at M = 0.42, and the reason for this is not known. The trend of these differences with Mach number is similar to that reported previously for the NACA 0012 airfoil (ref. 7). The magnitude and trend of the $c_{l,\max}$ degradation for the RC(5)-10 and VR-7 airfoils would be expected to be similar to those of the RC(4)-10.

Maximum lift coefficient. The maximum lift coefficients determined from the 6×28TT data figures are presented in figure 15 for Mach numbers from 0.34 to 0.54. The trend of the maximum lift coefficient to decrease with increasing Mach number is common to the three airfoils with the RC(5)-10 and VR-7 data displaying about the same slope but the RC(4)-10 data displaying a much steeper slope. The maximum lift coefficients of the RC(4)-10 are higher than those of the other two airfoils at Mach numbers from 0.34 to about 0.42. The maximum lift coefficients of the RC(4)-10 were 1.57 at $M = 0.34$ and 1.42 at $M = 0.42$, whereas those of the baseline airfoil were 1.47 at $M = 0.34$ and 1.38 at $M = 0.42$. The maximum lift coefficients of the VR-7 are higher than those of the RC(5)-10 by about 0.05 or less for the range of Mach numbers presented. An increase in the maximum thickness of the RC(5)-10 of 1 to 2 percent chord would be expected to raise the $c_{l,\max}$ values to at least the same level as those of the VR-7. Examination of the pressure distributions for these three airfoils indicates that $c_{l,\max}$ decreases with increasing Mach number because of the development of shock waves which cause the upper-surface boundary layer to separate. The development of supercritical flow first occurs at progressively lower angles of attack with increasing Mach number; thus a strong shock develops sooner that limits the maximum lift value.

The maximum lift coefficients of the RC(4)-10 measured in both the LTPT and the 6×28TT are presented in figure 16. The highest $c_{l,\max}$ value is 1.74 and it occurs at Mach numbers from 0.10 to 0.20. Above $M = 0.20$, the maximum lift coefficients decrease with increasing Mach number until at $M = 0.49$, they decrease to 1.18.

The data in figures 15 and 16 indicate that neither of the two new airfoils completely met the two $c_{l,\max}$ design goals. The RC(4)-10 attained a $c_{l,\max}$ value of 1.45 at a Mach number of 0.40 (which meets the design goal) and a value of 1.18 at a Mach number of 0.5 (which is slightly below the design goal). The RC(5)-10 met the design goal for $M = 0.5$ by attaining a value of $c_{l,\max}$ of 1.25, but it did not meet the desired value for $M = 0.4$ by attaining a value of 1.39. Depending on the particular rotor requirements, the application of both sections to a rotor may result in a better rotor design than the use of just one of these sections. For example, using the RC(4)-10 from near the root end to about 75 percent of the rotor blade radius and then using the RC(5)-10 from 80 to 85 percent may result in a better rotor design than using the RC(4)-10 from near the root end to 85 percent of the rotor blade radius.

The maximum lift coefficients of the RC(4)-10 at Mach numbers of 0.10 and 0.20 are increased significantly by increases in the Reynolds number as shown in figure 16. This effect is typical of that shown for many airfoils at subcritical flow conditions (ref. 21). At Mach numbers from 0.34 to 0.49, the maximum lift coefficients of the RC(4)-10 are nearly unchanged by increases in Reynolds number from about 4×10^6 to 6×10^6 as shown in figures 9 and 12. An examination of the pressure distributions indicates that supercritical flow is present over a significant region of the upper surface near the leading edge at high angles of attack at Mach numbers of 0.34 and higher. Apparently the supercritical flow effects (which limit $c_{l,\max}$) predominate over the Reynolds number effects (which increase $c_{l,\max}$) for the stated conditions.

The effect of fixing transition on the maximum lift coefficients of the RC(4)-10 was determined for only one condition and is shown in figure 14. The addition of the grit strip resulted in an unexpected increase in $c_{l,\max}$ of about 0.06 and a softening of the stall characteristics. The roughness strip apparently causes the development of an upper-surface turbulent boundary layer that is more resistant to separation than the natural turbulent boundary layer resulting from the reattachment of a separation bubble.

Both the RC(4)-10 and the RC(5)-10 have a trailing-edge type of stall. This kind of gradual stall is characterized by a rounding of the lift curve near the maximum lift coefficient caused by a progressive movement of the upper-surface boundary-layer separation point toward the airfoil leading edge. The lift curves shown in figures 9(a) and 10(a) display this rounding, and the pressure distributions shown in figures 24 and 25 indicate a loss in pressure recovery on the upper surface near the airfoil trailing edge (typical of separated flow) at the angle of attack for $c_{l,\max}$. This type of static stall usually forecasts favorable dynamic stall characteristics. The abrupt drop in lift of the RC(4)-10 at the highest angles of attack shown in figure 12(a) is due to the

boundary-layer separation point moving from near 80 percent chord to near 20 percent chord for the small change in angle of attack. (See fig. 26(c).)

Pitching Moment

The pitching-moment coefficients measured in the 6×28TT are presented as a function of lift coefficient in figures 9(b), 10(b), and 11(b) for the RC(4)-10, RC(5)-10, and VR-7, respectively. The pitching-moment coefficients of the RC(4)-10 measured in the LTPT are similarly presented in figure 12(b). In general, the two new airfoils have very low pitching moments for lift coefficients from zero to near maximum lift for Mach numbers up to about 0.63. At Mach numbers above 0.63, the range of lift coefficients for near-zero pitching moment is reduced because of compressibility effects. The RC-series airfoils have a near-zero pitching moment over a broader range of lift coefficients than the baseline VR-7 until compressibility effects begin to dominate at $M = 0.63$. The pitching-moment coefficient about the aerodynamic center (c_m at $c_l = 0$) becomes more nose-down with increasing Mach number for all three airfoils (fig. 17). This trend for the RC-series airfoils is due to the development of a supersonic zone on the lower surface near the leading edge with increasing Mach number followed by an expansion of the supersonic flow on the upper surface between about 40 to 60 percent chord at the highest Mach numbers. The $c_{m,o}$ values of the new airfoils are less than -0.015 for Mach numbers up to about 0.75. Thus, all the pitching-moment design goals for the RC-series airfoils were satisfied. The positive value of the $c_{m,o}$ of the VR-7 at the lowest Mach number is due to the upward deflection of the trailing-edge tab. This tab results in a more nose-up pitching moment for the VR-7 than for the RC-series airfoils for Mach numbers up to about 0.81.

Increasing the Reynolds number has little effect on the pitching-moment characteristics of the RC(4)-10 other than delaying the nose-down break in the curve to higher lift coefficients because of the stall delay (figs. 9(b) and 12(b)). Fixing transition has no effect on the pitching moment coefficients of the RC(4)-10 (fig. 14).

Drag

The drag coefficients measured in the 6×28TT are presented in figures 9(c), 10(c), and 11(c) for the RC(4)-10, RC(5)-10, and VR-7, respectively, and those measured in the LTPT for the RC(4)-10 are presented in figure 12(c). Some 6×28TT data for the three airfoils are cross-plotted as a function of Mach number in figure 18. In general, the RC-series airfoils have lower drag coefficients than the baseline airfoil except at the higher lift coefficients at Mach numbers from about 0.49 to 0.64.

Minimum drag. The RC(5)-10 has a drag level of 0.0070 for lift coefficients from 0 to 0.3 for subcritical Mach numbers; this compares with a drag level of 0.0075 for the RC(4)-10 and of 0.0085 for the VR-7 (fig. 18). At zero lift, supercritical flow effects cause both the RC(4)-10 and RC(5)-10 curves to cross over that of the VR-7. This crossover results in a significant increase in drag level at Mach numbers between 0.67 and 0.80 for the RC(4)-10 and a much smaller increase ($\Delta c_{d,o} < 0.0005$) at Mach numbers near 0.73 for the RC(5)-10. At lift coefficients from 0.1 to 0.3, compressibility effects cause significant differences between airfoils with the new airfoils having much lower drag levels than the baseline airfoil.

A "bucket" is evident in the RC(4)-10 drag curves measured in the LTPT that is not shown in the 6×28TT data (fig. 13(c)). The free-stream turbulence level in the LTPT is very low, thus permitting an extensive run of laminar flow; whereas that in the 6×28TT is high enough to cause an early transition to turbulent flow, thus eliminating the bucket. The new airfoils were never designed with the intention of utilizing a significant chordwise extent of laminar flow since a full-scale-rotor boundary layer would be expected to be fully turbulent. At lift coefficients outside the range of the bucket and not near $c_{l,\max}$, the drag coefficients measured in the two facilities show close agreement.

The differences in the minimum drag coefficients of the RC(4)-10 at Mach numbers from about 0.34 to 0.49 due to changes in Reynolds number from nominally 4×10^6 to 6×10^6 are generally within the accuracy of the 6×28TT data. The LTPT data measured at $M = 0.34$ also indicate small differences for this same change in Reynolds number. However, the LTPT data measured at $M = 0.10$ and 0.20 indicate significant Reynolds number effects. At $M = 0.10$, the sharpness of the bucket is reduced and the c_l range of the bucket is shifted to higher lift coefficients with increases in Reynolds number. At $M = 0.20$, the upper edge of the bucket is extended to a higher lift coefficient because of the increase in Reynolds number. Outside the minimum drag range and at lift coefficients above the linear range of the lift curves, the 6×28TT and LTPT drag coefficients show the expected decrease with increasing Reynolds number.

Fixing transition eliminates the bucket in the RC(4)-10 drag curve, thus substantially increasing the minimum c_d as shown in figure 14. Fixing transition generally increases the drag level at low to

moderate lift coefficients outside the bucket by about 0.0010.

Drag divergence. The RC(5)-10 airfoil has a higher drag-divergence Mach number than the VR-7 at lift coefficients from 0 to 0.3, whereas the RC(4)-10 has a higher drag-divergence Mach number than the VR-7 at lift coefficients from 0.1 to 0.3 (fig. 18). For the RC(4)-10 and RC(5)-10 at zero lift, $M_{\mathrm{dd}} = 0.74$ and 0.79, respectively, thus meeting the design goal for this parameter. The drag-divergence Mach number at zero lift for the baseline airfoil is 0.75. Increasing the lift coefficient decreases M_{dd} for the RC(5)-10 but increases it for the RC(4)-10. The RC(4)-10 has a higher drag-divergence Mach number than the RC(5)-10 at lift coefficients of 0.2 and 0.3, but because of drag creep it generally has a higher drag level than the RC(5)-10 in the vicinity of M_{dd}.

Lift-to-drag ratio. The lift-to-drag ratios calculated from the 6×28TT measurements are presented as a function of angle of attack in figures 9(d), 10(d), and 11(d). The maximum lift-to-drag ratio exceeds 100 for Mach numbers up to 0.44 for the RC(4)-10, for Mach numbers up to 0.54 for the RC(5)-10, and for Mach numbers up to 0.59 for the VR-7. Above these Mach numbers, $(l/d)_{\max}$ for these airfoils decreases continuously with increasing Mach number.

The maximum lift-to-drag ratio of the RC(4)-10 determined from the LTPT measurements (fig. 12(d)) decreases from about 140 to 130 as M increases from 0.10 to 0.20. For Mach numbers from 0.30 to 0.44, $(l/d)_{\max}$ for the RC(4)-10 varies from about 120 to 130. The sharp peak in some of the l/d curves of the RC(4)-10 is due to the laminar-flow bucket in the LTPT drag curves. Similarly, the $(l/d)_{\max}$ values determined from the LTPT data are higher than those determined from the 6×28TT data because of the lower drag levels obtainable in the LTPT.

Increasing the Reynolds number causes increases in $(l/d)_{\max}$ for the RC(4)-10 with the largest difference occurring at $M = 0.10$ (fig. 12(d)). At $M = 0.34$, the LTPT data (fig. 12(d)) indicate a very small effect of Reynolds number on $(l/d)_{\max}$, whereas the 6×28TT data (fig. 9(d)) indicate a significant effect. The larger Reynolds number effect in the 6×28TT data is caused by the lack of data points in the drag curve at the lower test Reynolds number between $c_l \approx 0.95$ and 1.35.

Comparison With Theory

The basic aerodynamic characteristics of the RC(4)-10 and RC(5)-10 airfoils at selected Mach numbers are compared with theory in figures 19 to 21. Data/theory comparisons of the variation of $c_{m,o}$ with Mach number and of $c_{d,o}$ with Mach number for these two airfoils are presented in figures 22 and 23, respectively.

For subcritical flow conditions, the multicomponent airfoil analysis (MCARFA) computer code was used for comparison with the experimental data. The MCARFA code (refs. 22 and 23) is a viscous, compressible analysis that is limited to subcritical flows and does not account for the effects of boundary-layer separation. When turbulent boundary-layer separation is predicted by MCARFA to occur forward of the airfoil trailing edge, the calculated pressure coefficients aft of the predicted separation point do not become significantly less positive (or become negative for massive separation) as they do experimentally. Instead, at the airfoil trailing edge the calculated pressure coefficients recover to a positive value that is not much different from that of a case without any separation predicted. As a result, the predicted lift coefficients continue to vary almost linearly with angle of attack even though separation has occurred.

For some subcritical and all supercritical flow conditions, the Korn-Garabedian-Bauer (KGB) theory (ref. 9) was used for the comparisons. The KGB code is a viscous, transonic analysis applicable to airfoils with turbulent boundary layers. This code does not make the appropriate adjustment to the pressure distribution when boundary-layer separation is predicted to occur ahead of the airfoil trailing edge. The pressure coefficients aft of the predicted boundary-layer separation point calculated by the KGB code continue to recover to a positive value at the airfoil trailing edge that is close to that of a fully attached flow case. Thus, the predicted lift coefficients continue to vary almost linearly with α even though separation has occurred.

Lift. The experimental lift curve of the RC(4)-10 is matched nearly identically by the lift curve calculated with the MCARFA code at Mach numbers of 0.20 and 0.30. At both Mach numbers, the MCARFA code predicts that the separation point of the upper-surface boundary layer $(x/c)_{\mathrm{sep}}$ will occur earlier than indicated by the experimental data. This could lead to a significant underestimate of the $c_{l,\max}$ capability of an airfoil. The predicted separation point at an angle of attack of about 13° at $M = 0.20$ is $(x/c)_{\mathrm{sep}} = 0.84$, whereas the experimental pressure distribution indicates attached flow to $(x/c)_{\mathrm{sep}} = 0.99$ on the upper surface.

At Mach numbers of 0.39 and 0.49, the KGB theory is used for the comparisons. The lift-curve slope determined from the KGB theory is lower than that determined from the experimental data for both airfoils at $M = 0.39$ and 0.49, but it matches the

experimental slope more closely at $M = 0.49$ for both airfoils. Since the experimental angle of attack has been corrected for wind-tunnel boundary effects, it is not clear how one can determine the part of the difference due to inadequacy of the theory and the part due to inadequacy of the correction to angle of attack. The predicted upper-surface boundary-layer separation point $(x/c)_{\text{sep}}$ is close to the experimental separation point at $M = 0.39$ for both airfoils. At $M = 0.49$, the predicted $(x/c)_{\text{sep}}$ occurs later than that indicated by the experiment for the RC(4)-10, but it occurs sooner than that shown by the experiment for the RC(5)-10. This highlights the uncertainty that an airfoil designer faces in selecting an airfoil when the primary design goal is to achieve $c_{l,\max}$ at Mach numbers of 0.4 and 0.5.

Pitching moment. The pitching-moment coefficients predicted by MCARFA at $M = 0.2$ and 0.3 agree very well with the wind-tunnel data for the RC(4)-10 airfoil (figs. 19(a) and 19(b)). The pitching-moment coefficients calculated by the KGB code are in poor agreement with the experimental data measured at $M = 0.39$ and 0.49 for both airfoils in that the predicted c_m versus c_l curves are rotated in the nose-up direction about a low value of c_l relative to the experimental curves (figs. 19(c), 20, and 21). The variation of $c_{m,o}$ with Mach number indicates that the trend predicted by the KGB code for both airfoils is the same as the experimental data trend except that the predicted values for both airfoils are more nose-down at all Mach numbers than the wind-tunnel data (fig. 22).

Drag. The MCARFA theory generally agrees well with the RC(4)-10 drag coefficients measured in the LTPT up to a lift coefficient of about 1.0 where the theory begins to underpredict the drag level. The MCARFA theory predicts the presence of a laminar-flow bucket at $M = 0.2$ and 0.3 although the predicted minimum drag level in the bucket is higher than the minimum measured level. The agreement between the drag level of the RC(4)-10 predicted by the KGB theory and the fixed-transition drag level measured in the LTPT at $M = 0.39$ is generally good for lift coefficients up to about 1.3 (fig. 19(c)). The agreement between the drag coefficients predicted by the KGB theory and those measured in the 6×28TT for the RC(4)-10 is good at lift coefficients up to about 1.0 for $M = 0.49$. The agreement between the KGB theory and the 6×28TT drag coefficients for the RC(5)-10 is good at lift coefficients up to about 1.2 for $M = 0.39$ and at lift coefficients up to about 1.0 for $M = 0.49$. Above these lift coefficients at these Mach numbers, the KGB theory begins to underpredict the drag level of both airfoils. This good agreement with the 6×28TT data is partly fortuitous in that the high turbulence level in the 6×28TT causes the boundary-layer transition to occur near the leading edge on both surfaces.

The variation of $c_{d,o}$ with Mach number indicates that the KGB theory underpredicts the drag level of both airfoils at Mach numbers above about 0.65, a result indicative of a predicted wave drag that is lower than that occurring on the wind-tunnel models. A predicted wave drag that is too low results in a predicted drag-divergence Mach number that is too high for the RC(4)-10 but too low for the RC(5)-10.

A qualitative summary of the agreement of the theory relative to the experiment is given in the table below:

Airfoil	M	$dc_l/d\alpha$	$(x/c)_{\text{sep}}$	c_m	c_d
MCARFA theory					
RC(4)-10	0.20	Good	Low	Good	Good at $c_l \leq 1.0$; low at $c_l > 1.0$
	.30	Good	Low	Good	Good at $c_l \leq 1.0$; low at $c_l > 1.0$
KGB theory					
RC(4)-10	0.39	Low	Good	Poor	Good at $c_l \leq 1.3$; low at $c_l > 1.3$
	.49	Low	High	Poor	Good at $c_l \leq 1.0$; low at $c_l > 1.0$
RC(5)-10	0.39	Low	Good	Poor	Good at $c_l \leq 1.2$; low at $c_l > 1.2$
	.49	Low	Low	Poor	Good at $c_l \leq 1.0$; low at $c_l > 1.0$

Airfoil	M	$c_{m,o}$	$c_{d,o}$
KGB theory			
RC(4)-10	0.34–0.83	High at all M's; trend good	Good at $M \leq 0.65$; low at $M > 0.65$; M_{dd} high
RC(5)-10	0.34–0.84	High at all M's; trend good	Good at $M \leq 0.65$; low at $M > 0.65$; M_{dd} low

Conclusions

A wind-tunnel investigation has been conducted to determine the two-dimensional aerodynamic characteristics of two new rotorcraft airfoils designed

specifically for application to the inboard region (stations $\leq$85 percent radius) of a helicopter main rotor blade. The two new airfoils, the RC(4)-10 and RC(5)-10, and a baseline airfoil, the VR-7 which is currently in use, were all investigated in the Langley 6- by 28-Inch Transonic Tunnel (6×28TT) at Mach numbers from about 0.34 to 0.84 and at respective Reynolds numbers from about 4.7×10^6 to 9.3×10^6. In addition, the RC(4)-10 airfoil was investigated in the Langley Low-Turbulence Pressure Tunnel (LTPT) at Mach numbers from 0.10 to 0.44 and at respective Reynolds numbers from 1.4×10^6 to 5.4×10^6. Some of the experimental data for the two new airfoils were compared with two different theories. An analysis of the data has resulted in the following conclusions:

1. Of the three airfoils investigated in the 6×28TT, the RC(4)-10 airfoil had the highest maximum lift coefficients at Mach numbers M from 0.34 to about 0.42. The maximum lift coefficients of the RC(4)-10 were 1.57 at $M = 0.34$ and 1.42 at $M = 0.42$, whereas those of the baseline airfoil were 1.47 at $M = 0.34$ and 1.38 at $M = 0.42$. The maximum lift coefficients of the baseline airfoil were higher than those of the RC(5)-10 by about 0.05 or less for Mach numbers from 0.34 to 0.54. The highest maximum lift coefficient measured for the RC(4)-10 in the LTPT was 1.74 at Mach numbers of 0.10 and 0.20.

2. Neither the RC(4)-10 nor the RC(5)-10 met both design goals for maximum lift coefficient. The RC(4)-10 attained a value of maximum lift coefficient $c_{l,\max}$ of 1.45 at $M = 0.40$ which met the design goal ($c_{l,\max} > 1.40$) and a value of 1.18 at $M = 0.50$ which was slightly below the design goal ($c_{l,\max} > 1.20$). The RC(5)-10 attained a maximum lift coefficient of 1.39 at $M = 0.40$ and of 1.25 at $M = 0.50$.

3. The two new airfoils had very low pitching-moment coefficients (nearly zero) for lift coefficients from zero to near maximum lift for Mach numbers up to about 0.63. The new airfoils had a near-zero pitching-moment coefficient over a broader range of lift coefficients than the baseline airfoil until compressibility effects began to dominate at $M = 0.63$. The pitching-moment coefficient at zero lift for the new airfoils was less than -0.015 for Mach numbers up to about 0.75. Thus, the RC(4)-10 and RC(5)-10 met the pitching-moment-coefficient design criterion.

4. The drag-divergence Mach number of the RC(5)-10 airfoil was higher than that of the baseline airfoil for lift coefficients from 0.0 to 0.3, whereas the drag-divergence Mach number of the RC(4)-10 airfoil was higher than that of the baseline airfoil for lift coefficients from 0.1 to 0.3. The drag-divergence Mach number at zero lift coefficient was 0.79 for the RC(5)-10, 0.74 for the RC(4)-10, and 0.75 for the VR-7. For Mach numbers less than 0.63, the drag coefficients of the new airfoils were generally lower than those of the baseline airfoil. The new airfoils thus met all the design goals for drag coefficient.

5. The predictions of the Korn-Garabedian-Bauer (KGB) theory were compared with the 6×28TT experimental data for the RC(4)-10 and RC(5)-10 airfoils. The upper-surface boundary-layer separation point was well-predicted for the RC(5)-10 at $M = 0.39$ but poorly predicted for both airfoils at $M = 0.49$. The pitching-moment coefficients were poorly predicted for both airfoils. The drag coefficients at zero lift were underpredicted for both airfoils for Mach numbers greater than 0.65 which resulted in a poor prediction of the drag-divergence Mach number.

6. The predictions of the multicomponent airfoil analysis (MCARFA) computer code were compared with the experimental data for the RC(4)-10 airfoil measured at Mach numbers of 0.20 and 0.30. The MCARFA code prediction of the lift-curve slope, the pitching-moment coefficients, and the drag coefficients (for lift coefficients up to 1.0) agreed well with the experimental data at both Mach numbers. Also, at both Mach numbers the MCARFA code predicted that the upper-surface boundary layer would separate sooner than indicated by the experimental data.

NASA Langley Research Center
Hampton, VA 23665-5225
May 10, 1990

References

1. Bingham, Gene J.; and Noonan, Kevin W.: *Experimental Investigation of Three Helicopter Rotor Airfoils Designed Analytically.* NASA TP-1396, AVRADCOM TR 79-11, 1979.
2. Noonan, Kevin W.: *Experimental Investigation of a 10-Percent-Thick Helicopter Rotor Airfoil Section Designed With a Viscous Transonic Analysis Code.* NASA TP-1864, AVRADCOM TR 81-B-3, 1981.
3. Bingham, Gene J.; Noonan, Kevin W.; and Sewall, William G.: *Two-Dimensional Aerodynamic Characteristics of an Airfoil Designed for Rotorcraft Application.* NASA TP-1965, AVRADCOM TR 81-B-6, 1981.
4. Bingham, Gene J.; and Noonan, Kevin W.: *Two-Dimensional Aerodynamic Characteristics of Three Rotorcraft Airfoils at Mach Numbers From 0.35 to 0.90.* NASA TP-2000, AVRADCOM TR 82-B-2, 1982.
5. Dadone, Leo: *Rotor Airfoil Optimization: An Understanding of the Physical Limits.* Preprint No. 78-4, 34th Annual National Forum, American Helicopter Soc., Inc., May 1978.

6. Schrage, Daniel P.; and O'Malley, James A.: Performance and Aeroelastic Tradeoffs on Recent Rotor Blade Designs. *American Helicopter Society National Specialists' Meeting "Rotor System Design,"* Oct. 1980, pp. IV 5-1—IV-5-10.
7. Noonan, Kevin W.; and Bingham, Gene J.: *Two-Dimensional Aerodynamic Characteristics of Several Rotorcraft Airfoils at Mach Numbers From 0.35 to 0.90.* NASA TM X-73990, 1977.
8. Dadone, L.; and McMullen, J.: *HLH/ATC Rotor System Two-Dimensional Airfoil Test.* D301-10071-1 (Contract DAAJ01-71-C-0840(D40), Boeing Vertol Co., Dec. 1971.
9. Bauer, Frances; Garabedian, Paul; Korn, David; and Jameson, Antony: Supercritical Wing Sections II. *Volume 108 of Lecture Notes in Economics and Mathematical Systems,* M. Beckmann and H. P. Kuenzi, eds., Springer-Verlag, 1975.
10. Noonan, Kevin W.: *High Lift, Low Pitching Moment Airfoils.* U.S. Patent No. 4,776,531, Oct. 11, 1988.
11. Ladson, Charles L.: *Description and Calibration of the Langley 6- by 28-Inch Transonic Tunnel.* NASA TN D-8070, 1975.
12. Sewall, William G.: *Description of Recent Changes in the Langley 6- by 28-Inch Transonic Tunnel.* NASA TM-81947, 1981.
13. Barnwell, Richard W.: *Design and Performance Evaluation of Slotted Walls for Two-Dimensional Wind Tunnels.* NASA TM-78648, 1978.
14. Von Doenhoff, Albert E.; and Abbott, Frank T., Jr.: *The Langley Two-Dimensional Low-Turbulence Pressure Tunnel.* NACA TN 1283, 1947.
15. McGhee, Robert J.; Beasley, William D.; and Foster, Jean M.: *Recent Modifications and Calibration of the Langley Low-Turbulence Pressure Tunnel.* NASA TP-2328, 1984.
16. Baals, Donald D.; and Mourhess, Mary J.: *Numerical Evaluation of the Wake-Survey Equations for Subsonic Flow Including the Effect of Energy Addition.* NACA WR L-5, 1945. (Formerly NACA ARR L5H27.)
17. Braslow, Albert L.; and Knox, Eugene C.: *Simplified Method for Determination of Critical Height of Distributed Roughness Particles for Boundary-Layer Transition at Mach Numbers From 0 to 5.* NACA TN 4363, 1958.
18. Pankhurst, R. C.; and Holder, D. W.: *Wind-Tunnel Technique.* Sir Isaac Pitman & Sons, Ltd. (London), 1965.
19. Davis, Don D., Jr.; and Moore, Dewey: *Analytical Study of Blockage- and Lift-Interference Corrections for Slotted Tunnels Obtained by the Substitution of an Equivalent Homogeneous Boundary for the Discrete Slots.* NACA RM L53E07b, 1953.
20. Sewall, William Grier: *Application of a Transonic Similarity Rule To Correct the Effects of Sidewall Boundary Layers in Two-Dimensional Transonic Wind Tunnels.* M.S. Thesis, George Washington Univ., Aug. 1982. (Available as NASA TM-84847.)
21. Loftin, Laurence K., Jr.; and Smith, Hamilton A.: *Aerodynamic Characteristics of 15 NACA Airfoil Sections at Seven Reynolds Numbers From* 0.7×10^6 *to* 9.0×10^6. NACA TN 1945, 1949.
22. Stevens, W. A.; Goradia, S. H.; and Braden, J. A.: *Mathematical Model for Two-Dimensional Multi-Component Airfoils in Viscous Flow.* NASA CR-1843, 1971.
23. Brune, G. W.; and Manke, J. W.: *An Improved Version of the NASA-Lockheed Multielement Airfoil Analysis Computer Program.* NASA CR-145323, 1978.

Table I. Design Coordinates for RC(4)-10 Airfoil

[Stations and ordinates given in percent airfoil chord]

Upper surface		Lower surface	
Station	Ordinate	Station	Ordinate
0.0000	−0.5726	0.0000	−0.5726
.2864	.4313	.4687	−1.5907
.9072	1.3175	1.4350	−2.1823
2.3543	2.5980	1.6462	−2.2703
4.7036	3.8875	2.5184	−2.5664
7.3686	4.7953	3.5595	−2.8199
10.0188	5.3673	6.1865	−3.1576
12.6143	5.7324	8.4979	−3.2337
15.1842	5.9790	10.8242	−3.2011
17.7227	6.1579	13.2051	−3.1269
20.2556	6.2995	15.6116	−3.0611
22.7760	6.4163	18.0495	−3.0276
25.2956	6.5143	20.4930	−3.0257
30.3145	6.6614	22.9490	−3.0430
35.3142	6.7381	25.4059	−3.0703
37.8140	6.7422	30.3398	−3.1393
40.3297	6.7163	35.2929	−3.2090
42.8390	6.6543	37.7696	−3.2369
45.3678	6.5499	40.2303	−3.2553
47.8891	6.4013	42.6974	−3.2600
50.3763	6.2129	45.1451	−3.2474
52.8707	5.9876	47.6002	−3.2163
55.3618	5.7324	50.0894	−3.1659
57.8512	5.4510	52.5714	−3.0972
60.3417	5.1447	55.0567	−3.0090
62.8341	4.8144	57.5437	−2.9062
65.3244	4.4621	60.0297	−2.7933
67.8157	4.0912	62.5136	−2.6750
70.2978	3.7093	64.9997	−2.5542
72.7694	3.3251	67.4849	−2.4327
75.2502	2.9451	69.9792	−2.3108
77.7197	2.5808	72.4840	−2.1873
80.1713	2.2378	74.9797	−2.0610
82.6309	1.9139	77.4866	−1.9273
85.0970	1.6086	80.0114	−1.7818
87.5699	1.3211	82.5282	−1.6215
90.0509	1.0514	85.0386	−1.4420
92.5350	.8012	87.5421	−1.2443
95.0185	.5722	90.0374	−1.0312
97.5028	.3652	92.5298	−.8079
100.0000	.1785	95.0227	−.5728
		97.5148	−.3160
		100.0000	.0203

Table II. Design Coordinates for RC(5)-10 Airfoil

[Stations and ordinates given in percent airfoil chord]

Upper surface		Lower surface	
Station	Ordinate	Station	Ordinate
0.0000	−0.6628	0.0000	−0.6628
.2804	.2043	.3495	−1.4193
.9229	1.0156	1.1972	−1.8937
2.3372	2.1475	1.4150	−1.9692
4.7014	3.3786	2.2672	−2.1937
7.3268	4.2886	3.3442	−2.3815
9.9519	4.9191	5.9623	−2.6178
12.5345	5.3634	8.3193	−2.6954
15.0964	5.6898	10.6766	−2.7174
17.6322	5.9389	13.0763	−2.7247
20.1645	6.1379	15.4968	−2.7431
22.6856	6.3002	17.9434	−2.7824
25.2069	6.4343	20.3935	−2.8381
30.2312	6.6315	22.8548	−2.9009
35.2368	6.7354	25.3158	−2.9641
37.7395	6.7464	30.2563	−3.0826
40.2583	6.7237	35.2155	−3.1788
42.7706	6.6621	37.6951	−3.2134
45.3024	6.5566	40.1588	−3.2354
47.8267	6.4067	42.6288	−3.2420
50.3169	6.2175	45.0794	−3.2303
52.8143	5.9920	47.5374	−3.1997
55.3083	5.7368	50.0296	−3.1465
57.8007	5.4553	52.5146	−3.0745
60.2942	5.1488	55.0029	−2.9863
62.7896	4.8180	57.4929	−2.8855
65.2829	4.4654	59.9818	−2.7753
67.7772	4.0942	62.4687	−2.6595
70.2623	3.7121	64.9578	−2.5403
72.7368	3.3279	67.4460	−2.4202
75.2205	2.9477	69.9432	−2.2995
77.6930	2.5829	72.4511	−2.1778
80.1476	2.2394	74.9497	−2.0542
82.6101	1.9150	77.4597	−1.9242
85.0791	1.6094	79.9875	−1.7832
87.5550	1.3218	82.5073	−1.6277
90.0390	1.0519	85.0207	−1.4525
92.5260	.8016	87.5272	−1.2545
95.0125	.5726	90.0255	−1.0315
97.4998	.3655	92.5209	−.8026
100.0000	.1787	95.0168	−.5703
		97.5118	−.3169
		100.0000	.0204

Table III. Design Coordinates for VR-7 Airfoil With −4.6° Tab

[Stations and ordinates given in percent airfoil chord]

Upper surface		Lower surface	
Station	Ordinate	Station	Ordinate
0.0000	0.0000	0.0000	0.0000
.4950	1.6333	.4950	−.5700
.9900	2.1583	.9900	−.8000
1.9800	2.9500	1.9800	−1.0783
2.9700	3.5800	2.9700	−1.2767
3.9600	4.1083	3.9600	−1.4300
4.9500	4.5600	4.9500	−1.5683
5.9400	4.9750	5.9400	−1.6833
6.9300	5.3567	6.9300	−1.7867
8.4167	5.8717	8.4167	−1.9650
10.0983	6.3667	10.0983	−2.1233
11.8817	6.8417	11.8817	−2.2617
13.8617	7.2967	13.8617	−2.3867
15.8417	7.6733	15.8417	−2.4850
17.8217	8.0000	17.8217	−2.5750
19.8017	8.2967	19.8017	−2.6333
22.2767	8.5850	22.2767	−2.7033
25.2483	8.8317	25.2483	−2.7717
28.7133	9.0000	28.7133	−2.8217
32.6733	9.0500	32.6733	−2.8617
36.6333	8.9600	36.6333	−2.8717
40.5933	8.7817	40.5933	−2.8217
44.5550	8.4750	44.5550	−2.7233
48.5150	8.0800	48.5150	−2.5750
52.4750	7.5950	52.4750	−2.3767
56.4350	7.0300	56.4350	−2.1783
60.3967	6.3967	60.3967	−1.9700
64.3567	5.7433	64.3567	−1.7717
68.3167	5.0900	68.3167	−1.5650
72.2767	4.4250	72.2767	−1.3667
76.2383	3.7717	76.2383	−1.1583
80.1983	3.1183	80.1983	−.9600
83.6633	2.5450	83.6633	−.7833
87.1283	1.9700	87.1283	−.6067
90.0983	1.4750	90.0983	−.4550
92.5750	1.0667	92.5750	−.3283
94.5550	.7383	94.5550	−.2267
95.0500	.6550	95.0500	−.2017
100.0000	1.0533	100.0000	.1950

Table VI. Locations of Static Pressure Orifices for VR-7 Airfoil With −4.6° Tab

[Locations given in percent airfoil chord]

Upper-surface station	Lower-surface station
−0.068	−0.068
1.188	1.102
2.368	2.415
5.060	4.913
7.450	7.405
10.087	9.922
14.958	14.967
19.972	19.985
25.000	24.978
30.002	30.000
35.035	34.992
40.033	39.962
45.048	45.010
50.083	50.010
55.103	55.002
60.118	60.005
65.110	65.007
70.100	69.998
75.103	75.000
80.123	79.995
85.107	85.020
90.095	89.997
95.032	95.008

Table V. Locations of Static Pressure Orifices for RC(5)-10 Airfoil

[Locations given in percent airfoil chord]

Upper-surface station	Lower-surface station
0.000	0.000
1.263	1.282
2.528	2.543
4.997	5.027
7.525	7.517
10.047	10.013
14.978	15.018
20.038	20.018
25.028	25.007
29.988	30.052
35.010	35.035
40.015	40.037
45.000	45.060
50.025	50.052
55.013	54.983
60.000	60.008
65.025	65.000
70.022	70.040
75.035	75.013
80.048	80.033
85.062	85.062
90.068	90.065
94.997	95.080

Table IV. Locations of Static Pressure Orifices for RC(4)-10 Airfoil (6×28TT Model)

[Locations given in percent airfoil chord]

Upper-surface station	Lower-surface station
0.000	0.000
1.315	1.257
2.550	2.502
4.998	4.998
7.513	7.527
9.995	9.995
14.992	14.992
19.978	19.998
24.982	25.005
29.993	29.995
34.998	35.008
40.032	40.015
45.030	45.005
50.032	50.008
55.017	54.995
60.043	60.007
65.000	64.993
70.002	70.012
75.033	75.013
80.035	80.003
85.023	85.008
89.993	90.003
95.052	95.012

Table VII. Locations of Static Pressure Orifices for RC(4)-10 Airfoil (LTPT Model)

[Locations given in percent airfoil chord]

Upper-surface station	Lower-surface station
0.00	0.00
.41	.36
.99	.95
1.97	1.93
2.99	2.97
4.88	4.97
5.77	5.80
7.50	7.46
9.94	10.08
15.00	15.05
20.01	20.03
25.01	24.91
29.95	29.94
35.02	34.91
39.98	39.96
45.03	45.03
50.02	50.02
55.00	54.97
60.01	60.04
64.97	64.94
69.98	69.95
75.01	74.99
79.99	80.05
85.09	90.01
90.02	92.53
92.53	95.03
95.00	97.56
97.50	99.03
98.99	100.00
100.00	

Upper-surface spanwise station	
$x/c = 4.9$	$x/c = 79.9$
25.2	25.3
33.6	33.7
42.0	42.1
50.5	50.5
58.9	58.9
67.3	67.4
71.5	71.6

(a) Comparison of RC(4)-10 and RC(5)-10 profiles.

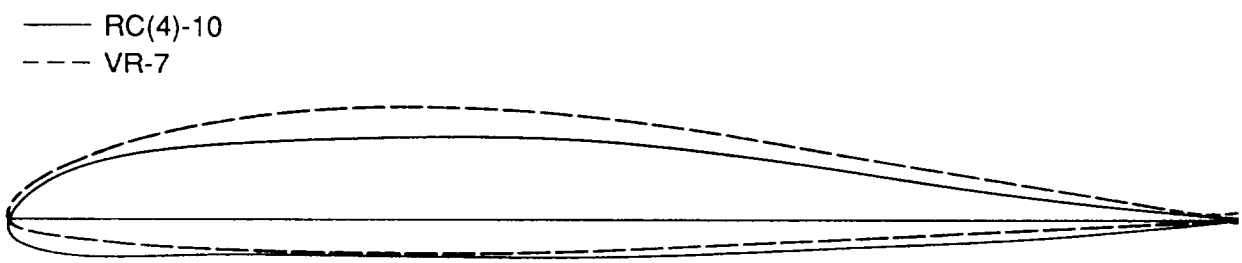

(b) Comparison of RC(4)-10 and VR-7 profiles.

Figure 1. Airfoil profiles.

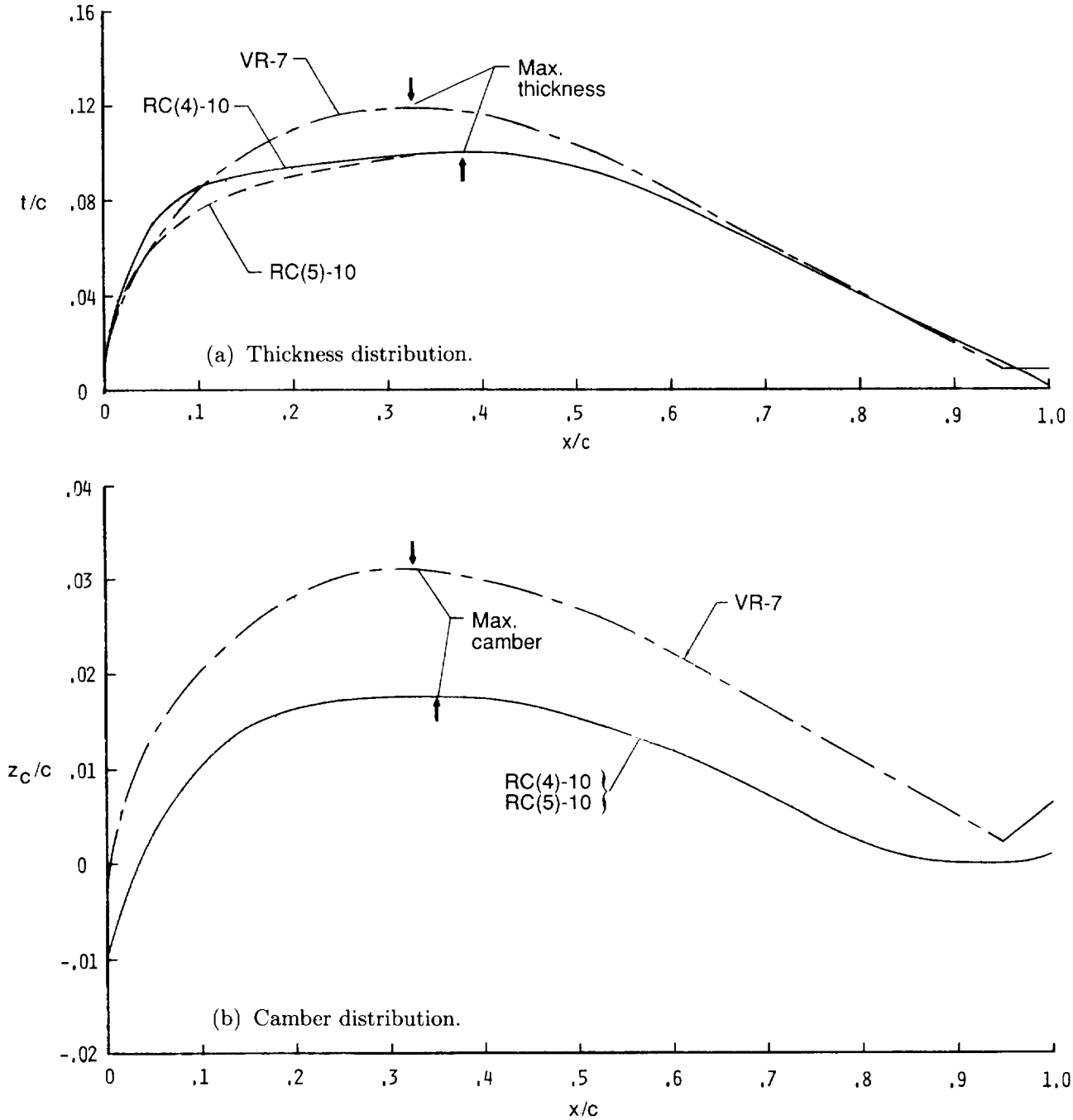

Figure 2. Thickness and camber distribution of RC(4)-10, RC(5)-10, and VR-7 airfoils.

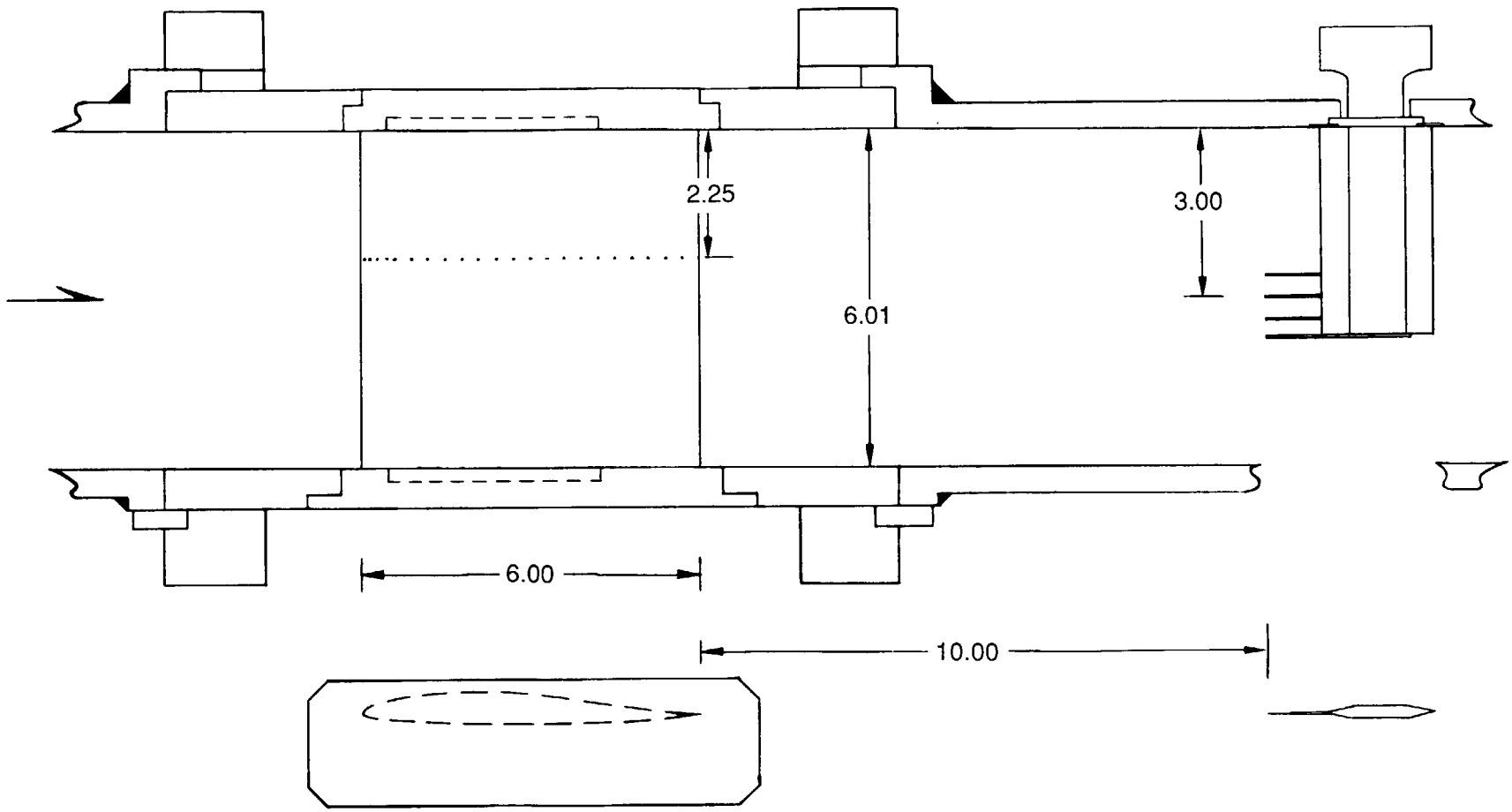

Figure 3. Model and wake-survey probe installation in the Langley 6×28TT. All dimensions are given in inches.

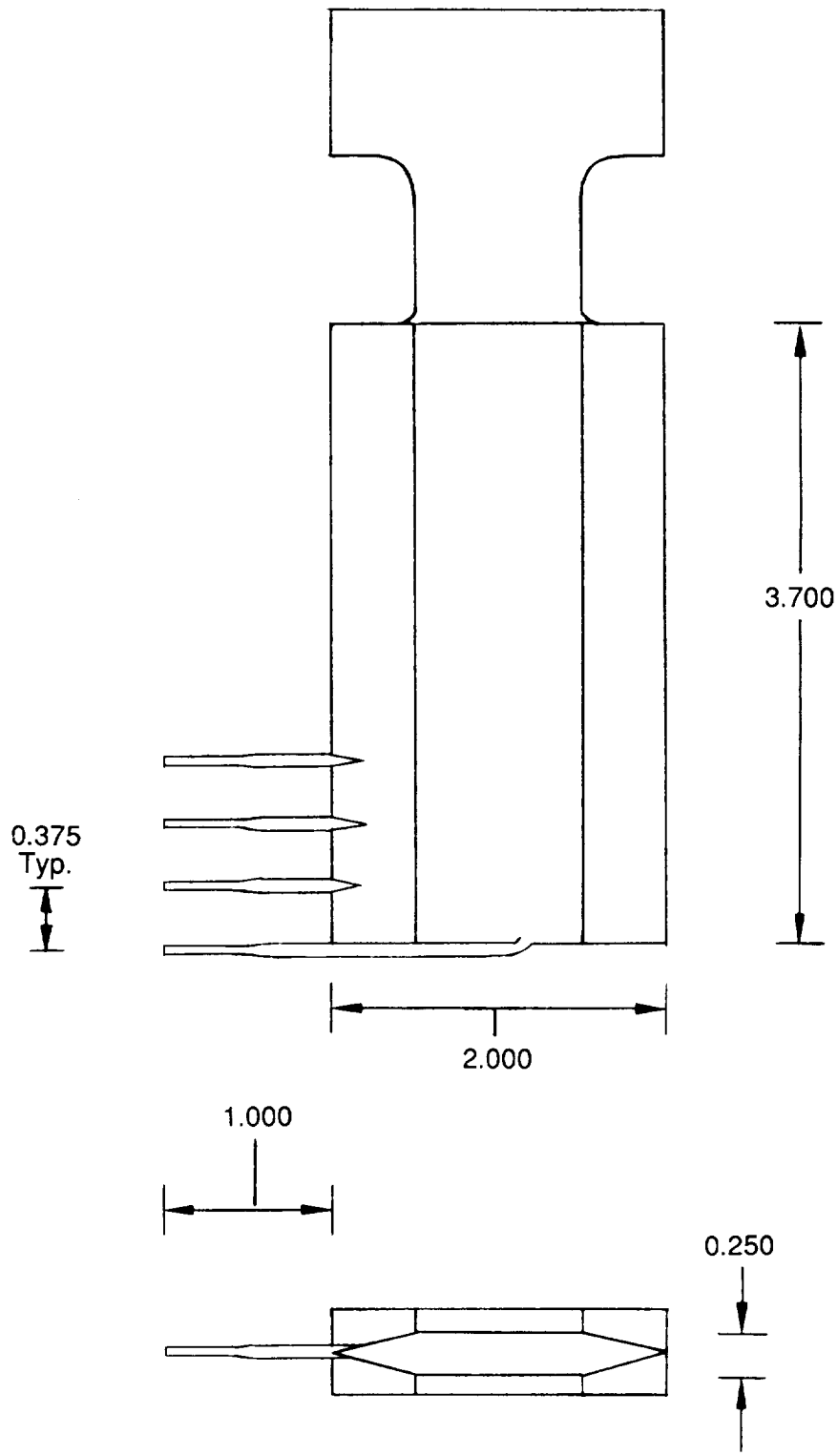

Figure 4. Wake-survey probe used in the Langley 6×28TT. All dimensions are given in inches.

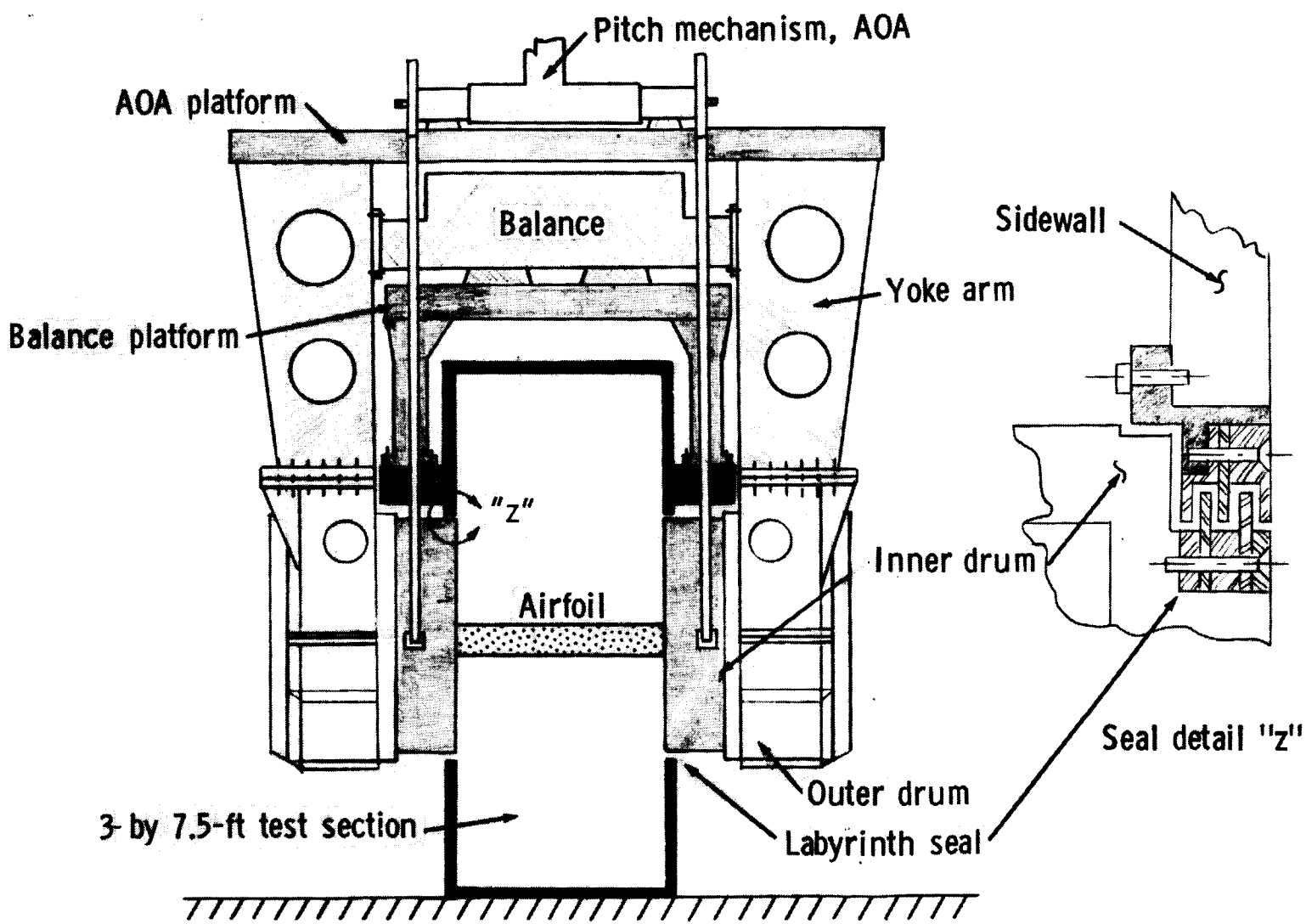

Figure 5. Model-support and force-balance system for the Langley LTPT. View looking upstream.

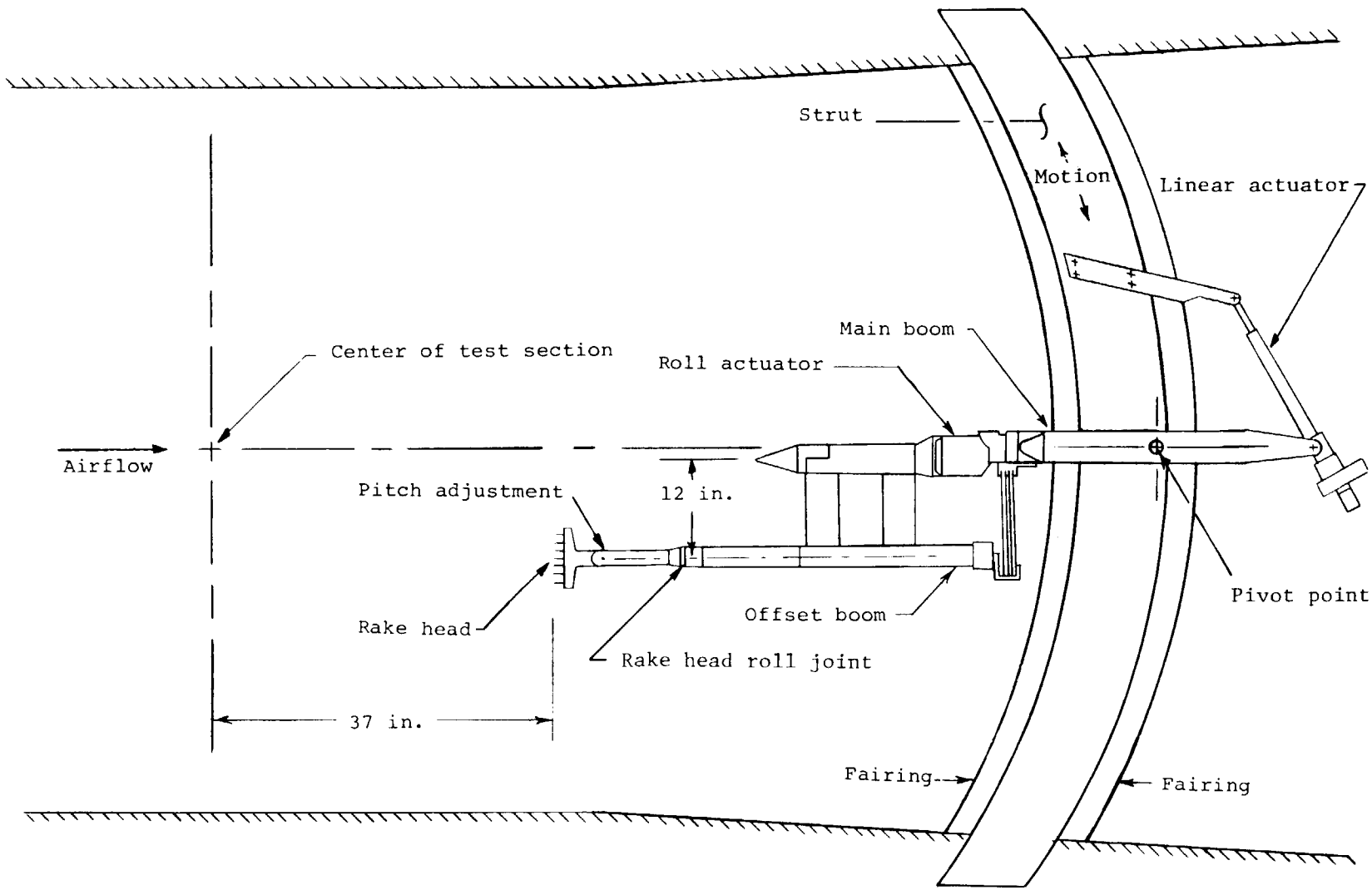

Figure 6. Sketch of remote-controlled survey apparatus for the Langley LTPT.

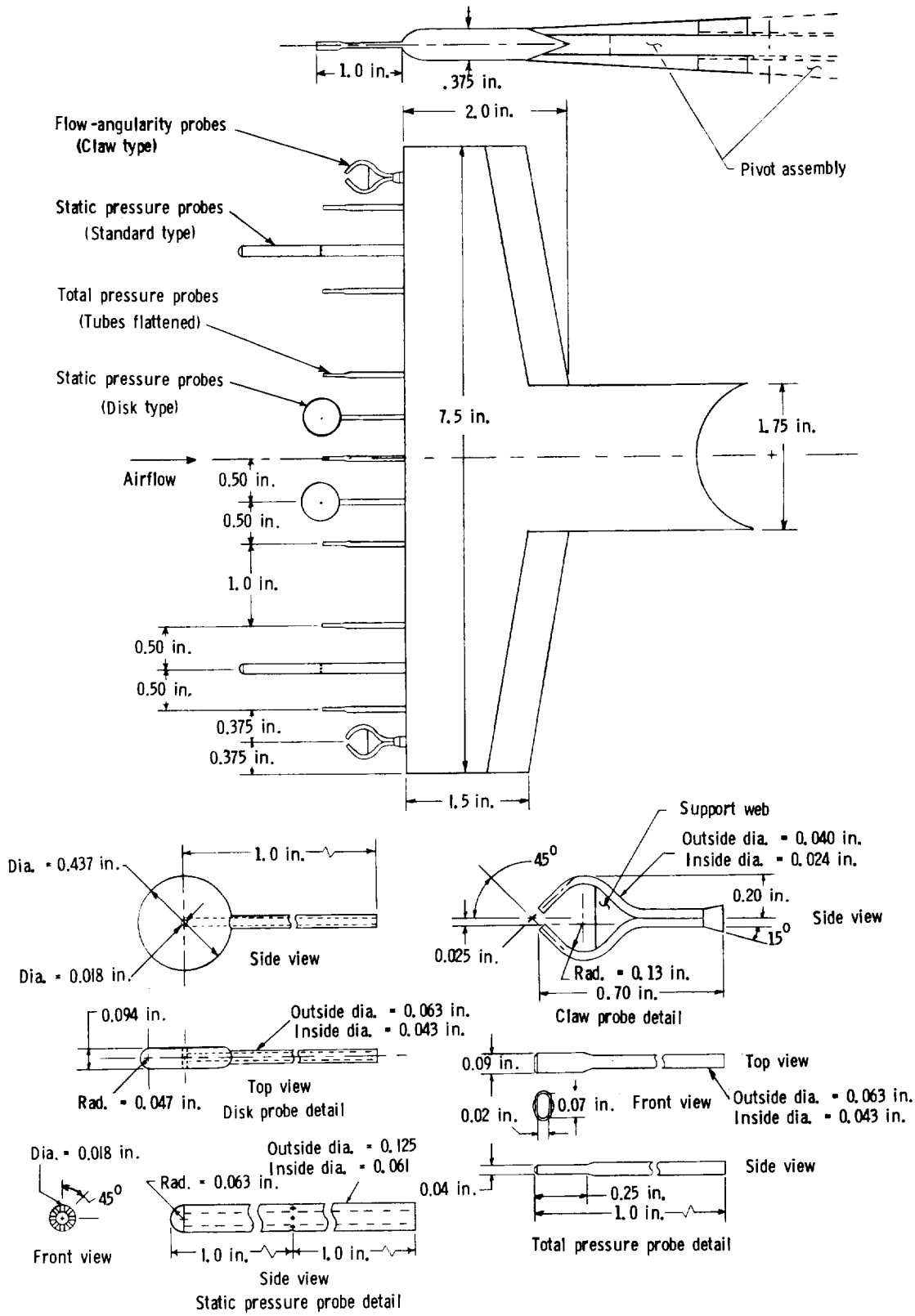

Figure 7. Details of wake-survey rake.

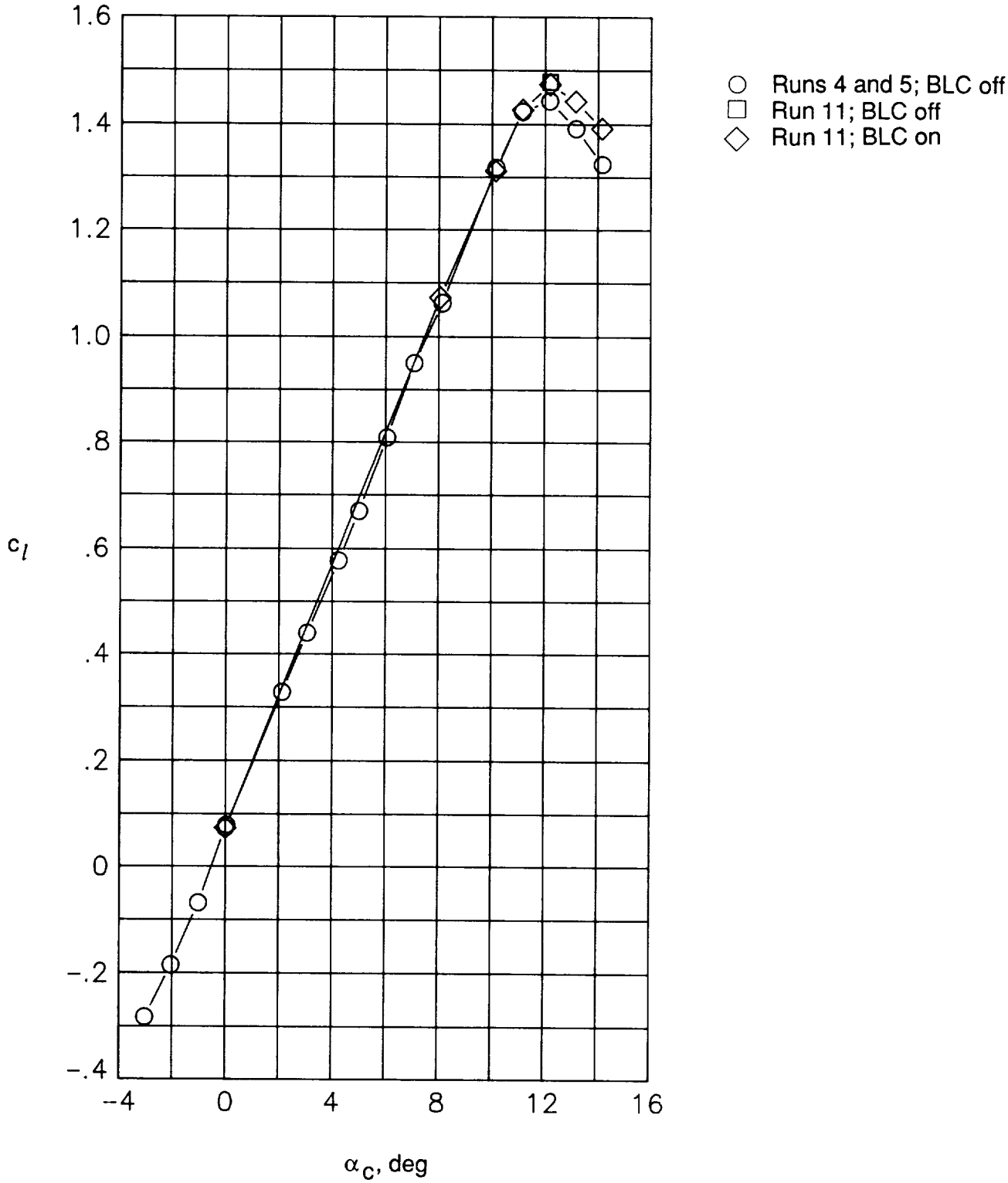

Figure 8. Effect of tunnel-wall boundary-layer control on lift characteristics of RC(4)-10 airfoil. $M = 0.39$; $R = 4.8 \times 10^6$; LTPT data.

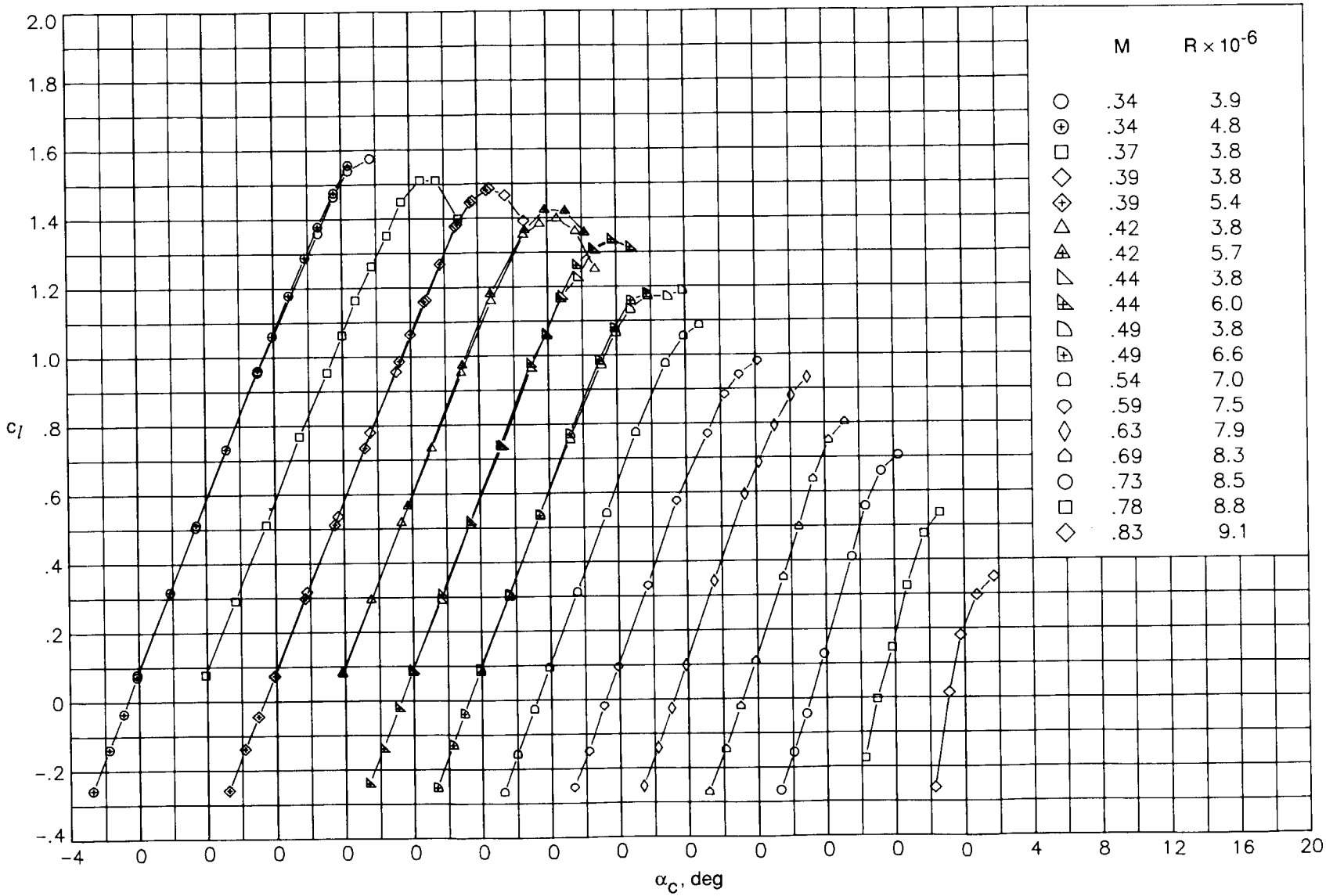

(a) Section lift coefficients.

Figure 9. Aerodynamic characteristics of RC(4)-10 airfoil measured in the Langley 6×28TT.

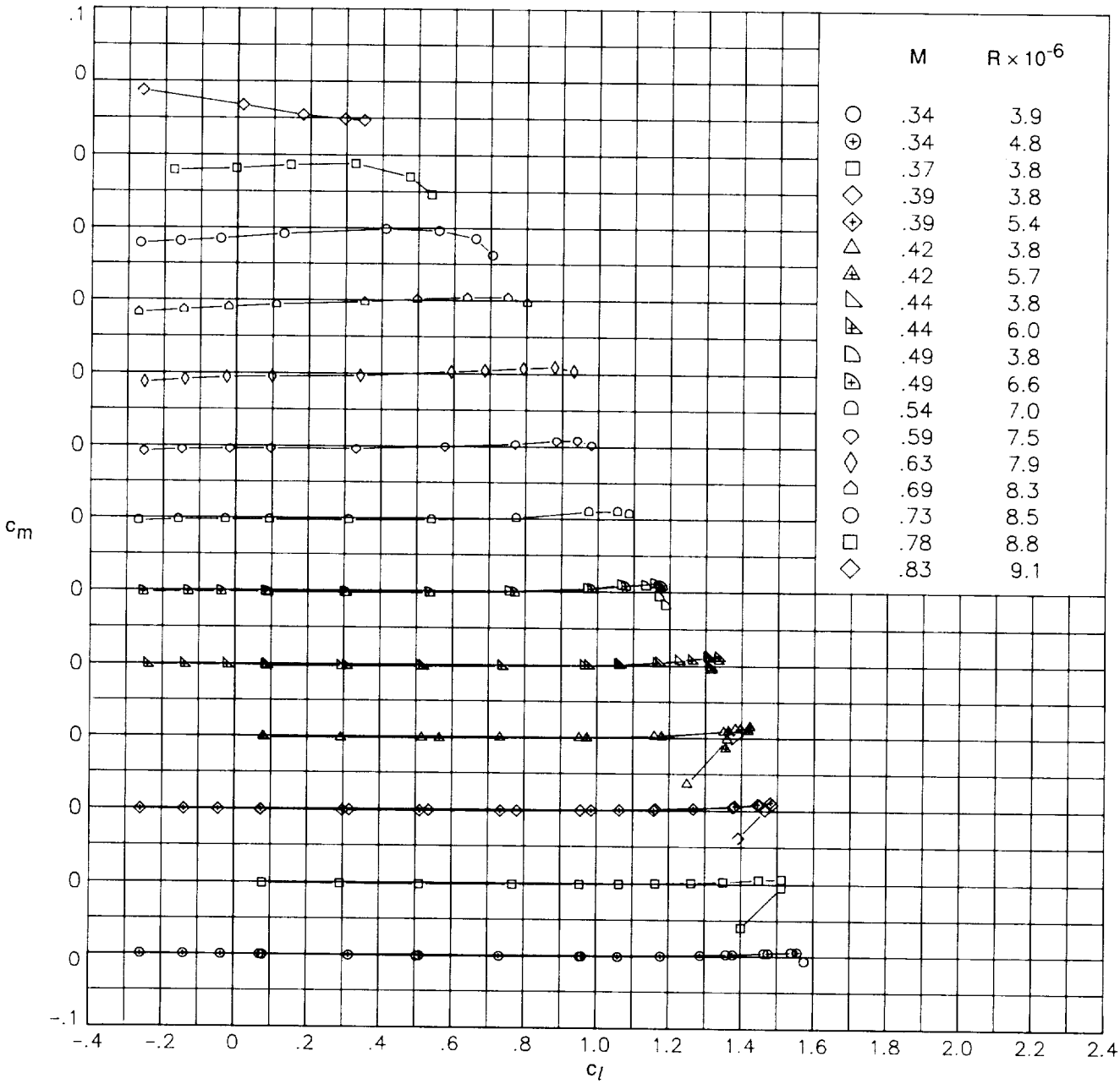

(b) Section pitching-moment coefficients.

Figure 9. Continued.

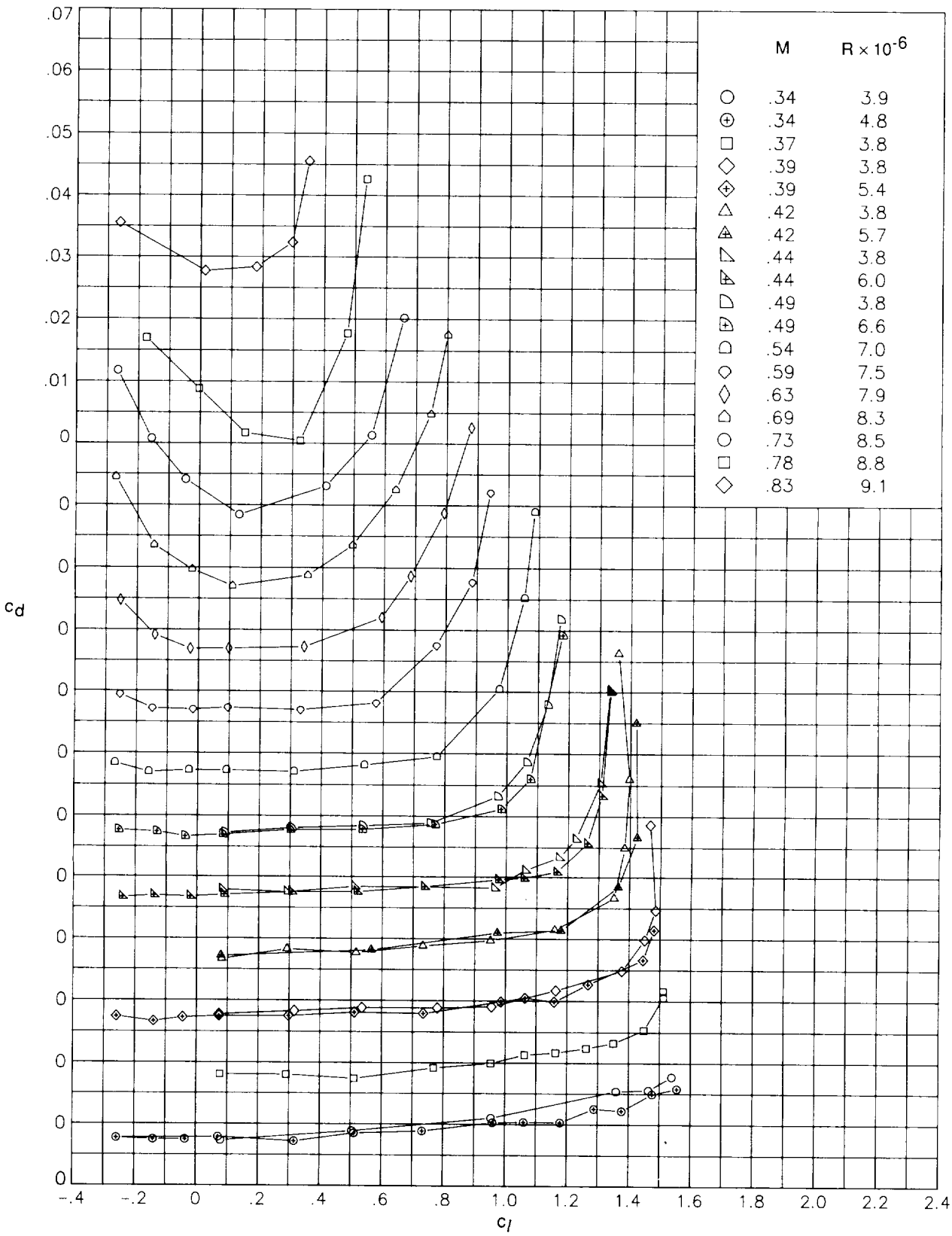

(c) Section drag coefficients.

Figure 9. Continued.

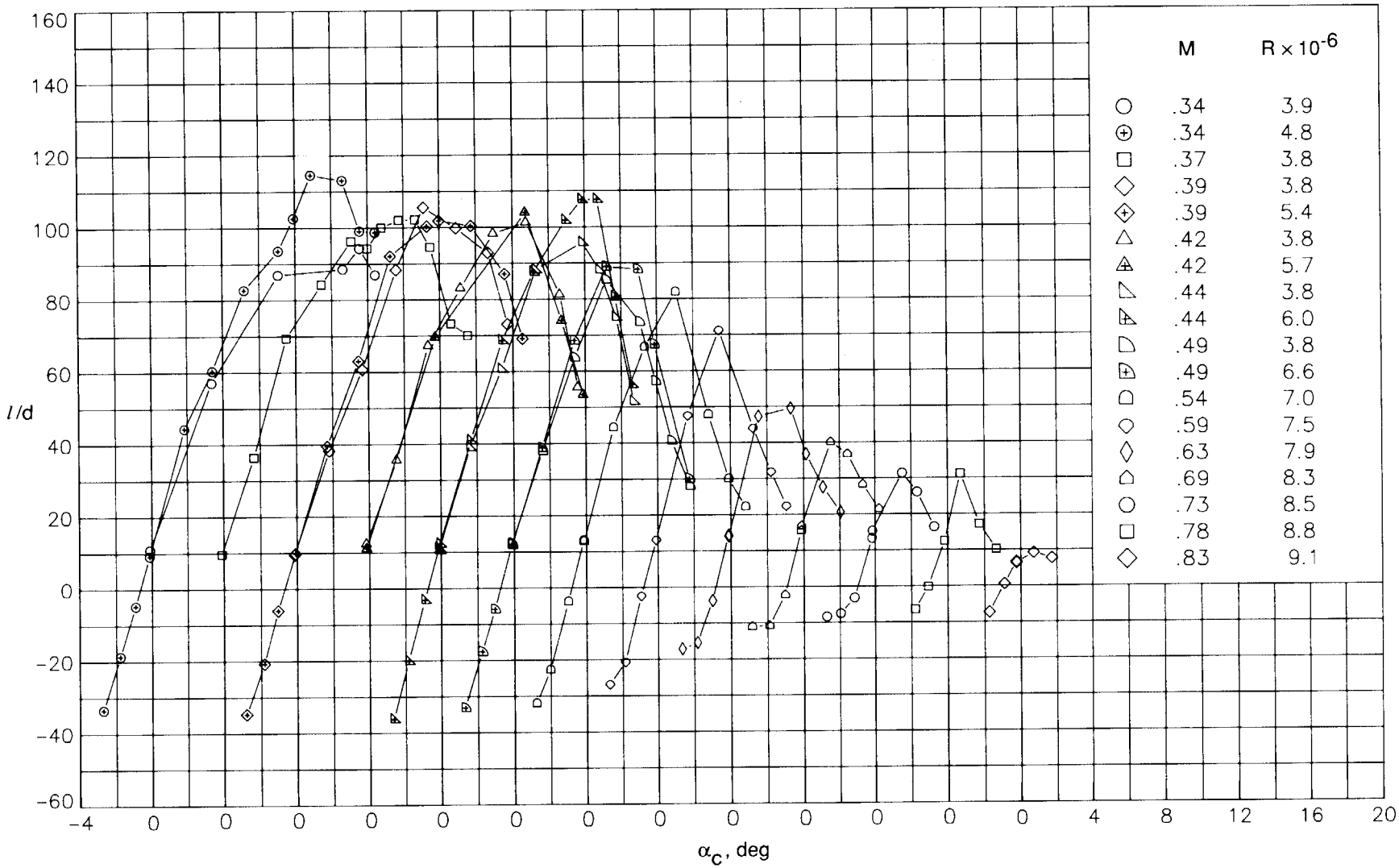

(d) Section lift-to-drag ratio.

Figure 9. Concluded.

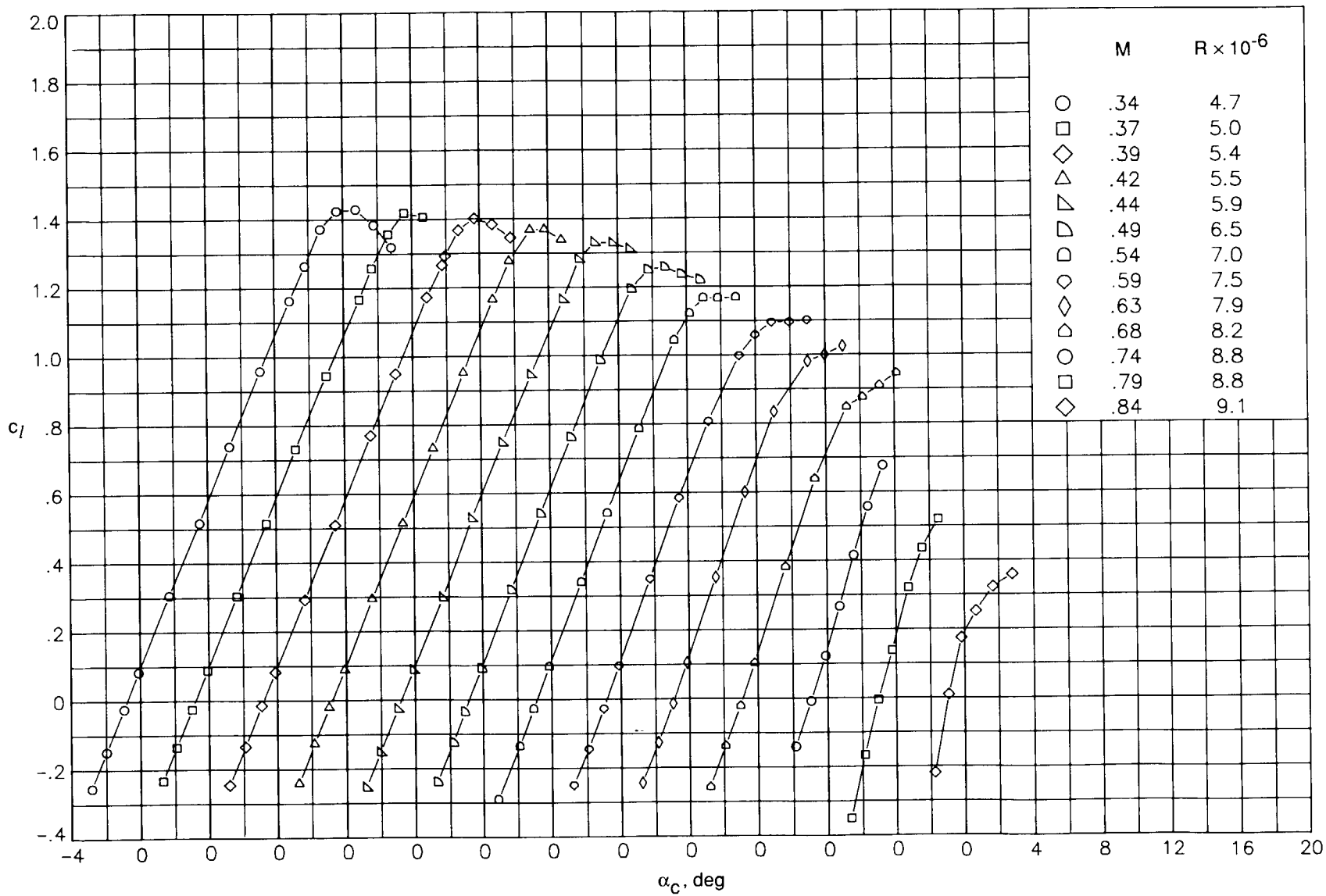

(a) Section lift coefficients.

Figure 10. Aerodynamic characteristics of RC(5)-10 airfoil measured in the Langley 6×28TT.

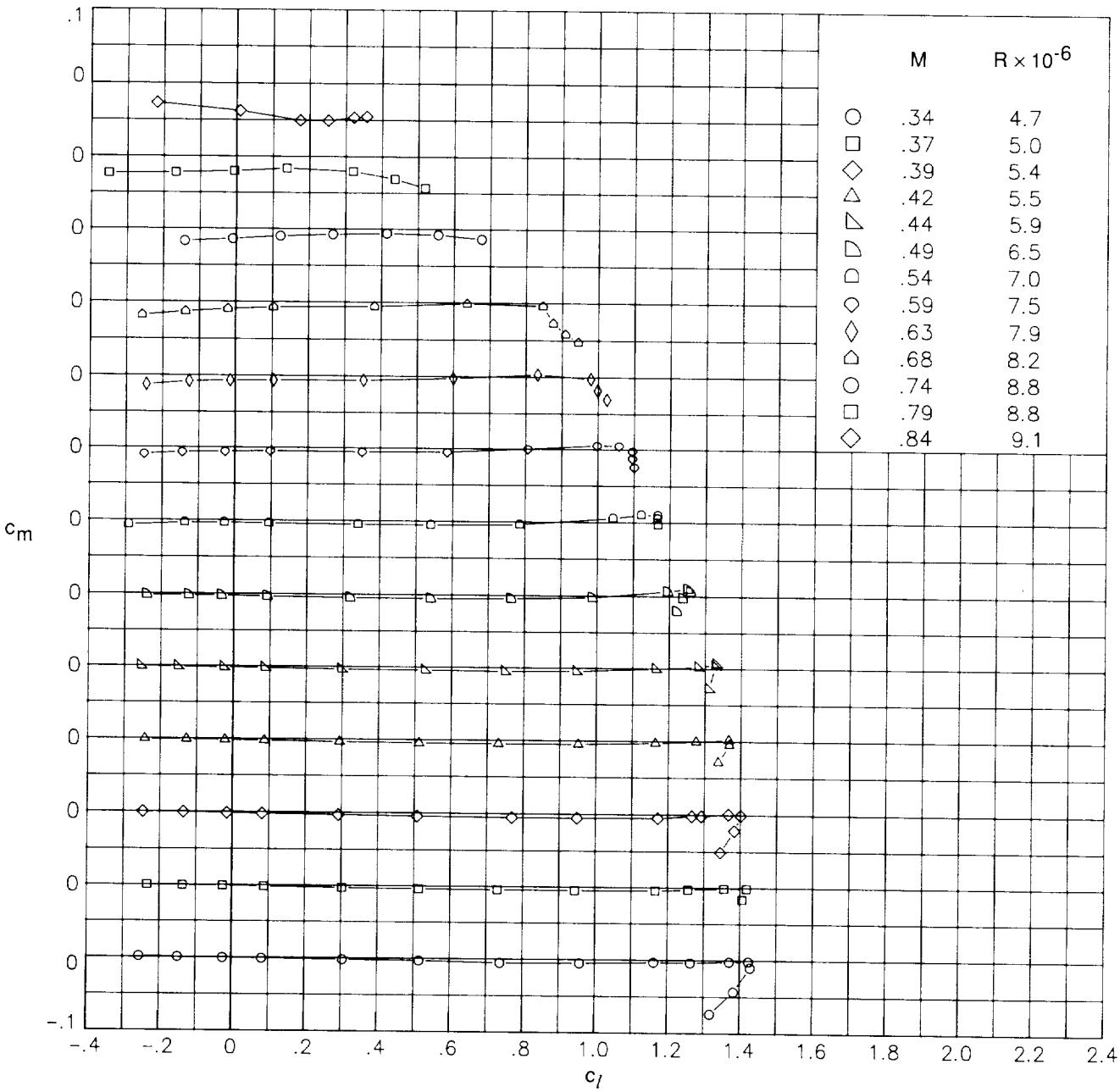

(b) Section pitching-moment coefficients.

Figure 10. Continued.

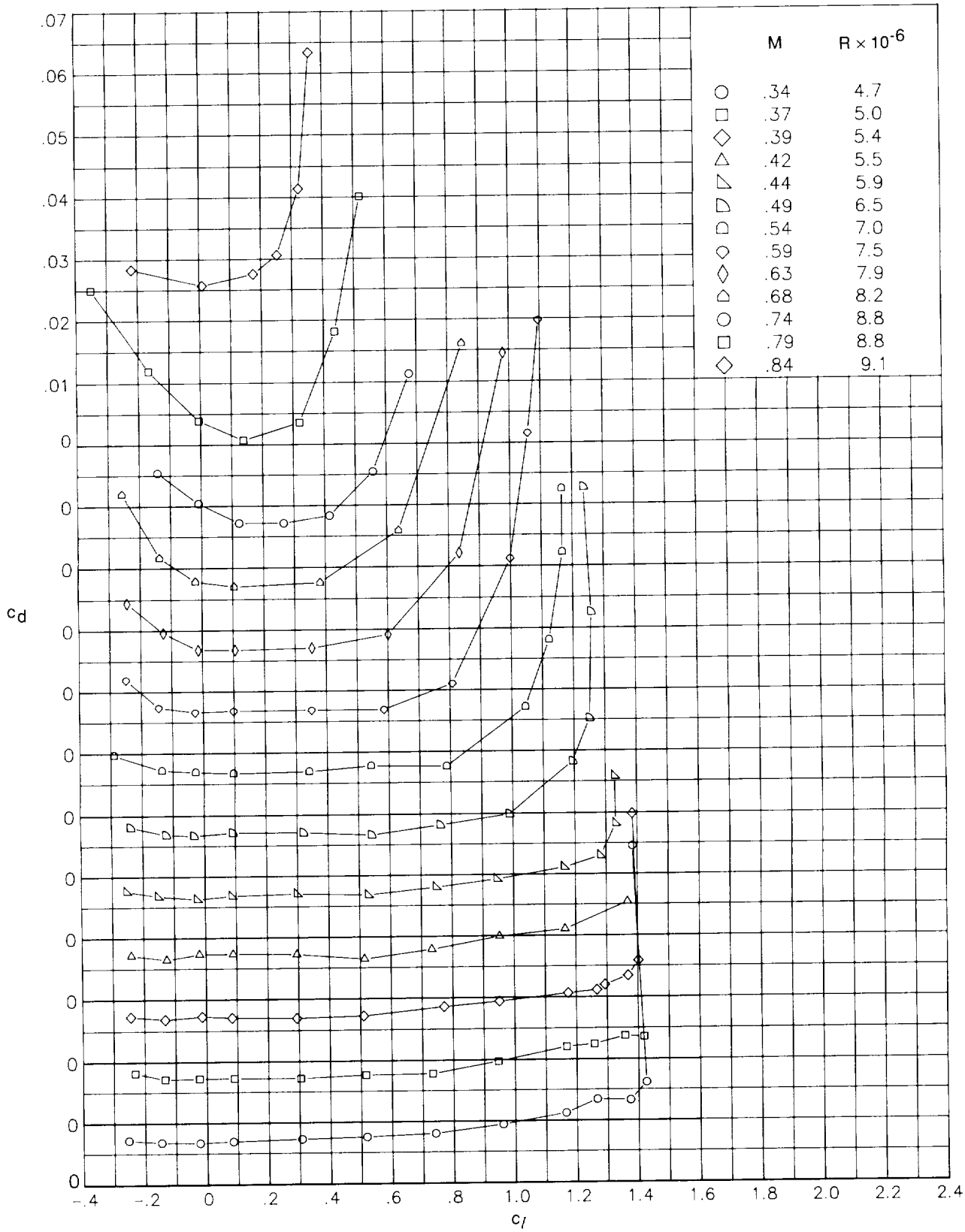

(c) Section drag coefficients.

Figure 10. Continued.

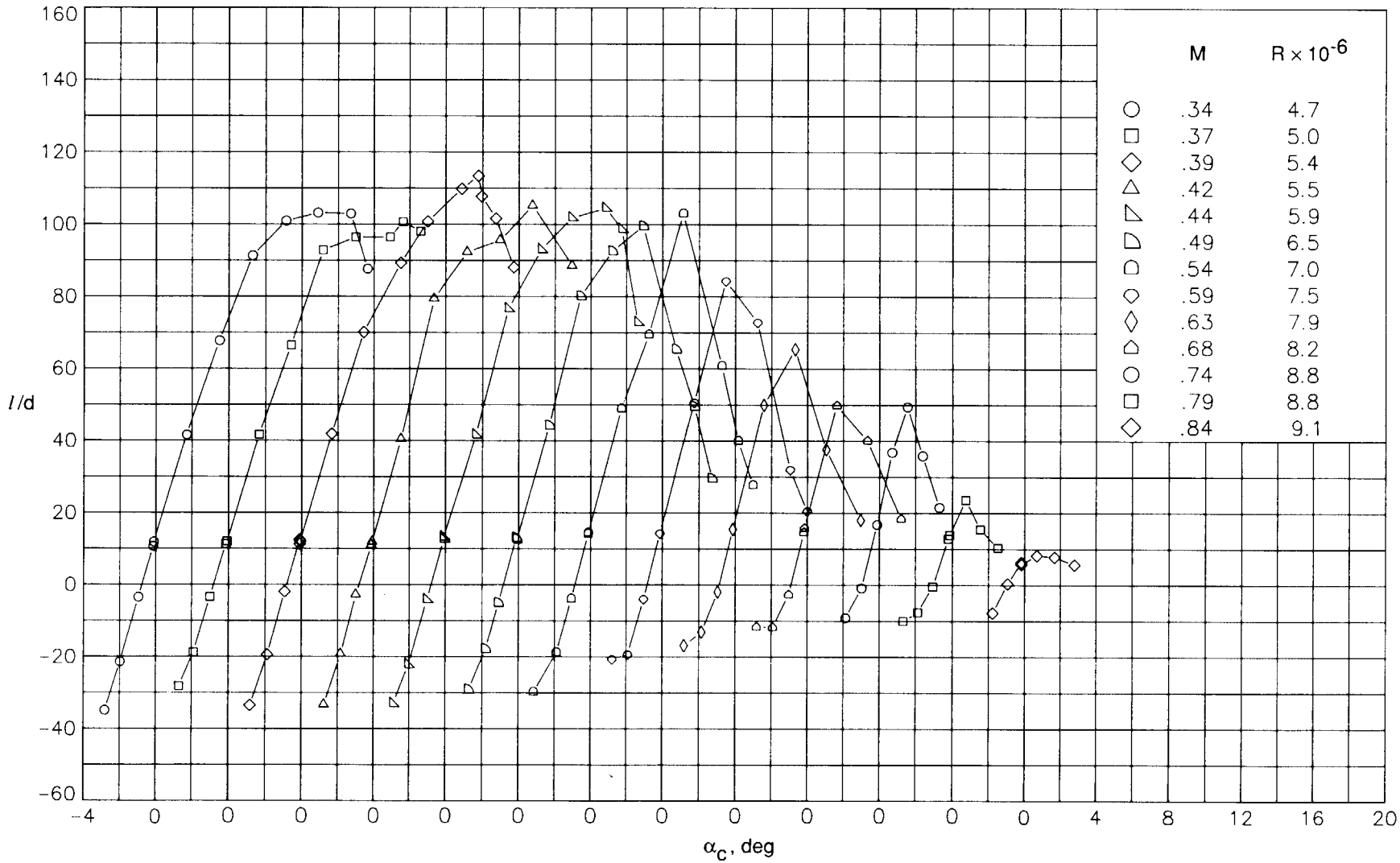

(d) Section lift-to-drag ratio.

Figure 10. Concluded.

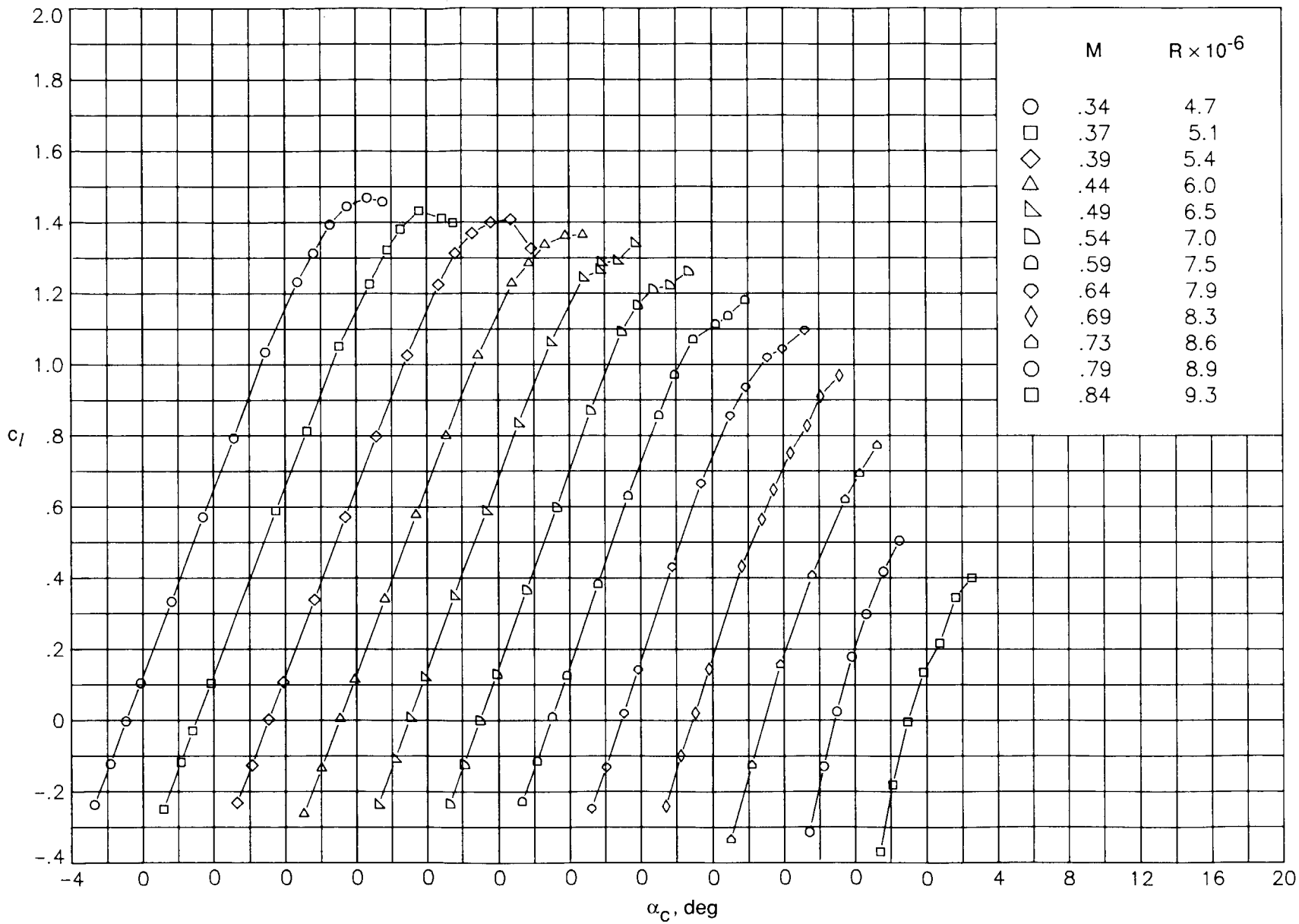

(a) Section lift coefficients.

Figure 11. Aerodynamic characteristics of VR-7 airfoil measured in the Langley 6×28TT.

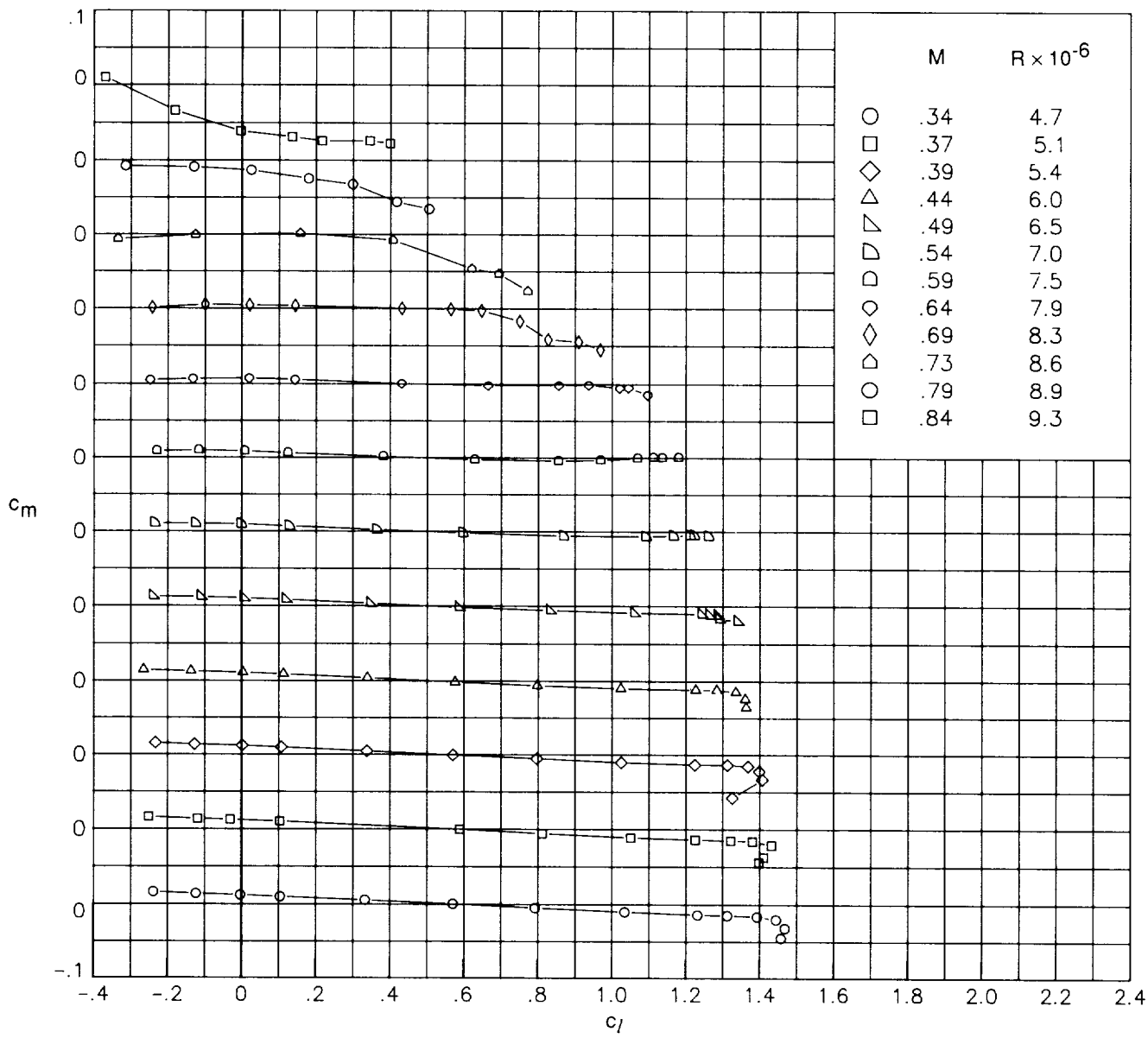

(b) Section pitching-moment coefficients.

Figure 11. Continued.

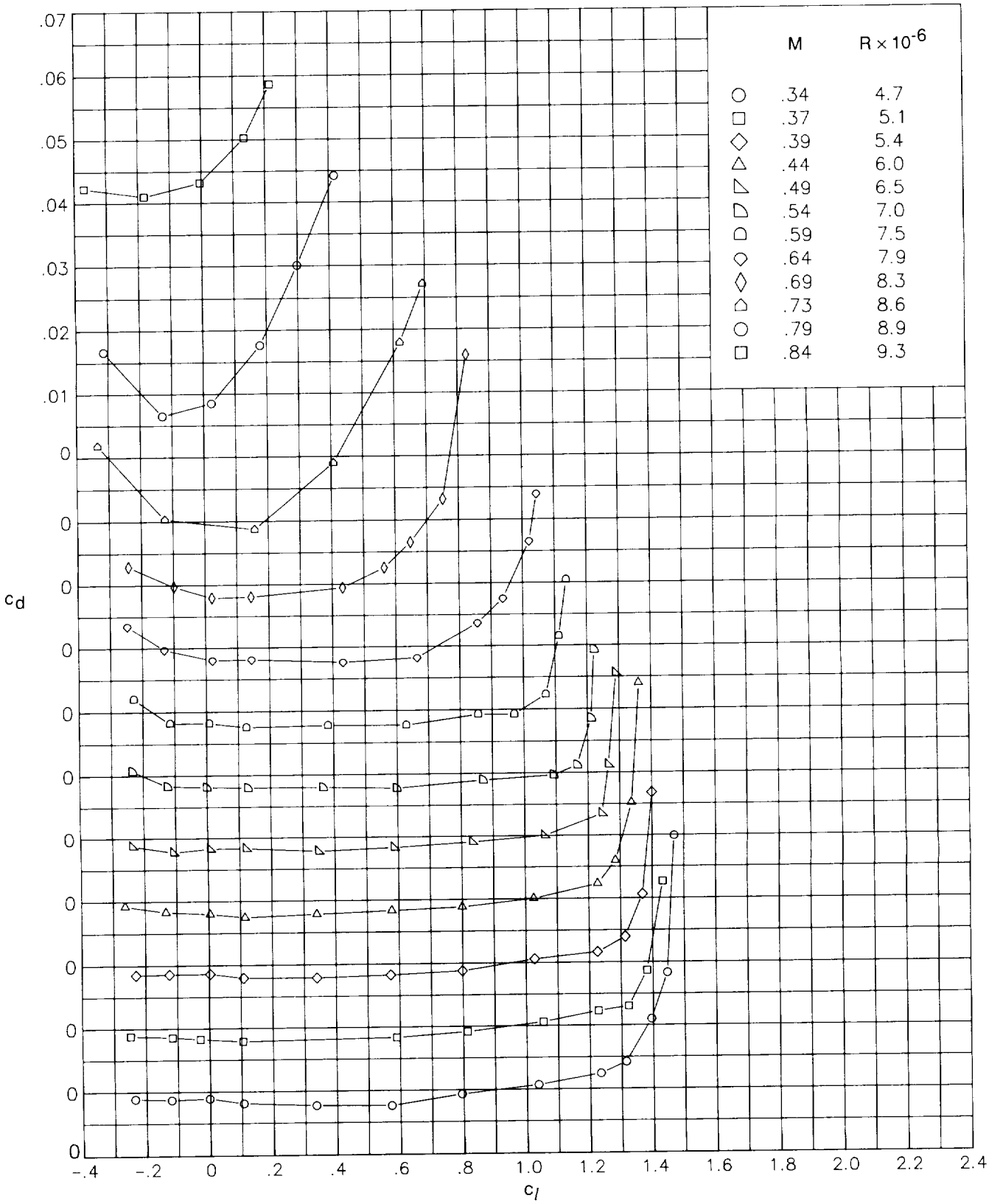

(c) Section drag coefficients.

Figure 11. Continued.

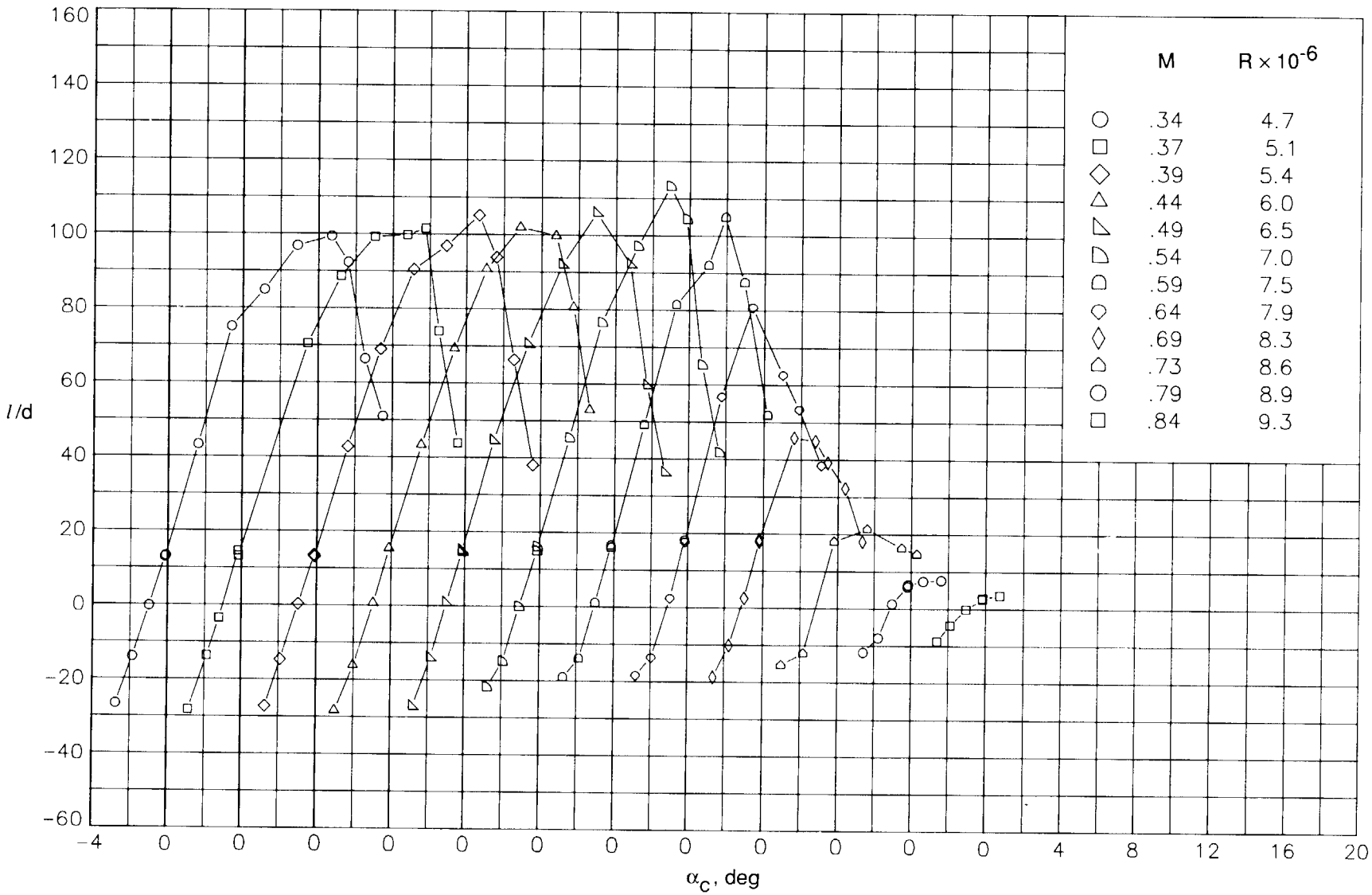

(d) Section lift-to-drag ratio.

Figure 11. Concluded.

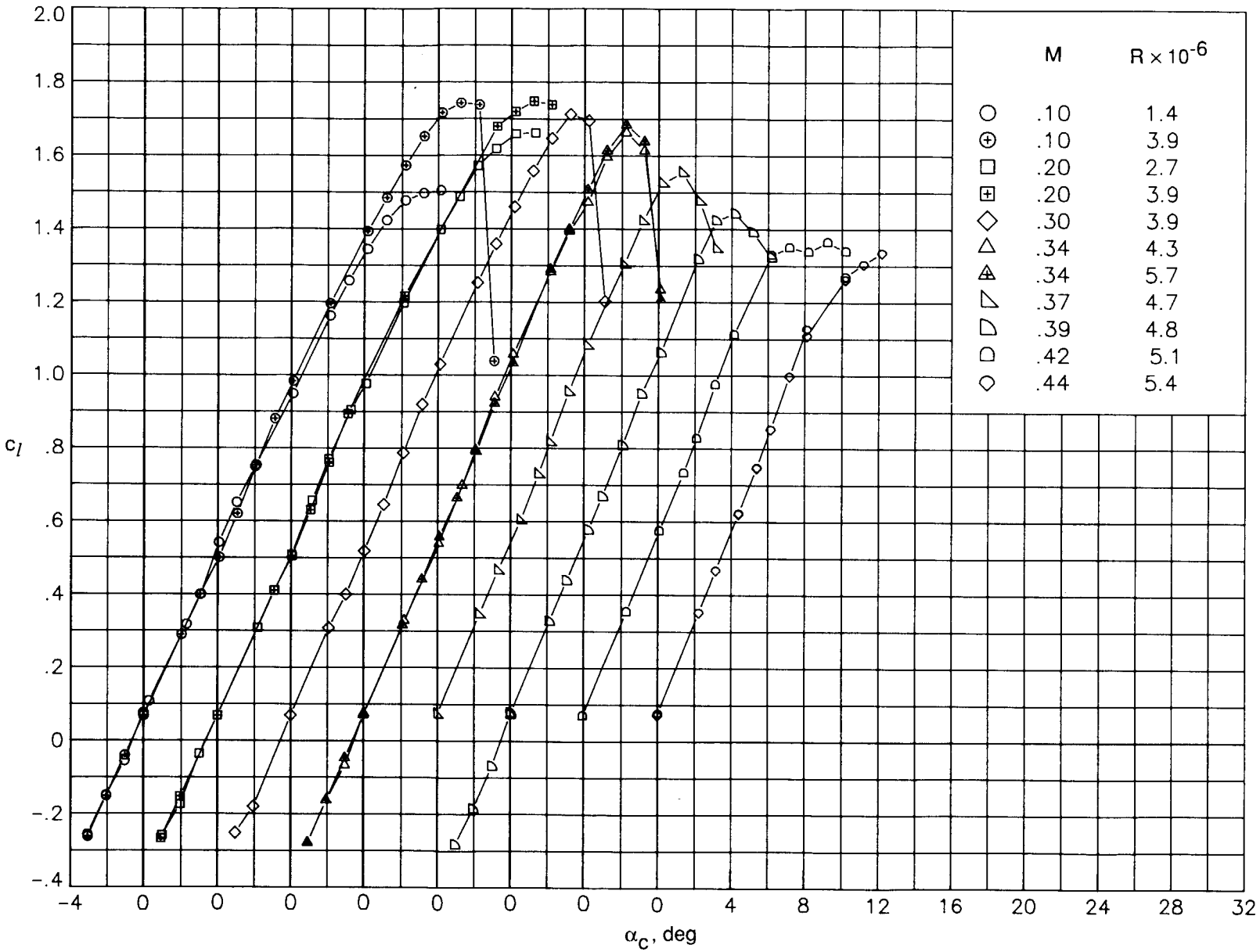

(a) Section lift coefficients.

Figure 12. Aerodynamic characteristics of RC(4)-10 airfoil measured in the Langley LTPT.

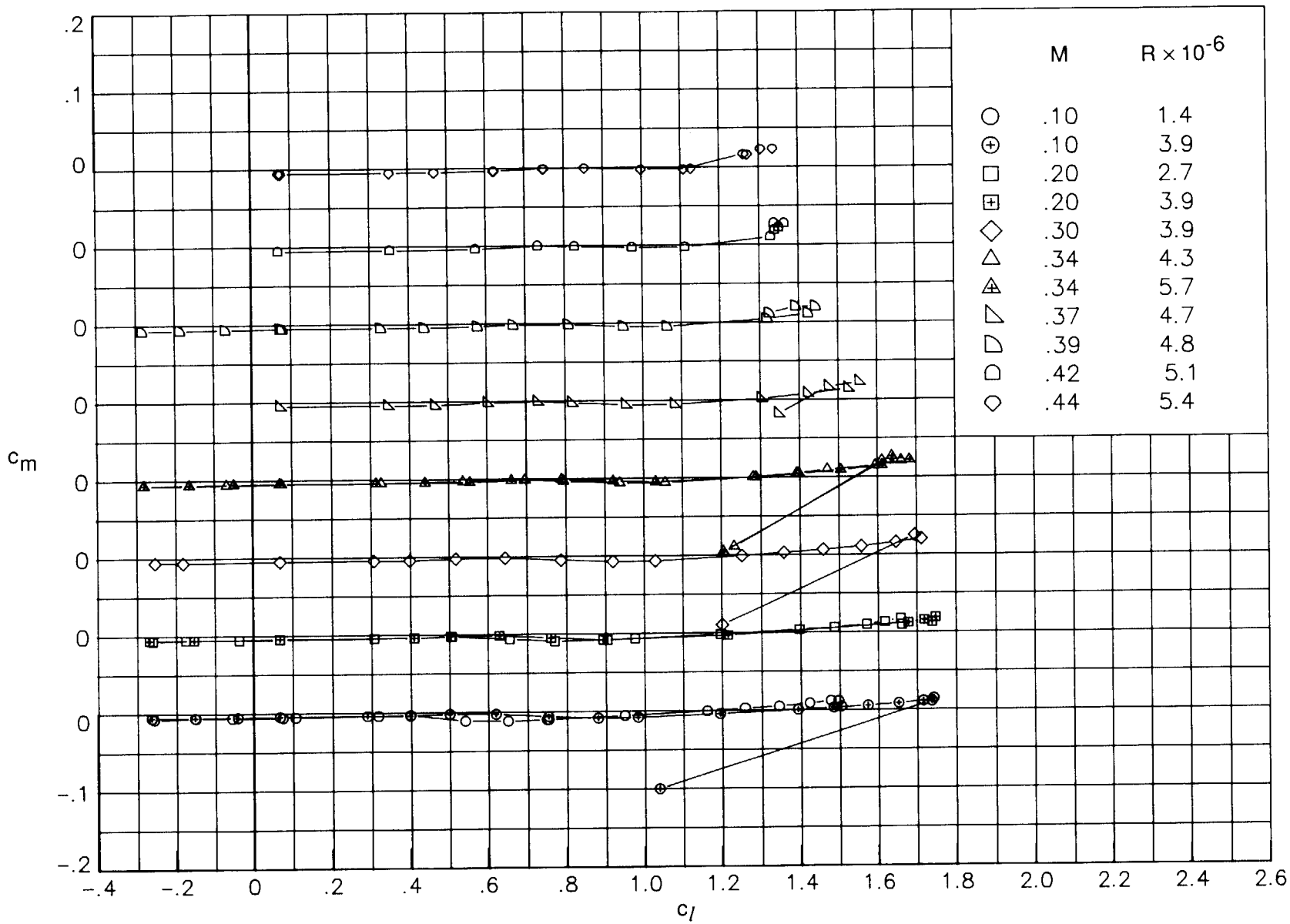

(b) Section pitching-moment coefficients.

Figure 12. Continued.

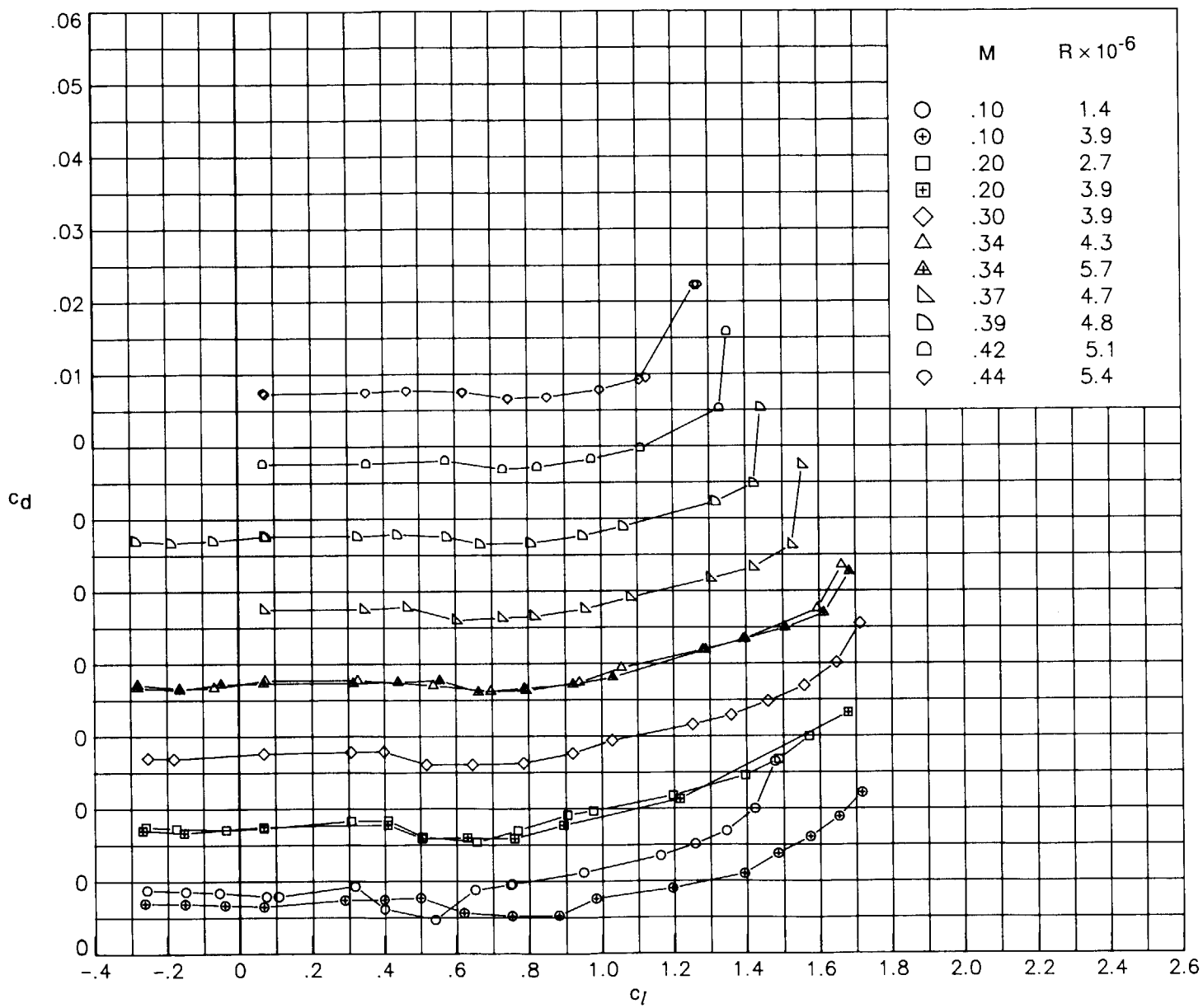

(c) Section drag coefficients.

Figure 12. Continued.

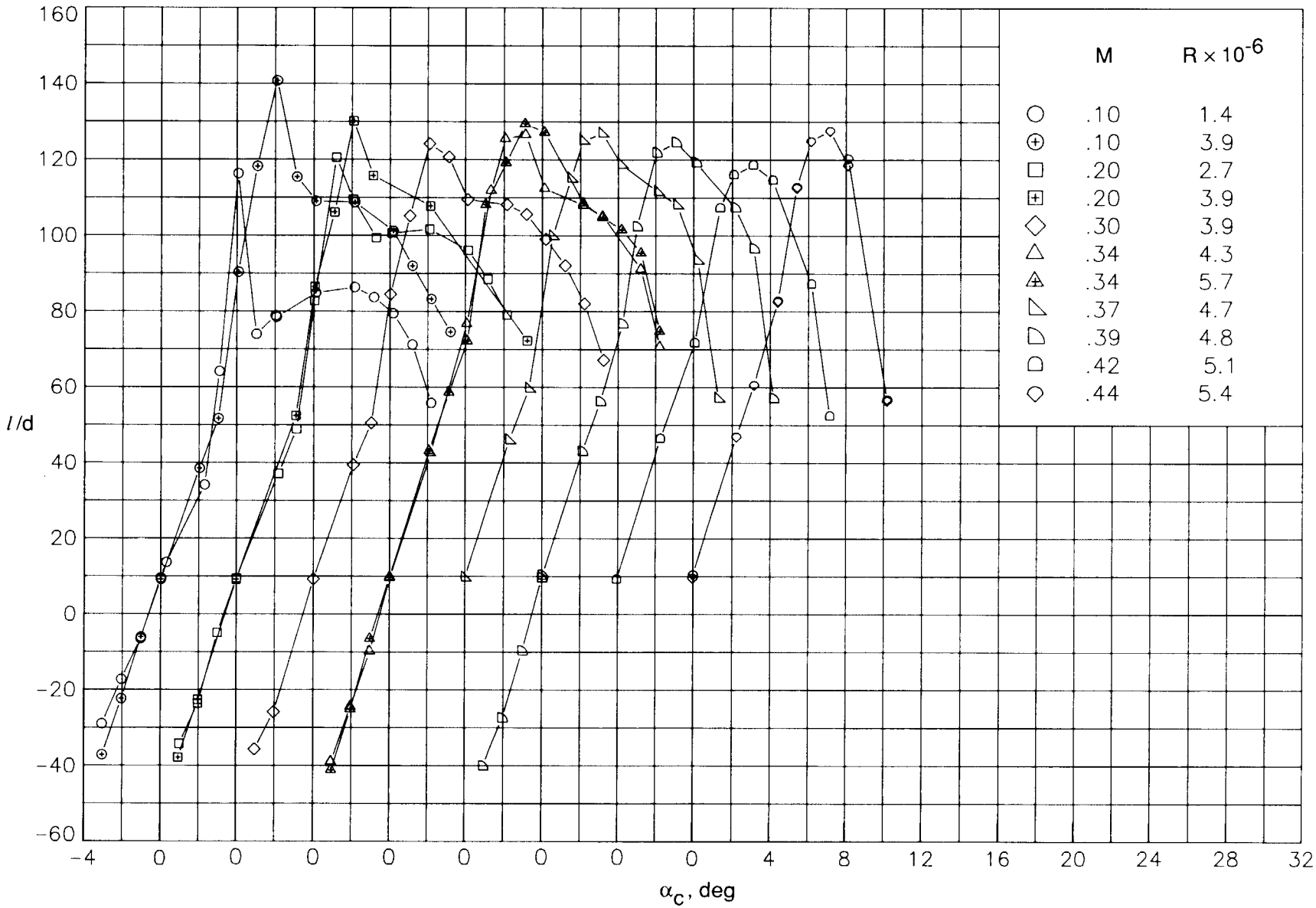

(d) Section lift-to-drag ratio.

Figure 12. Concluded.

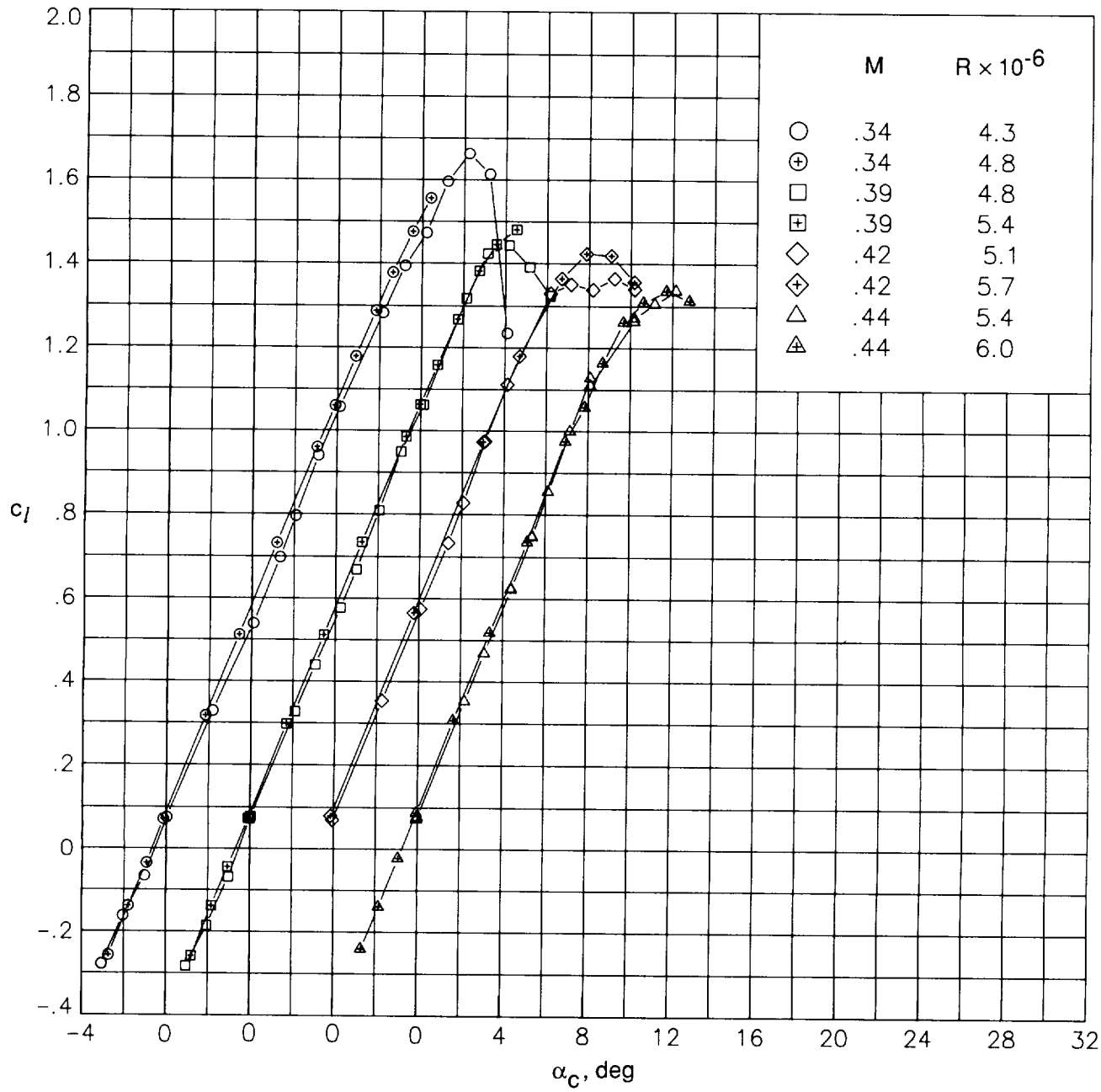

(a) Section lift coefficients.

Figure 13. Aerodynamic characteristics of RC(4)-10 airfoil measured in the Langley LTPT and 6×28TT. Open symbols indicate LTPT data and centered symbols indicate 6×28TT data.

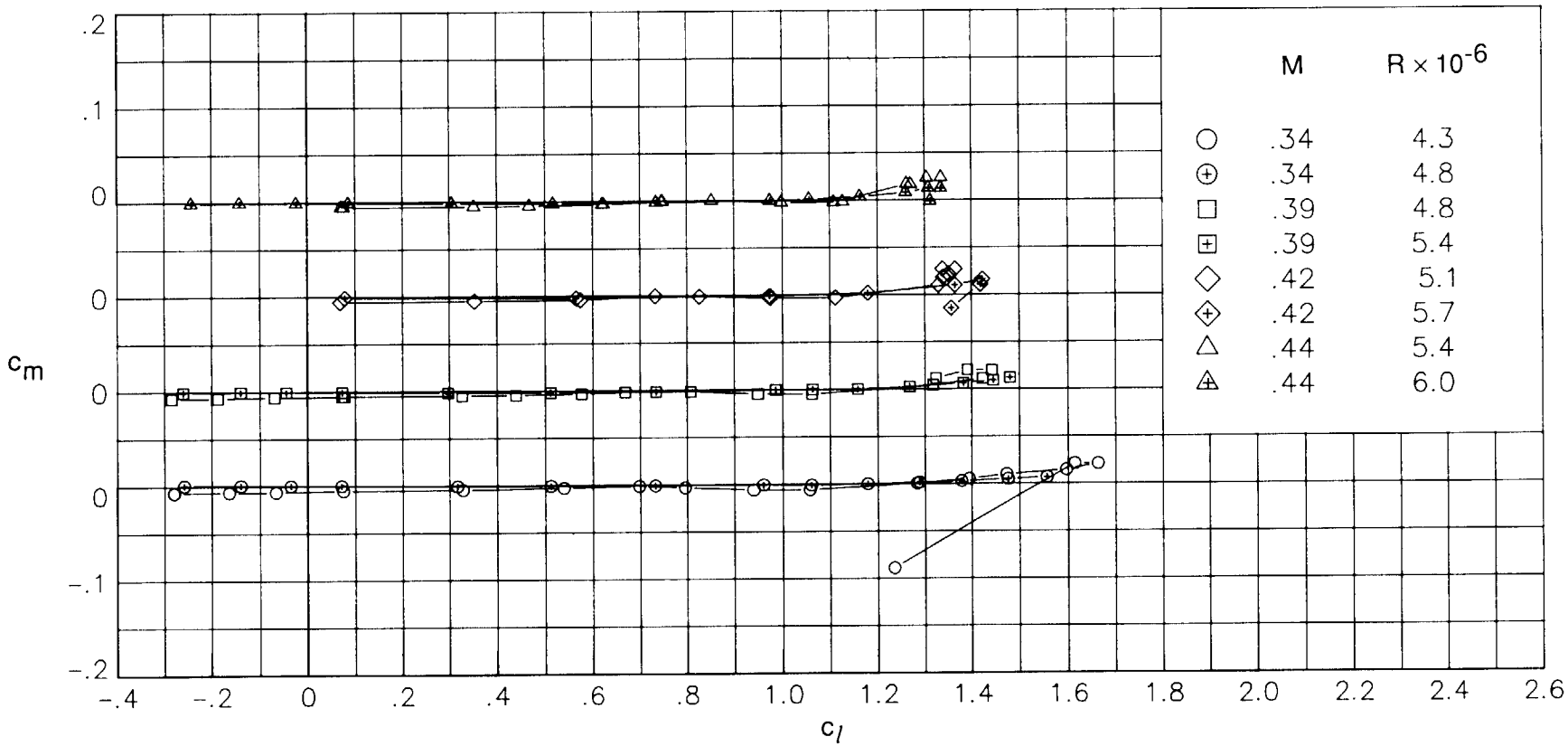

(b) Section pitching-moment coefficients.

Figure 13. Continued.

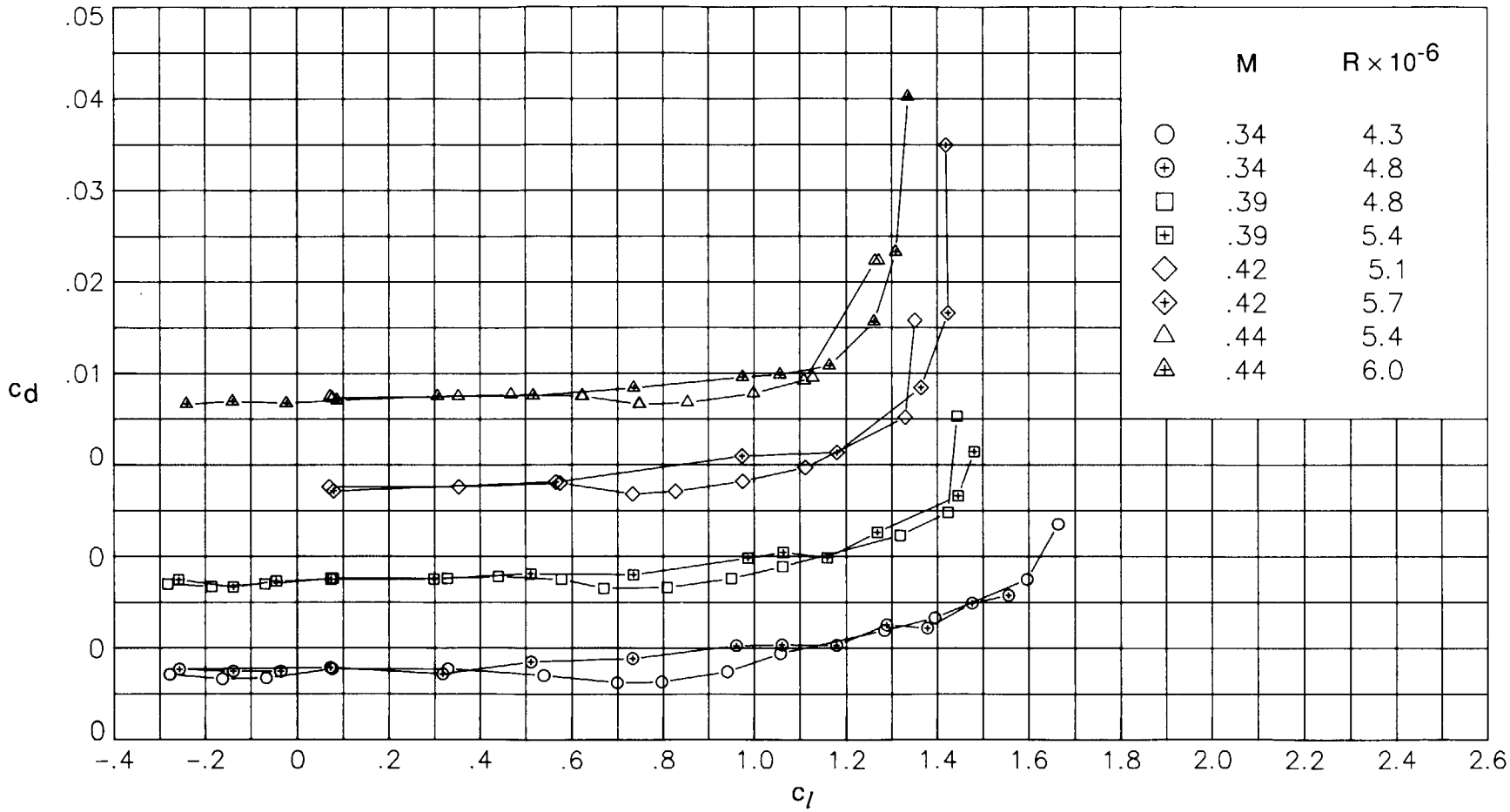

(c) Section drag coefficients.

Figure 13. Concluded.

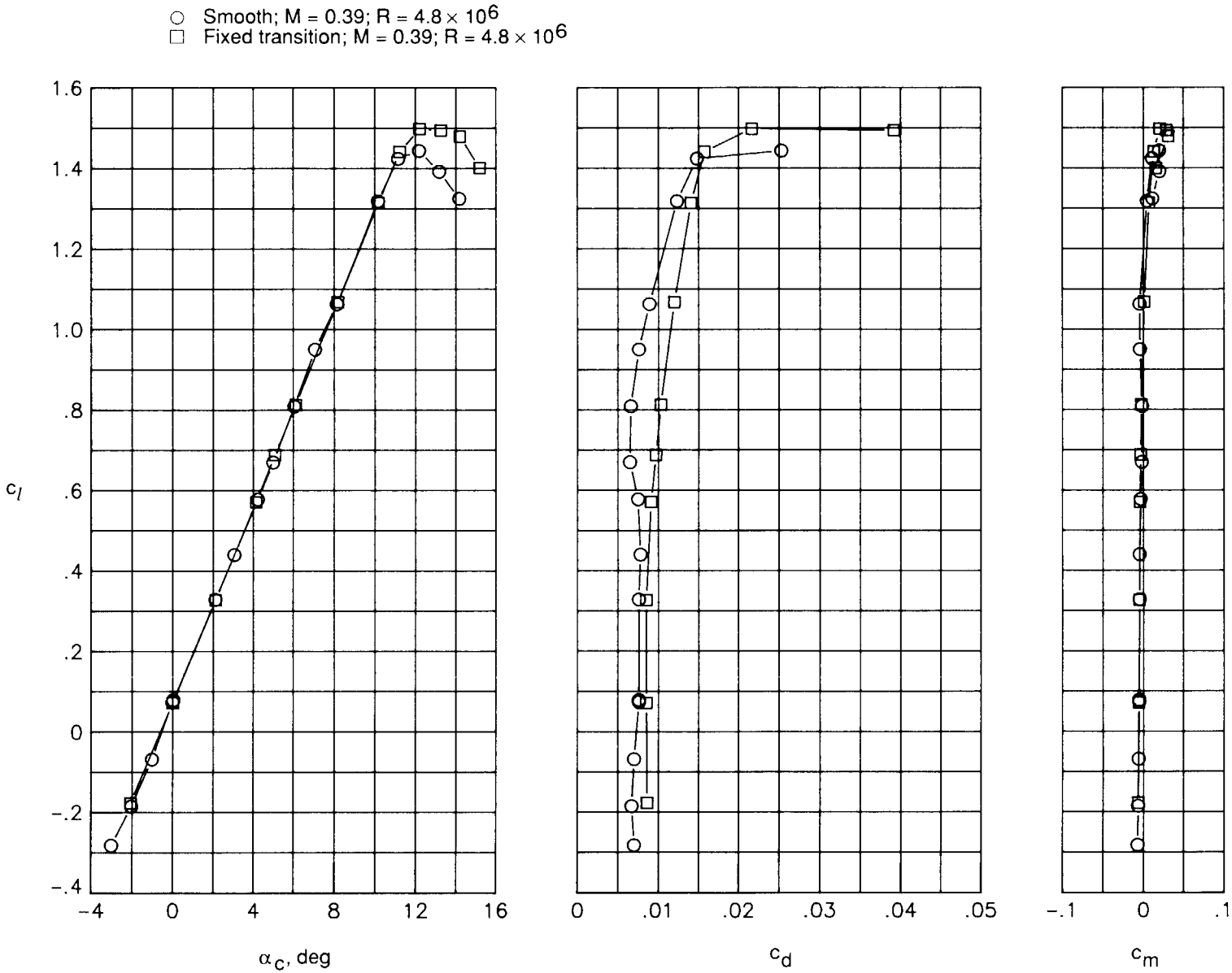

Figure 14. Effect of fixing transition on aerodynamic characteristics of RC(4)-10 airfoil measured in the Langley LTPT.

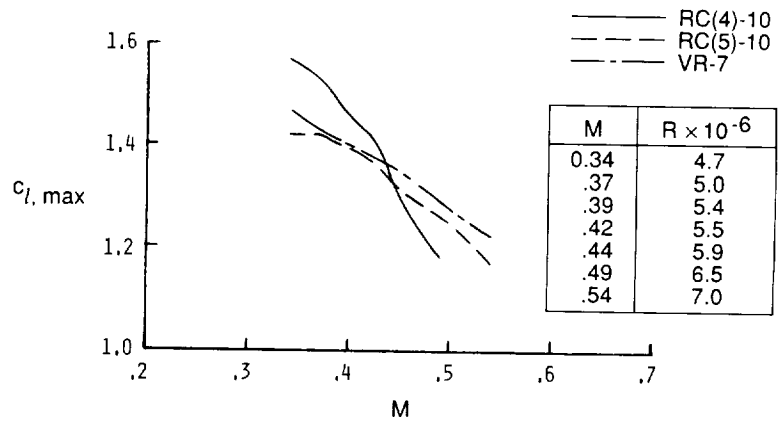

M	R × 10⁻⁶
0.34	4.7
.37	5.0
.39	5.4
.42	5.5
.44	5.9
.49	6.5
.54	7.0

Figure 15. Comparison of maximum lift coefficients of RC(4)-10, RC(5)-10, and VR-7 airfoils in the Langley 6×28TT.

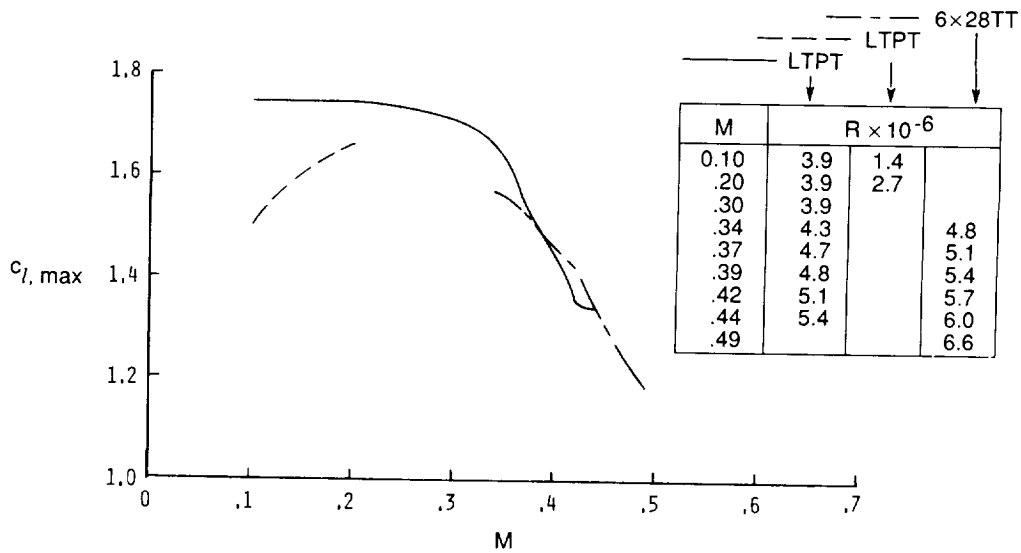

M	R × 10⁻⁶		
0.10	3.9	1.4	
.20	3.9	2.7	
.30	3.9		
.34	4.3		4.8
.37	4.7		5.1
.39	4.8		5.4
.42	5.1		5.7
.44	5.4		6.0
.49			6.6

Figure 16. Maximum lift coefficients of RC(4)-10 airfoil measured in the Langley LTPT and 6×28TT.

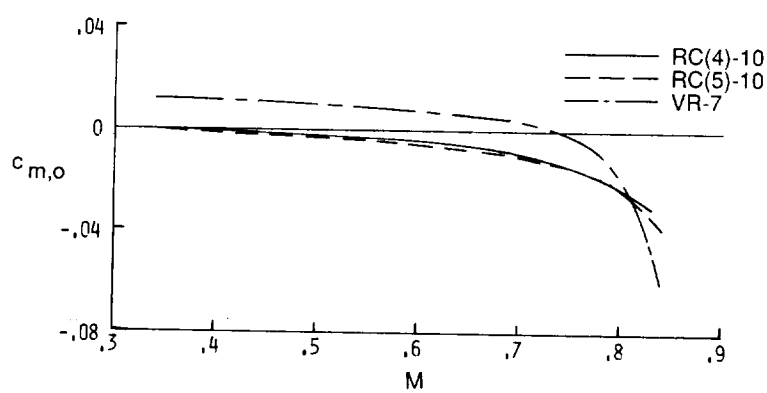

Figure 17. Comparison of pitching-moment coefficients at zero lift coefficient of RC(4)-10, RC(5)-10, and VR-7 airfoils in the Langley 6×28TT.

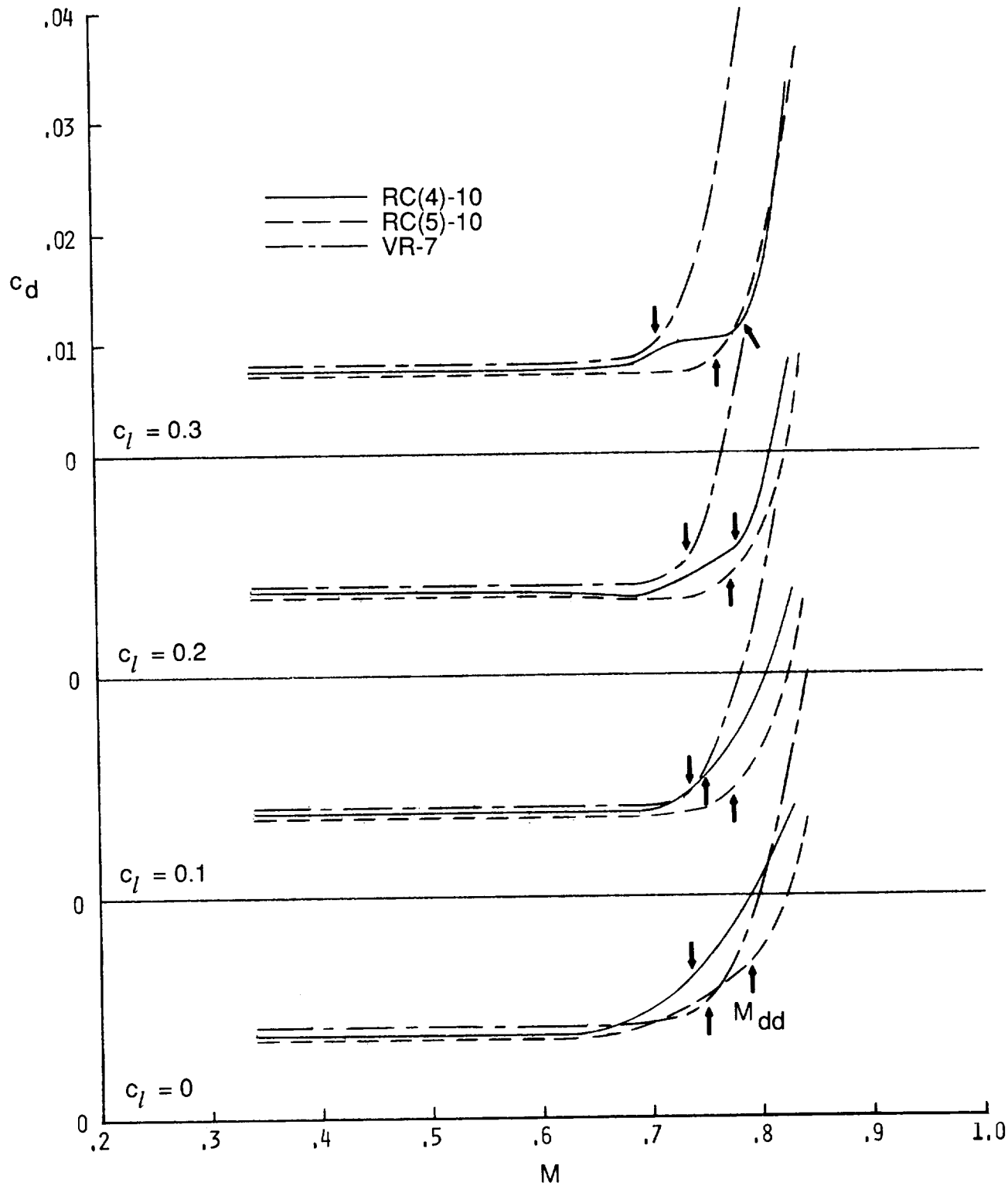

Figure 18. Comparison of drag-divergence characteristics of RC(4)-10, RC(5)-10, and VR-7 airfoils measured in the Langley 6×28TT.

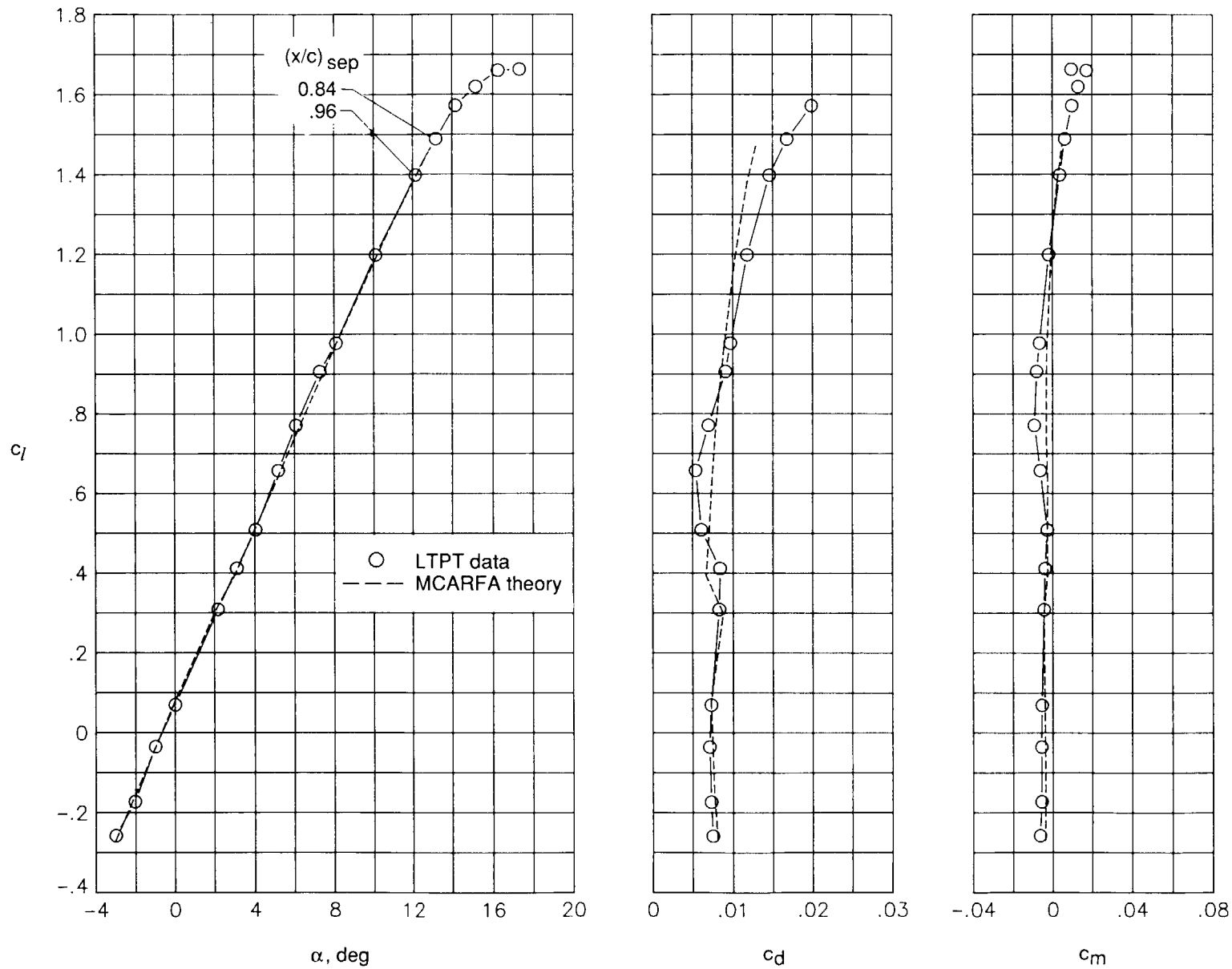

(a) $M = 0.20; R = 2.7 \times 10^6$.

Figure 19. Comparison of RC(4)-10 airfoil data measured in the Langley LTPT with theory.

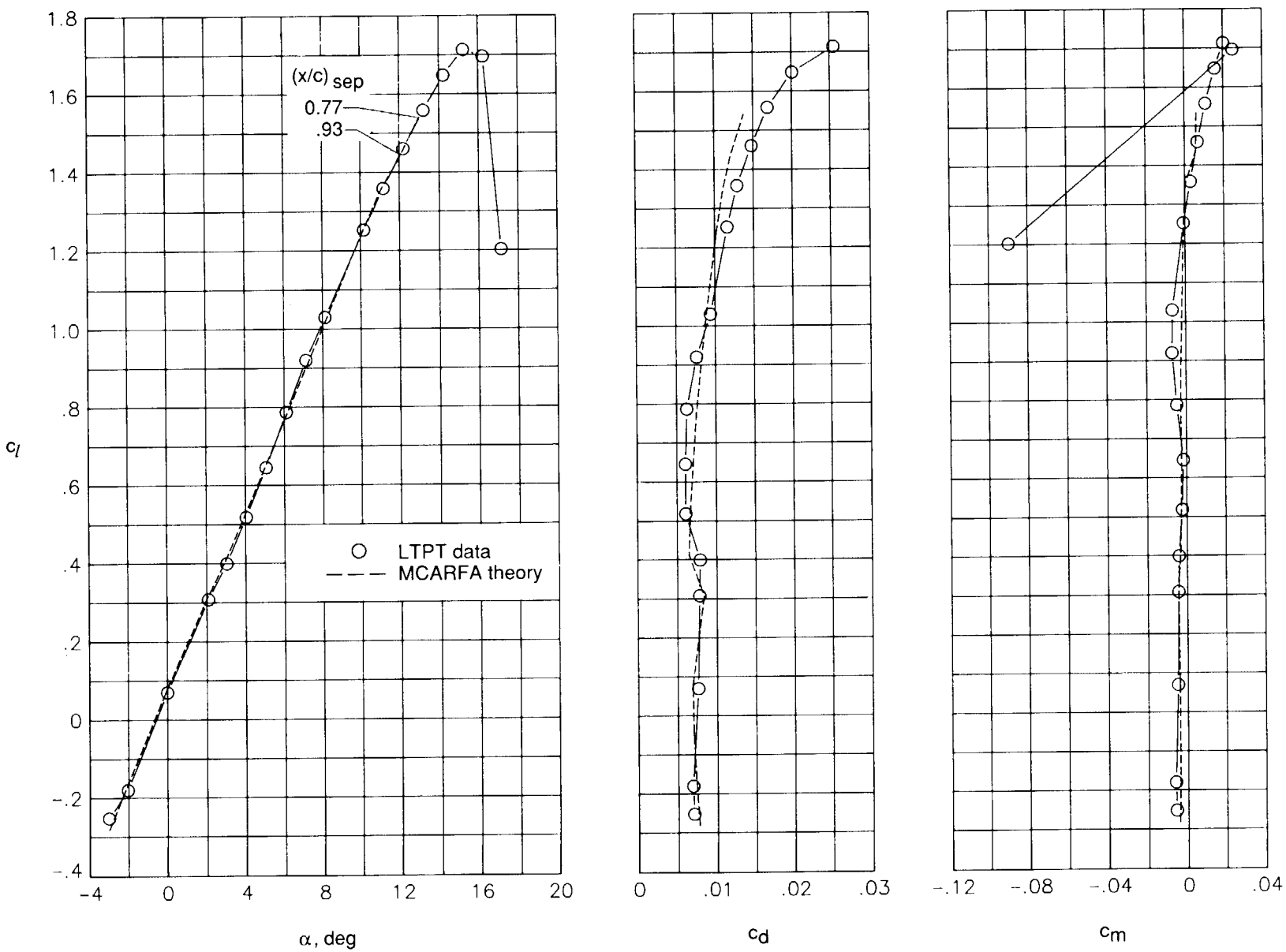

(b) $M = 0.30; R = 3.9 \times 10^6$.

Figure 19. Continued.

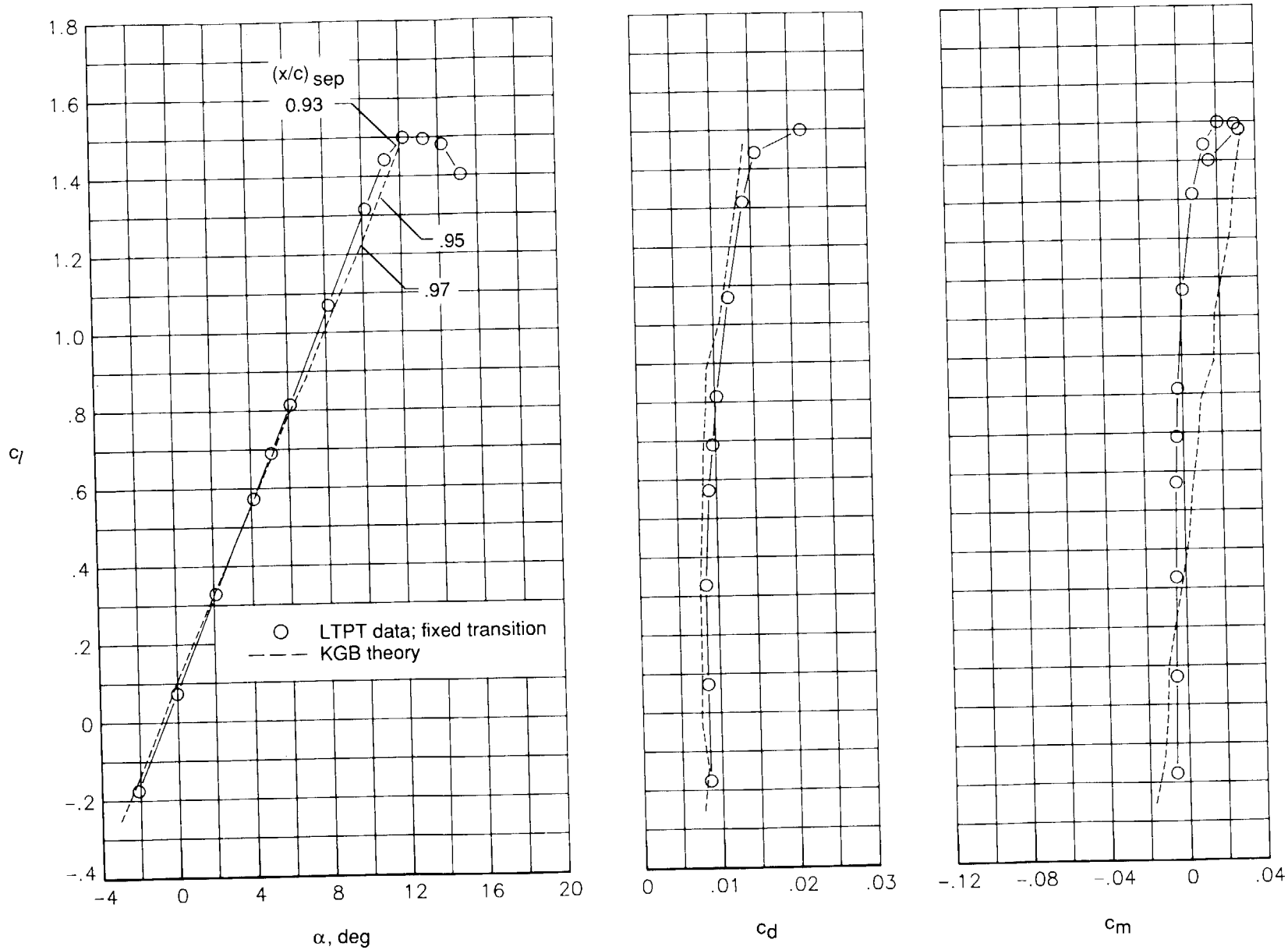

(c) $M = 0.39; R = 4.8 \times 10^6$.

Figure 19. Concluded.

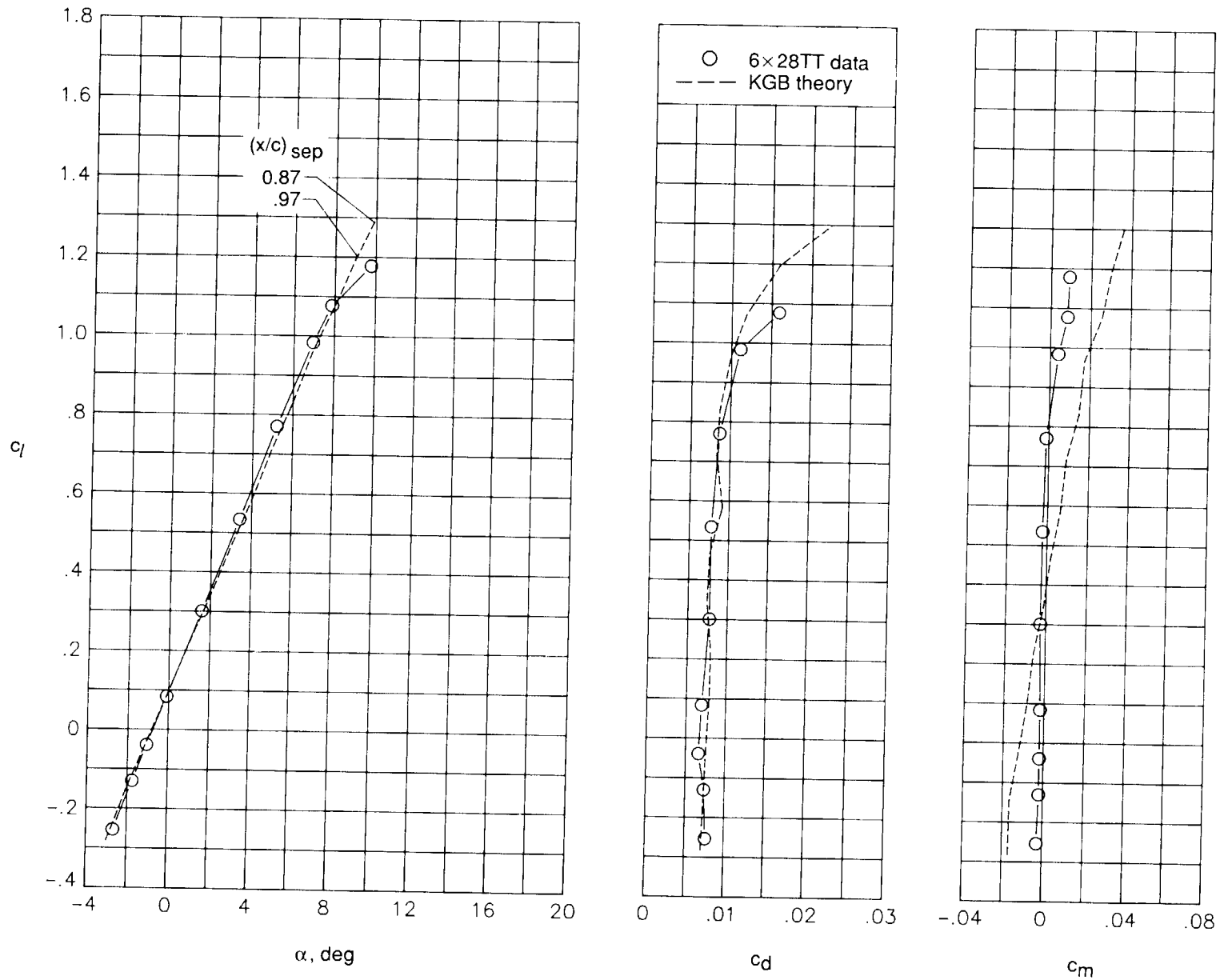

Figure 20. Comparison of RC(4)-10 airfoil data measured in the Langley 6 × 28TT with theory. $M = 0.49$; $R = 6.6 \times 10^6$.

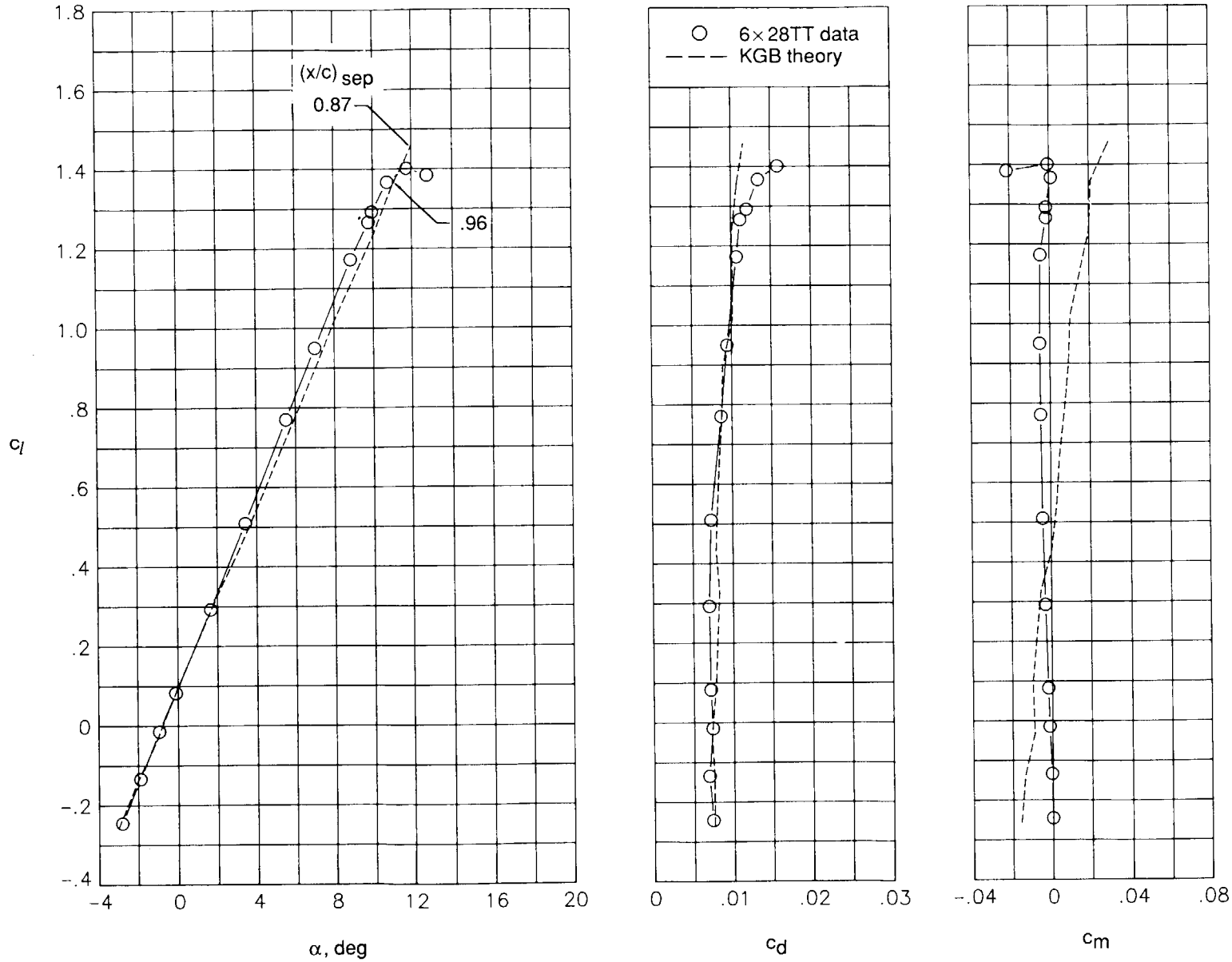

(a) $M = 0.39; R = 5.4 \times 10^6$.

Figure 21. Comparison of RC(5)-10 airfoil data measured in the Langley 6×28TT with theory.

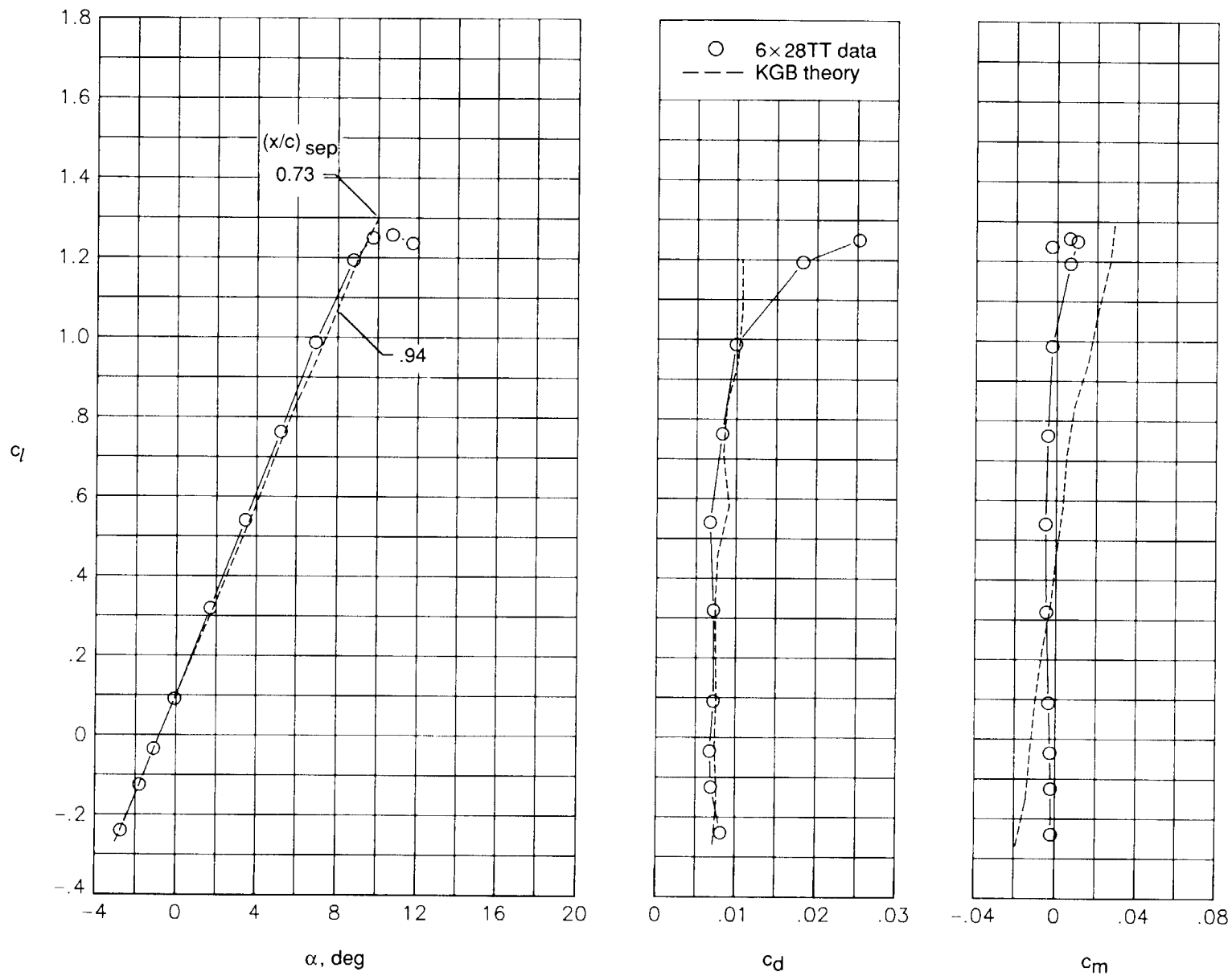

(b) $M = 0.49; R = 6.5 \times 10^6$.

Figure 21. Concluded.

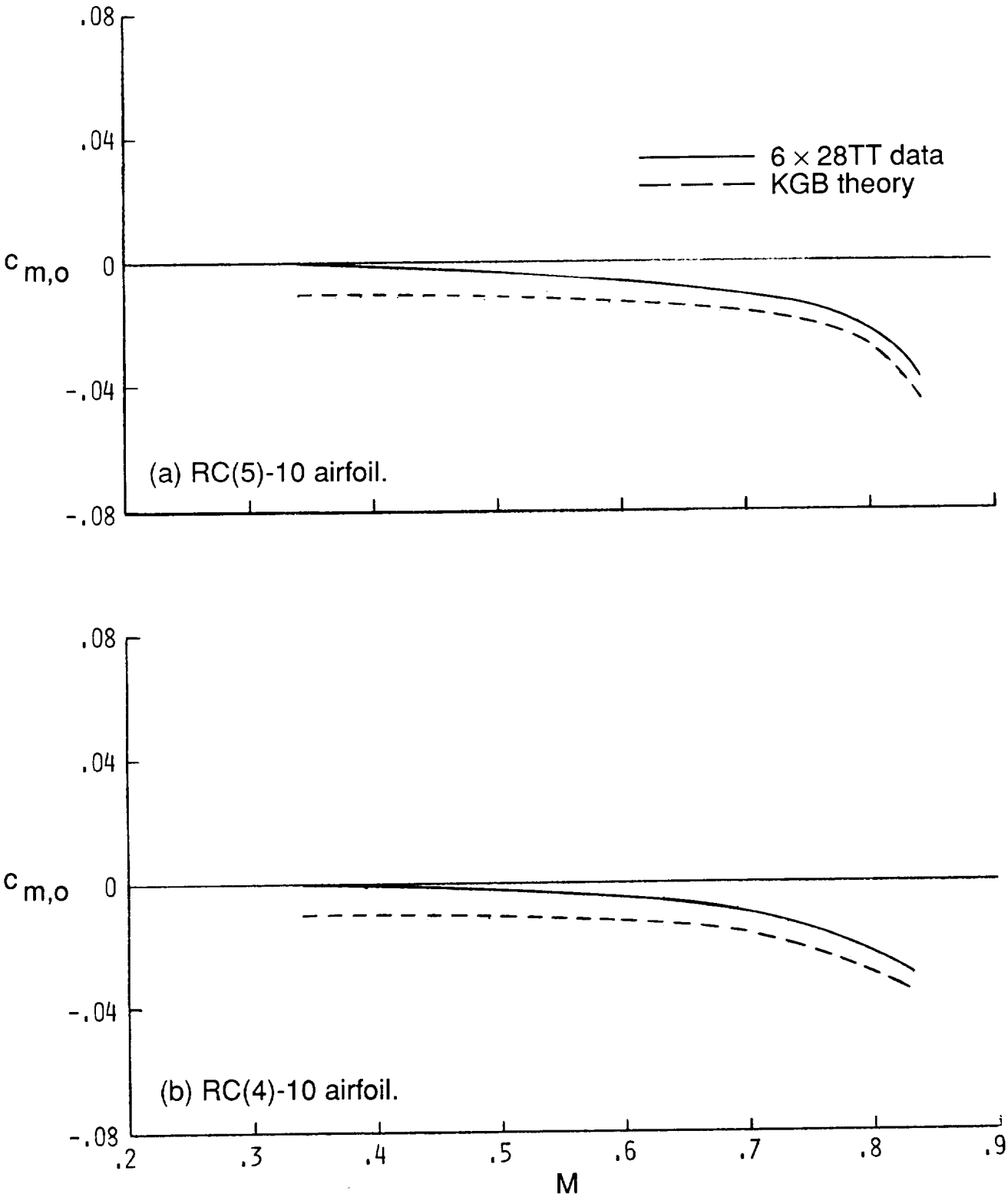

Figure 22. Comparison of experimental and theoretical variation of pitching-moment coefficient with Mach number for RC(4)-10 and RC(5)-10 airfoils at $c_l = 0$.

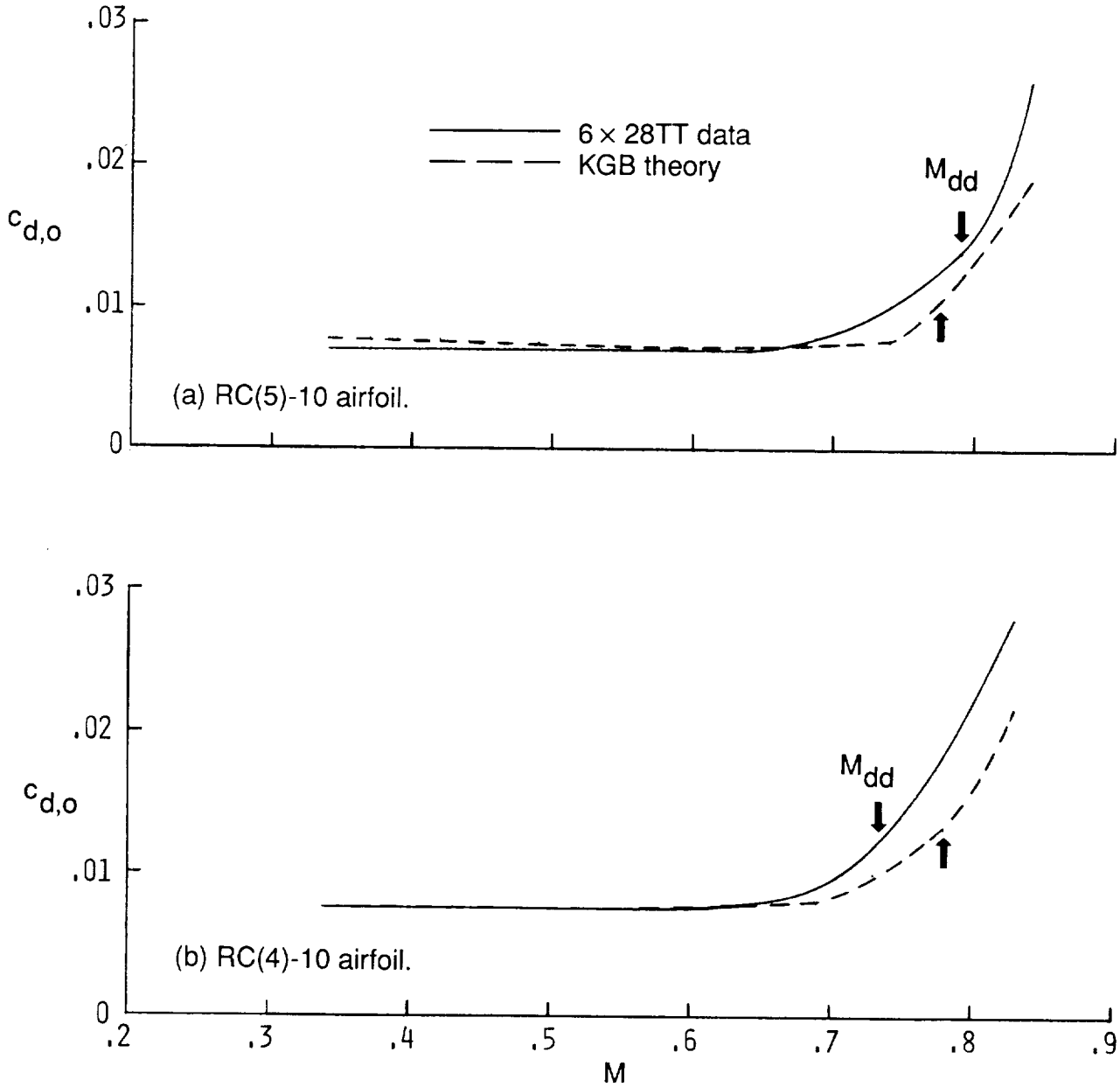

Figure 23. Comparison of experimental and theoretical variation of drag coefficient with Mach number for RC(4)-10 and RC(5)-10 airfoils at $c_l = 0$.

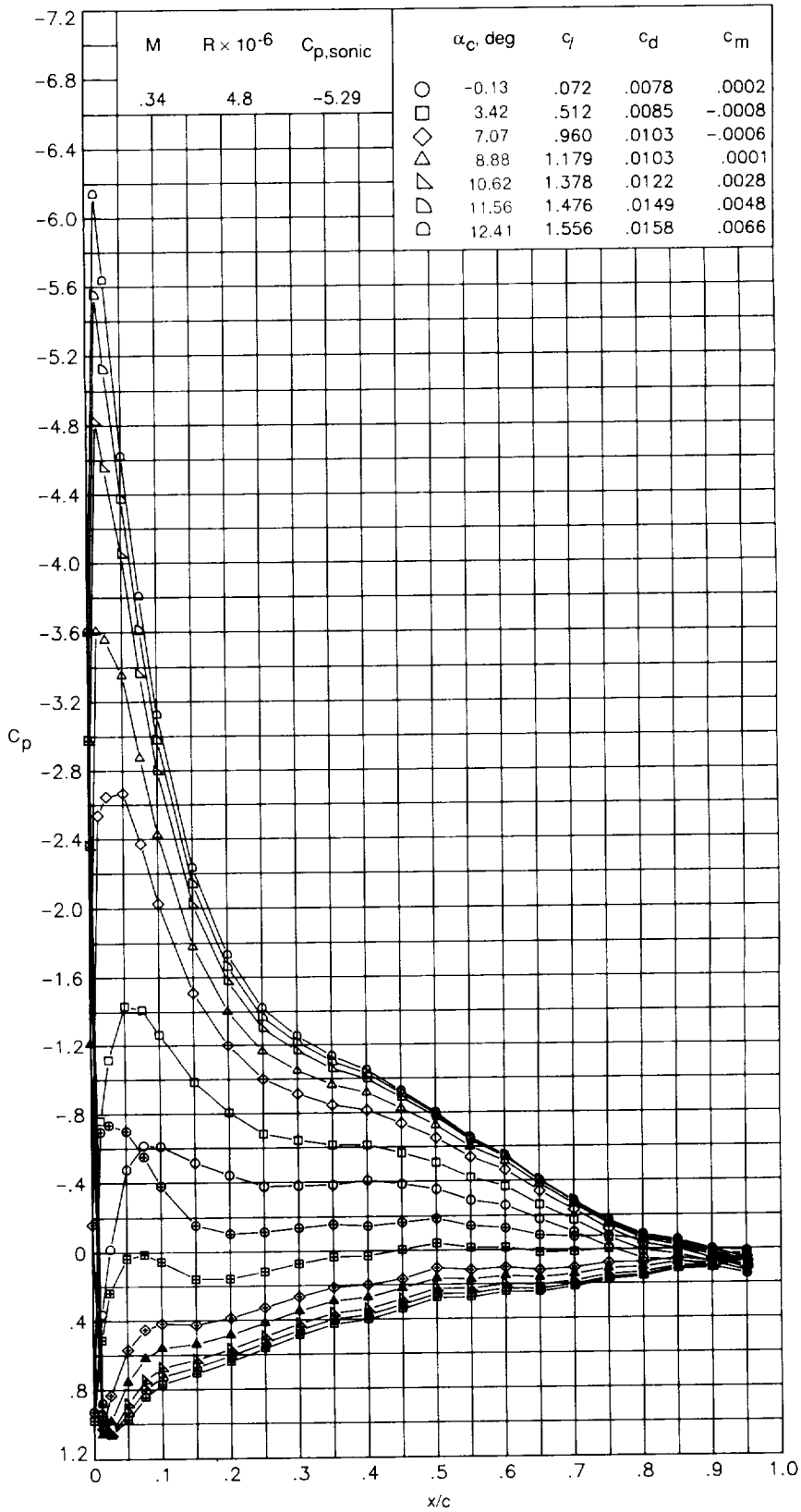

(a) $M = 0.34; R = 4.8 \times 10^6$.

Figure 24. Chordwise pressure distributions of RC(4)-10 airfoil measured in the Langley 6×28TT.

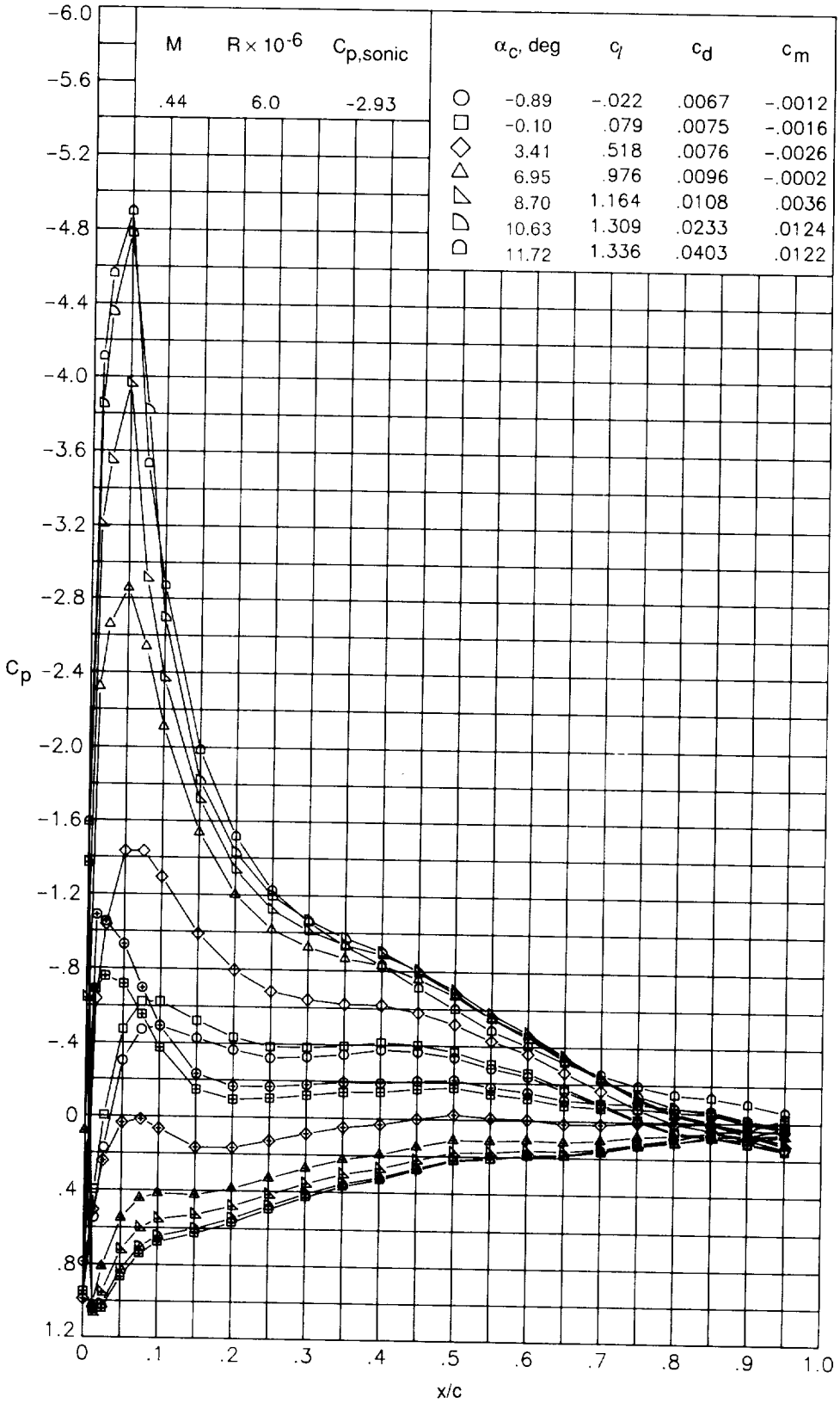

(b) $M = 0.44; R = 6.0 \times 10^6$.

Figure 24. Continued.

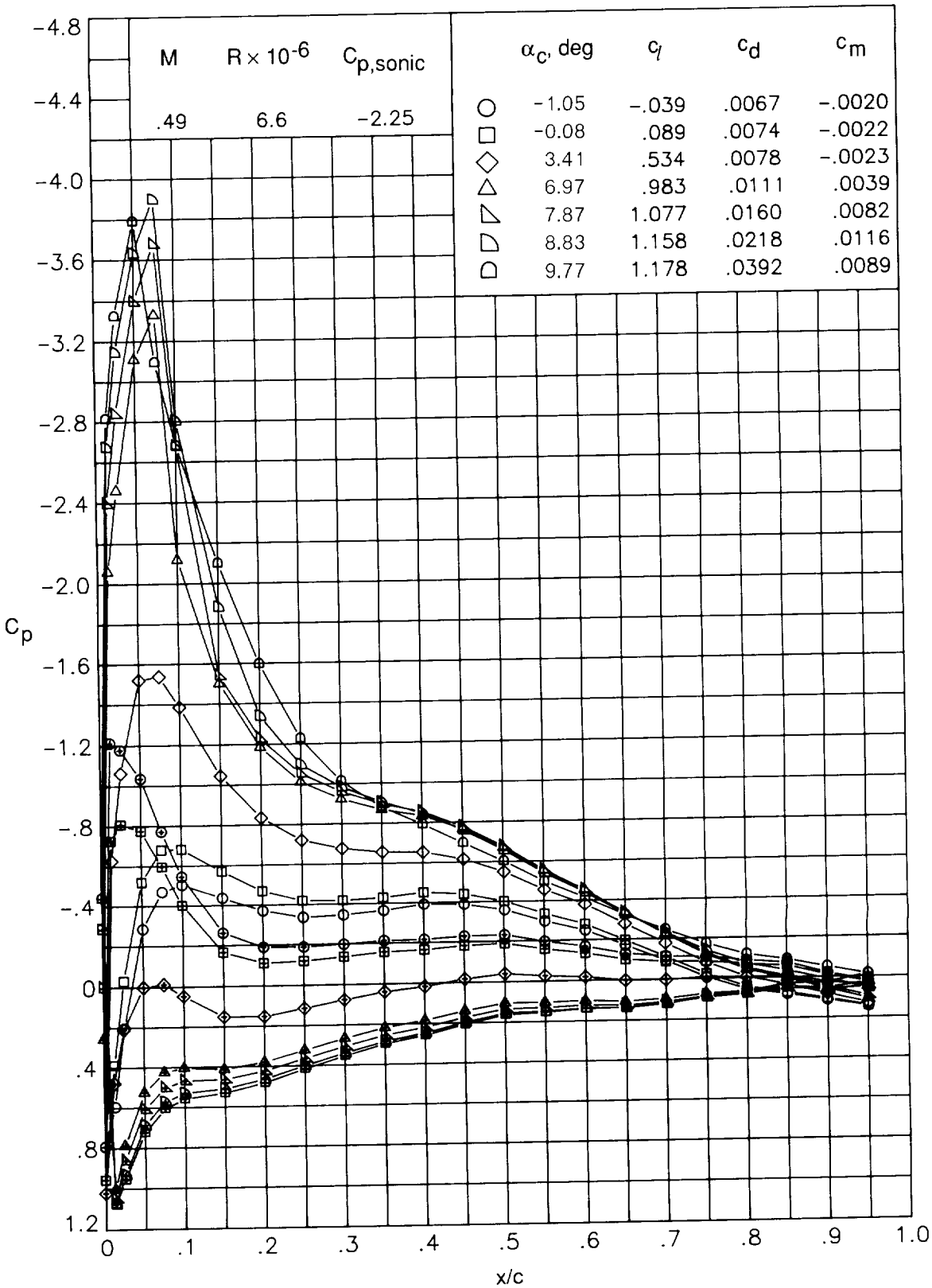

(c) $M = 0.49; R = 6.6 \times 10^6$.

Figure 24. Continued.

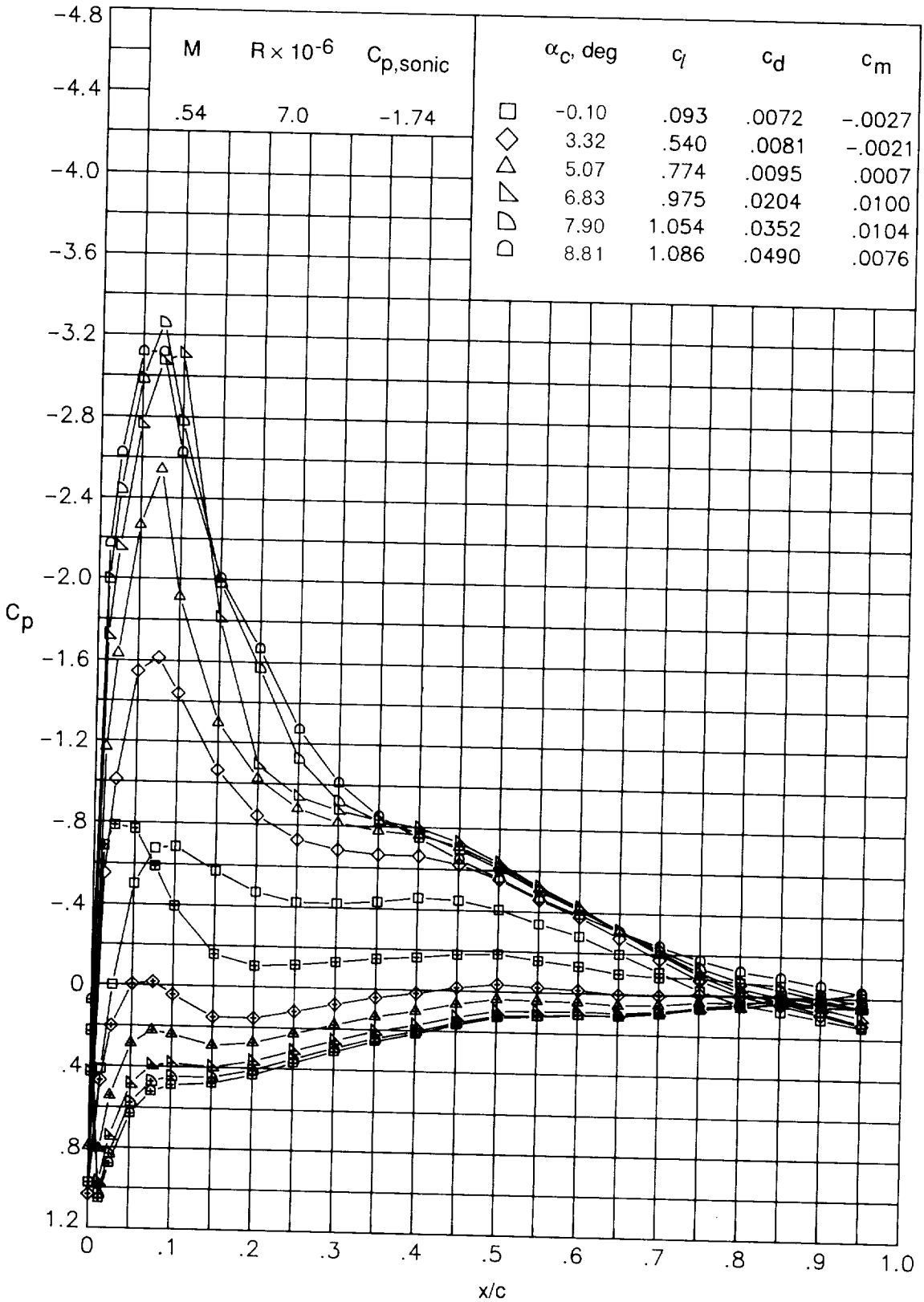

(d) $M = 0.54; R = 7.0 \times 10^6$.

Figure 24. Continued.

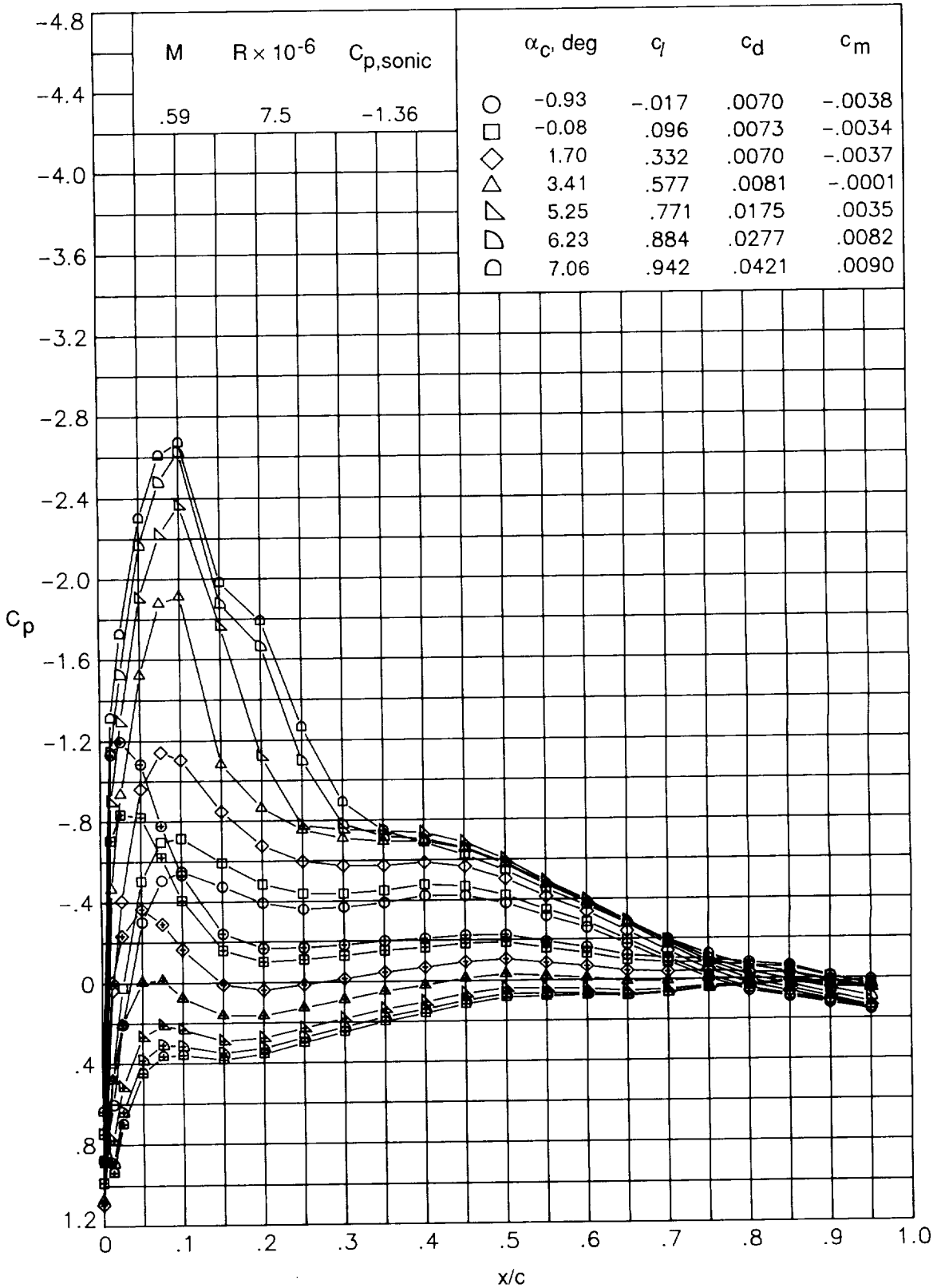

(e) $M = 0.59; R = 7.5 \times 10^6$.

Figure 24. Continued.

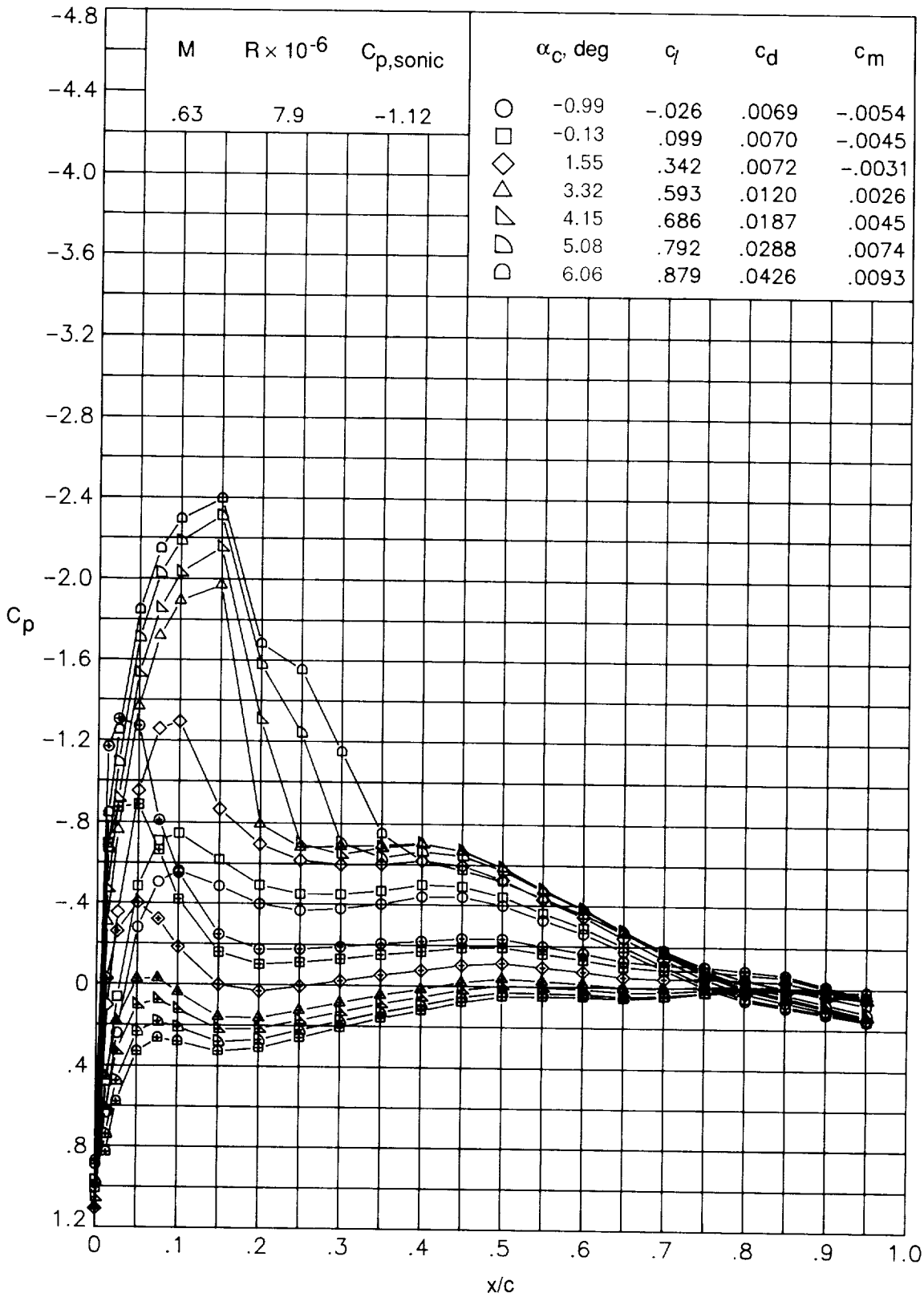

(f) $M = 0.63; R = 7.9 \times 10^6$.

Figure 24. Continued.

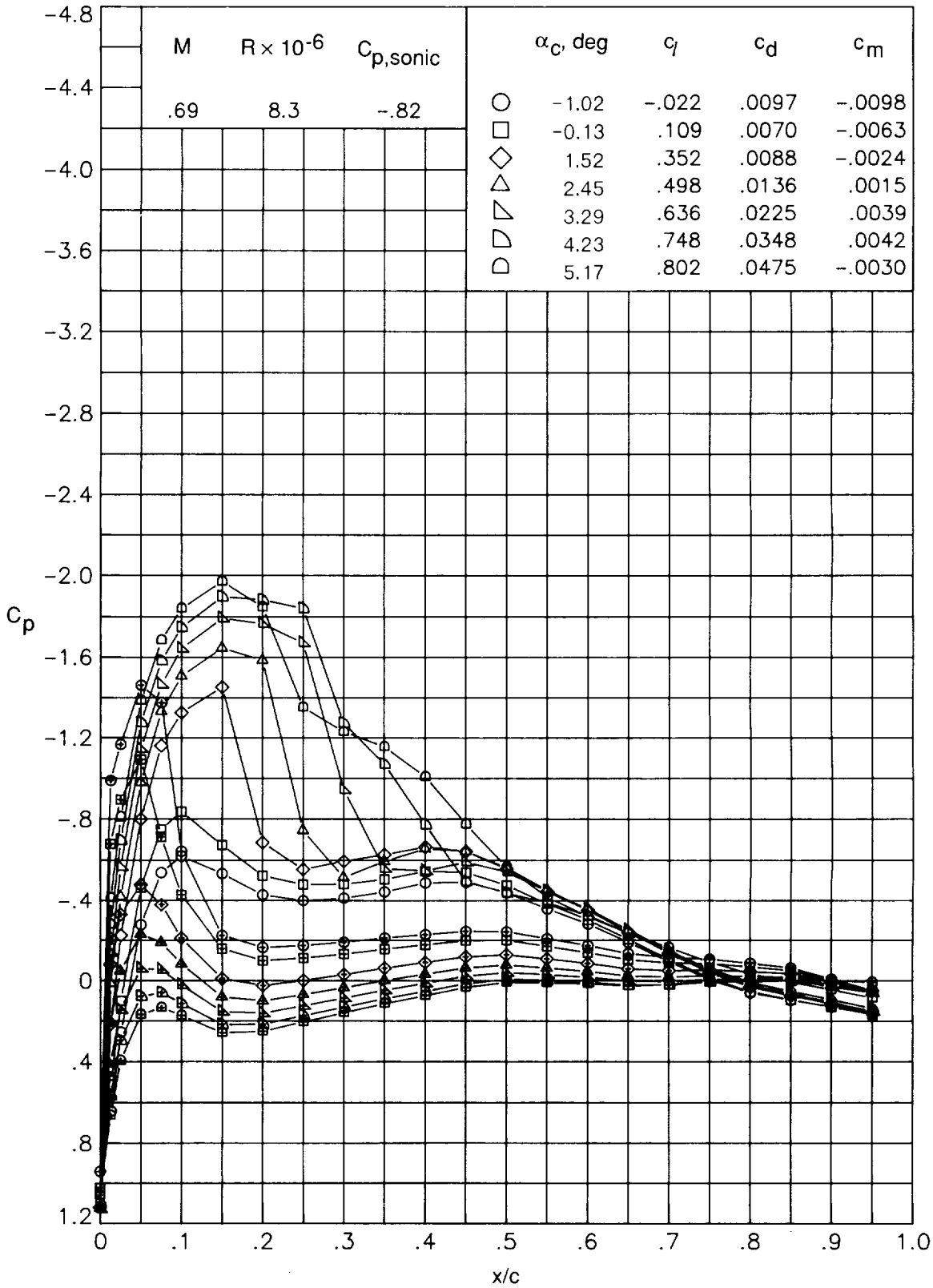

(g) $M = 0.69; R = 8.3 \times 10^6$.

Figure 24. Continued.

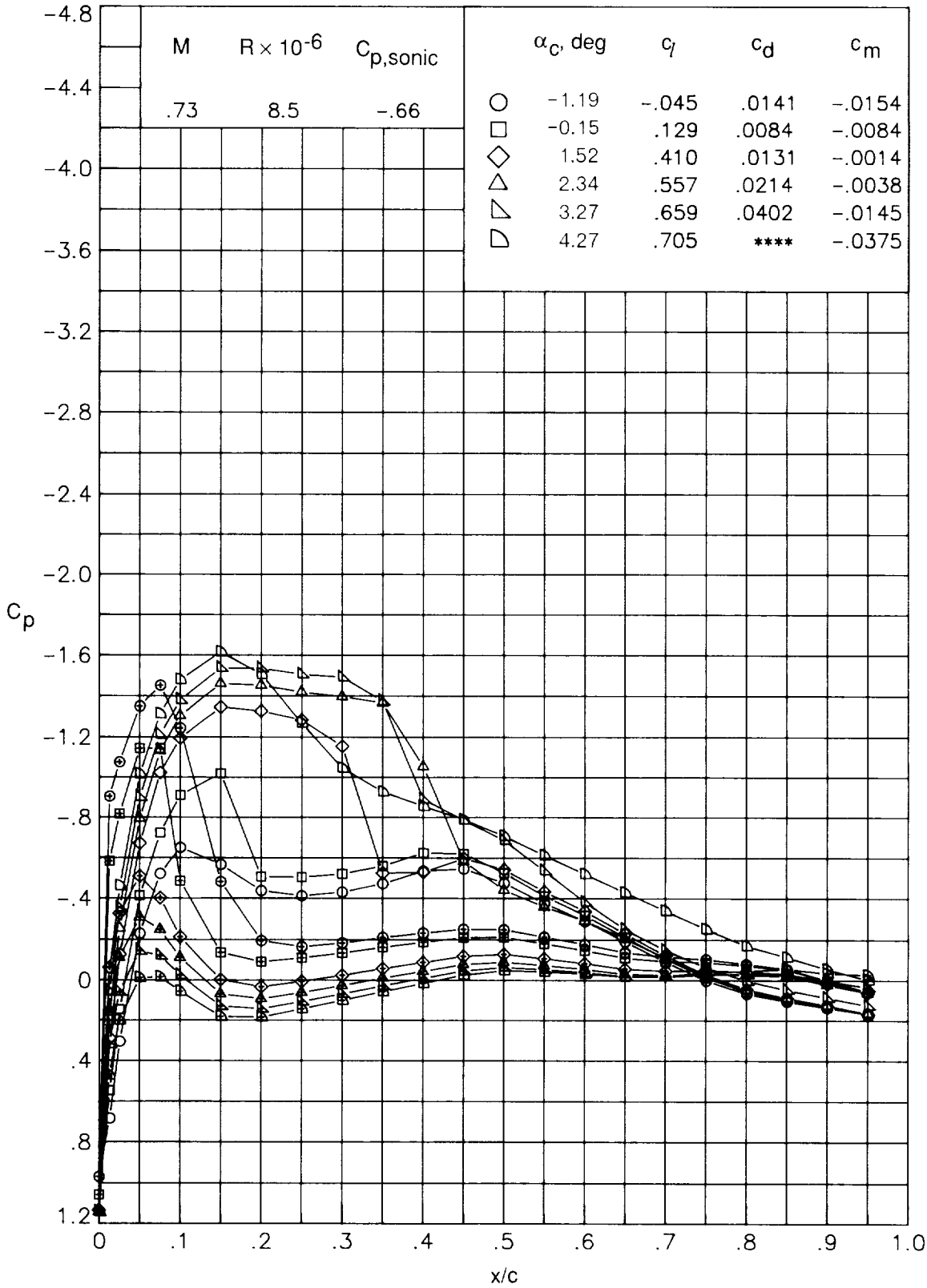

(h) $M = 0.73; R = 8.5 \times 10^6$.

Figure 24. Continued.

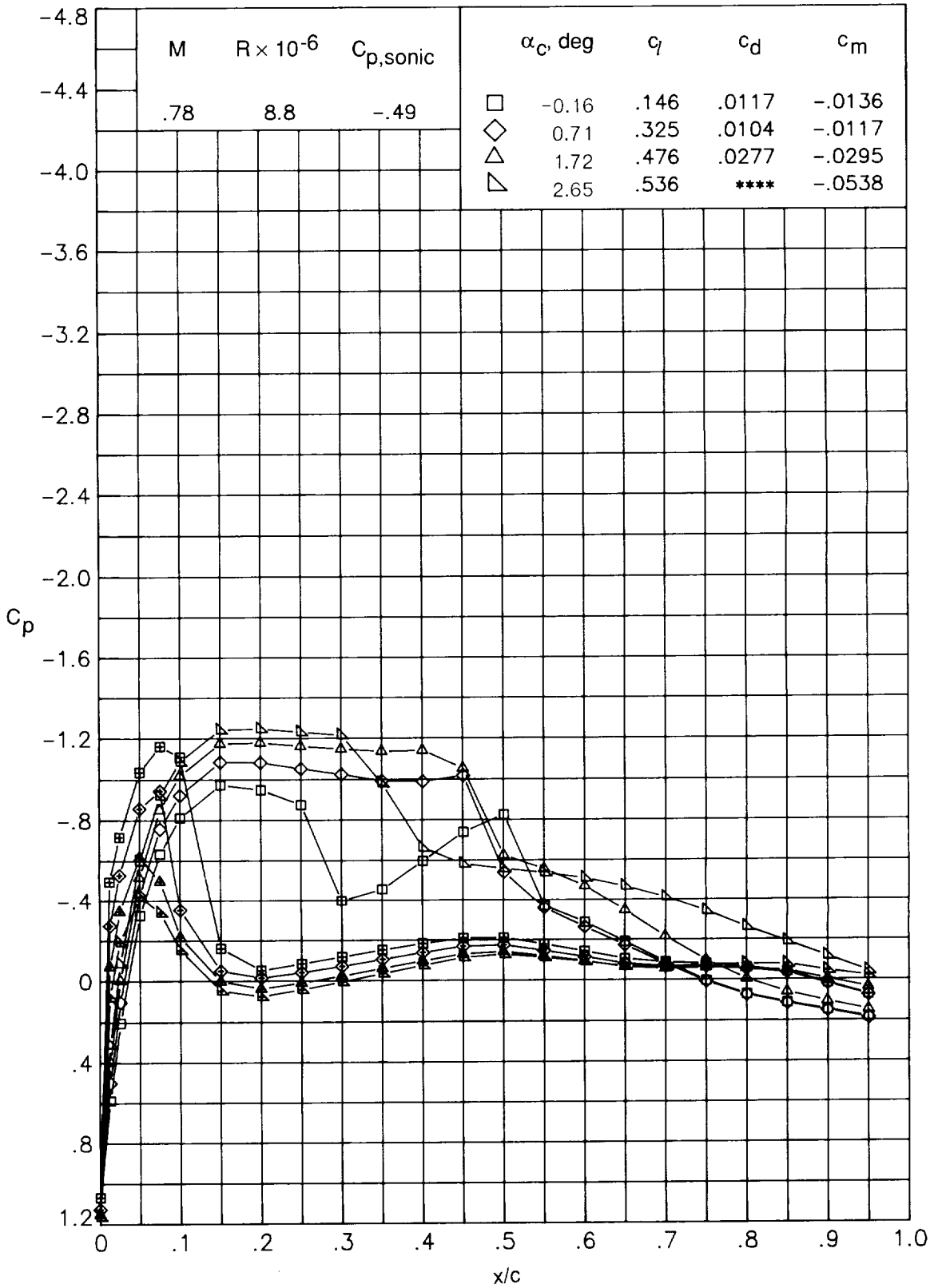

(i) $M = 0.78; R = 8.8 \times 10^6$.

Figure 24. Continued.

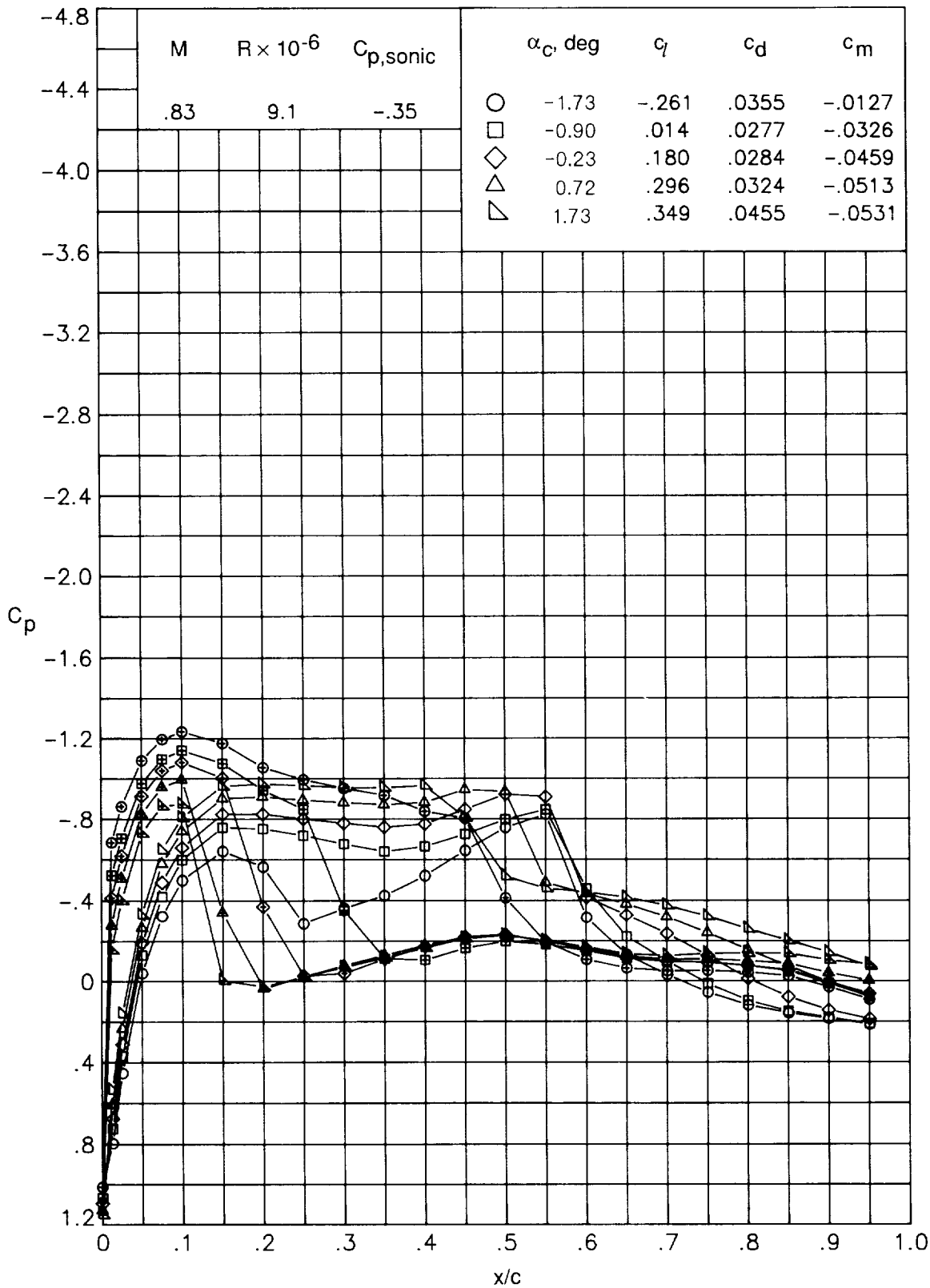

(j) $M = 0.83; R = 9.1 \times 10^6$.

Figure 24. Concluded.

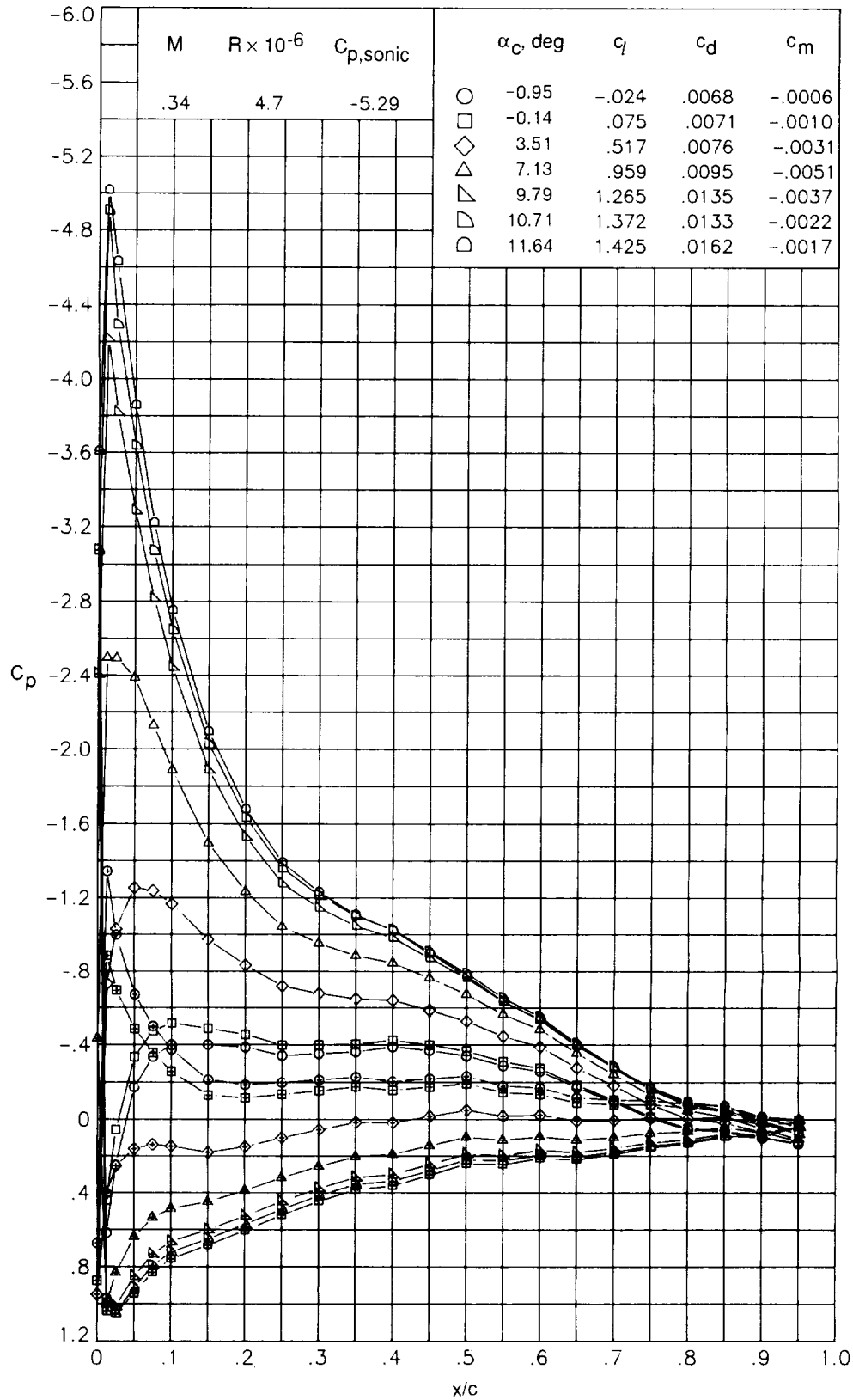

(a) $M = 0.34; R = 4.7 \times 10^6$.

Figure 25. Chordwise pressure distributions of RC(5)-10 airfoil measured in the Langley 6×28TT.

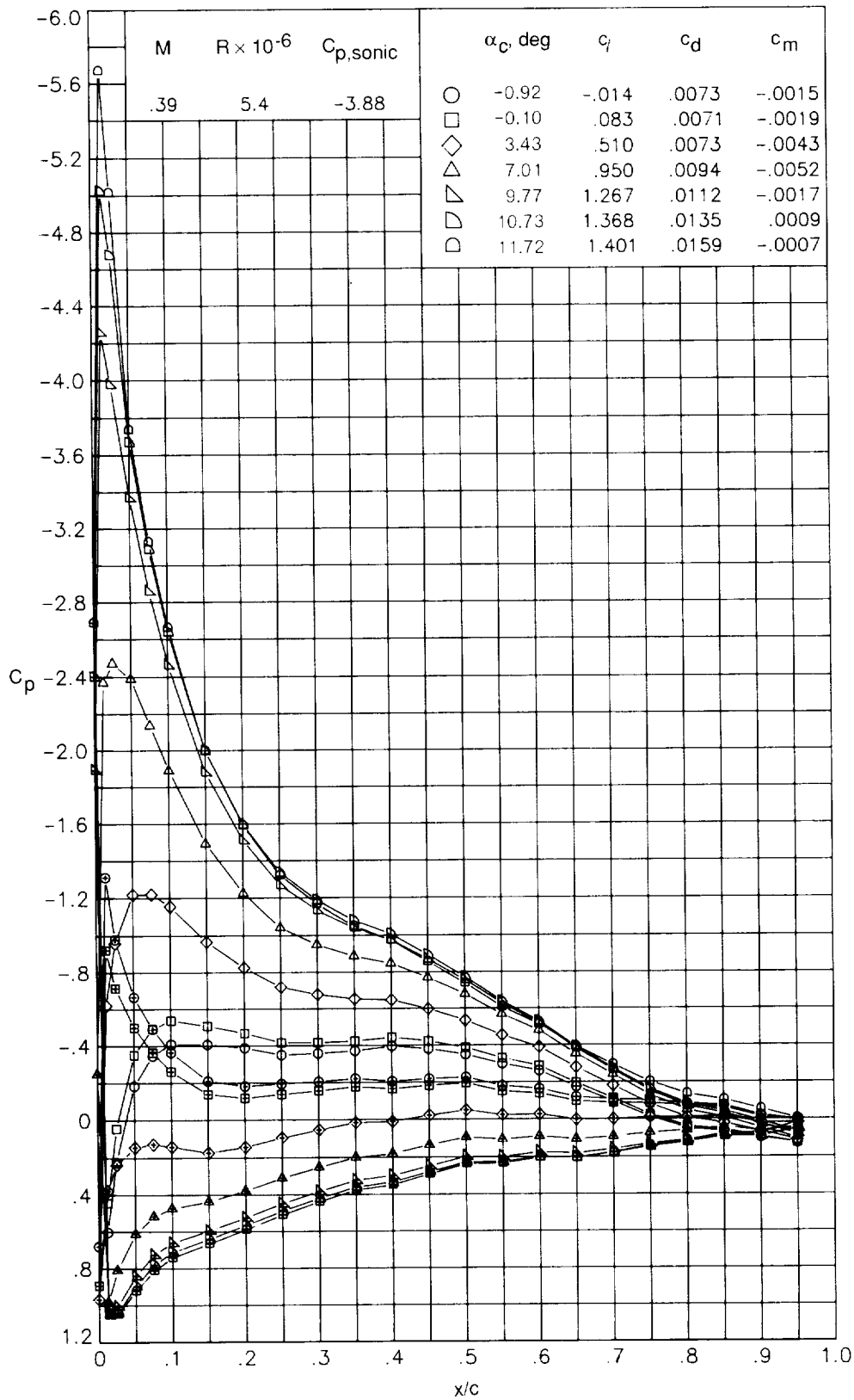

(b) $M = 0.39; R = 5.4 \times 10^6$.

Figure 25. Continued.

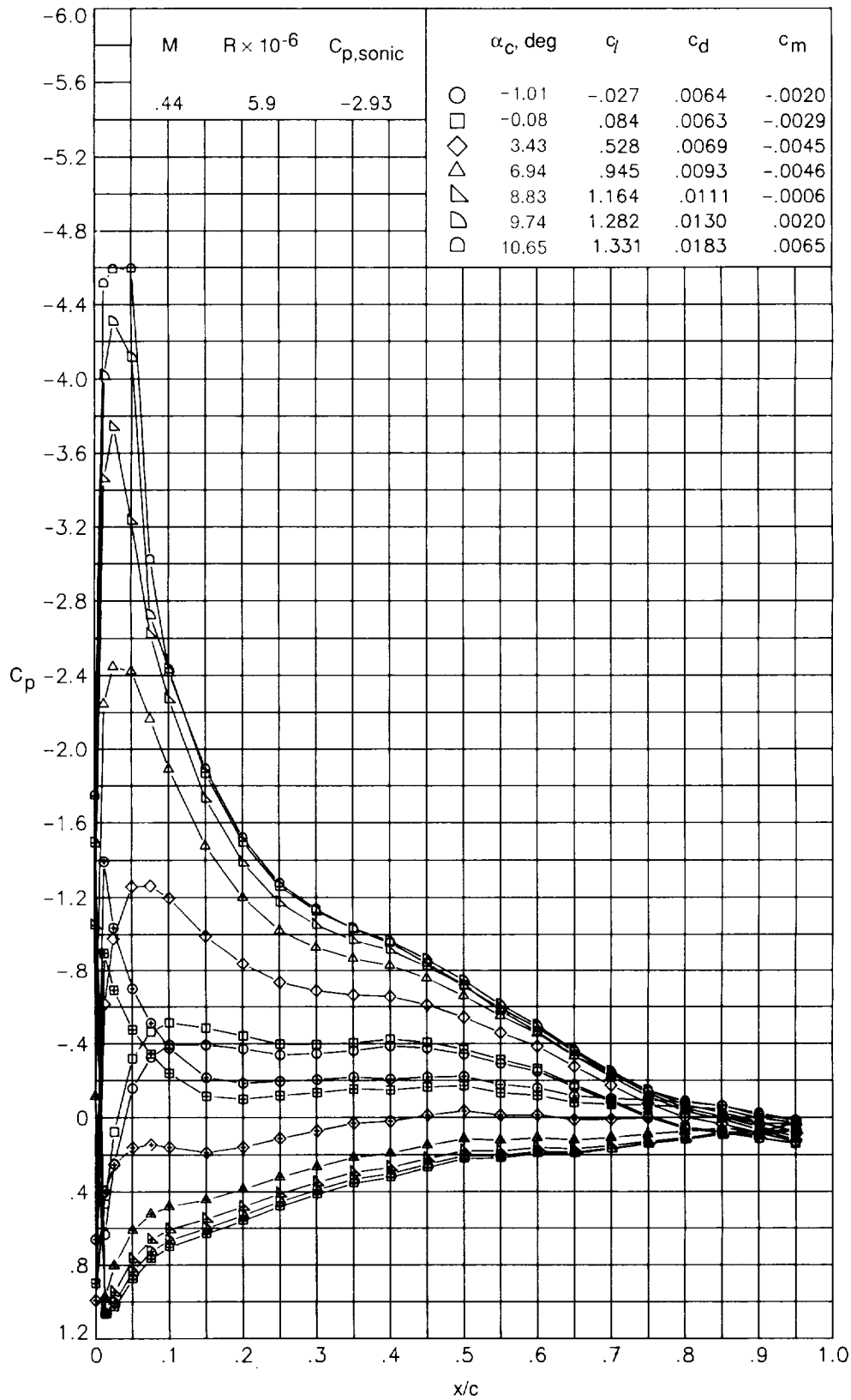

(c) $M = 0.44; R = 5.9 \times 10^6$.

Figure 25. Continued.

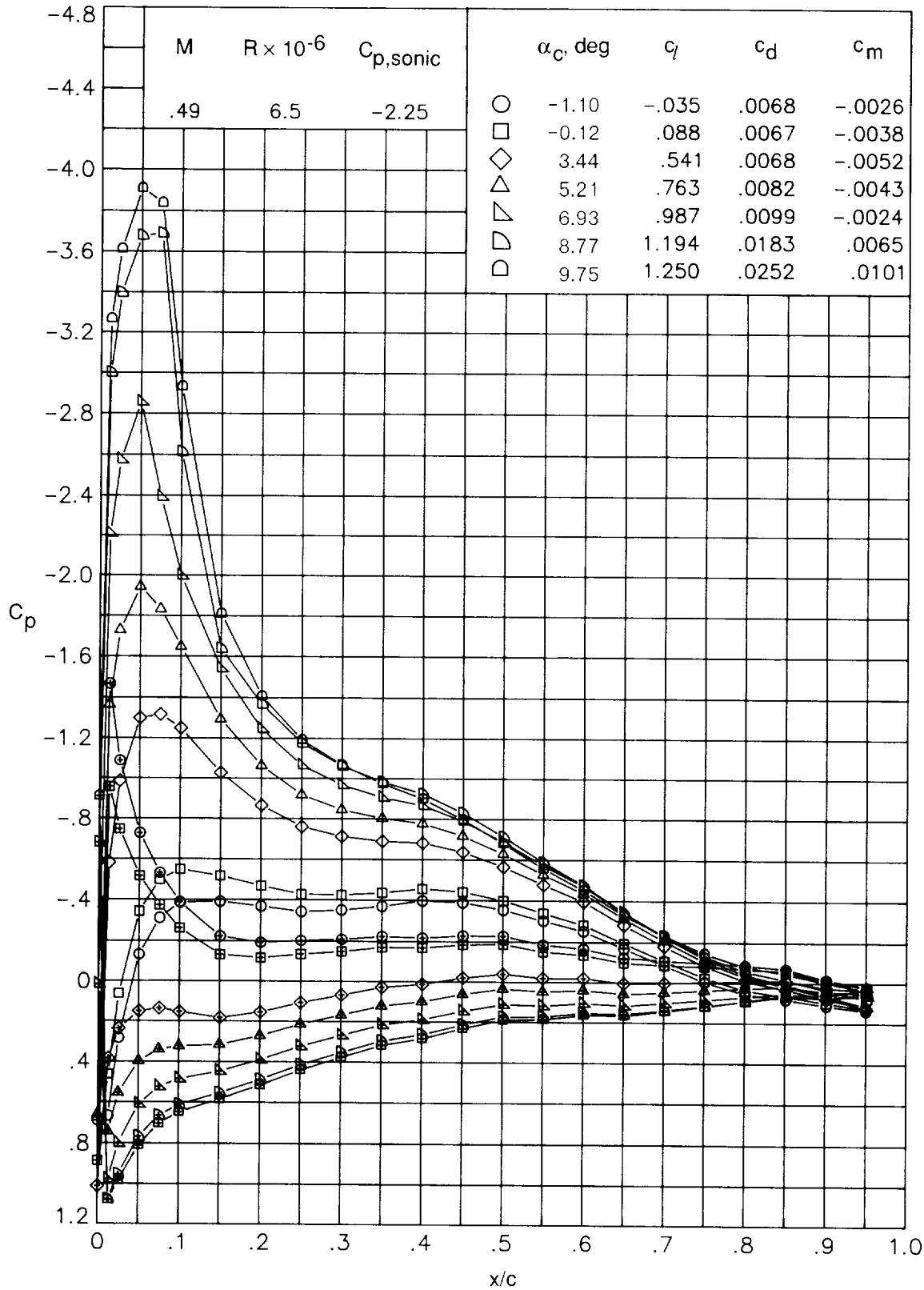

(d) $M = 0.49; R = 6.5 \times 10^6$.

Figure 25. Continued.

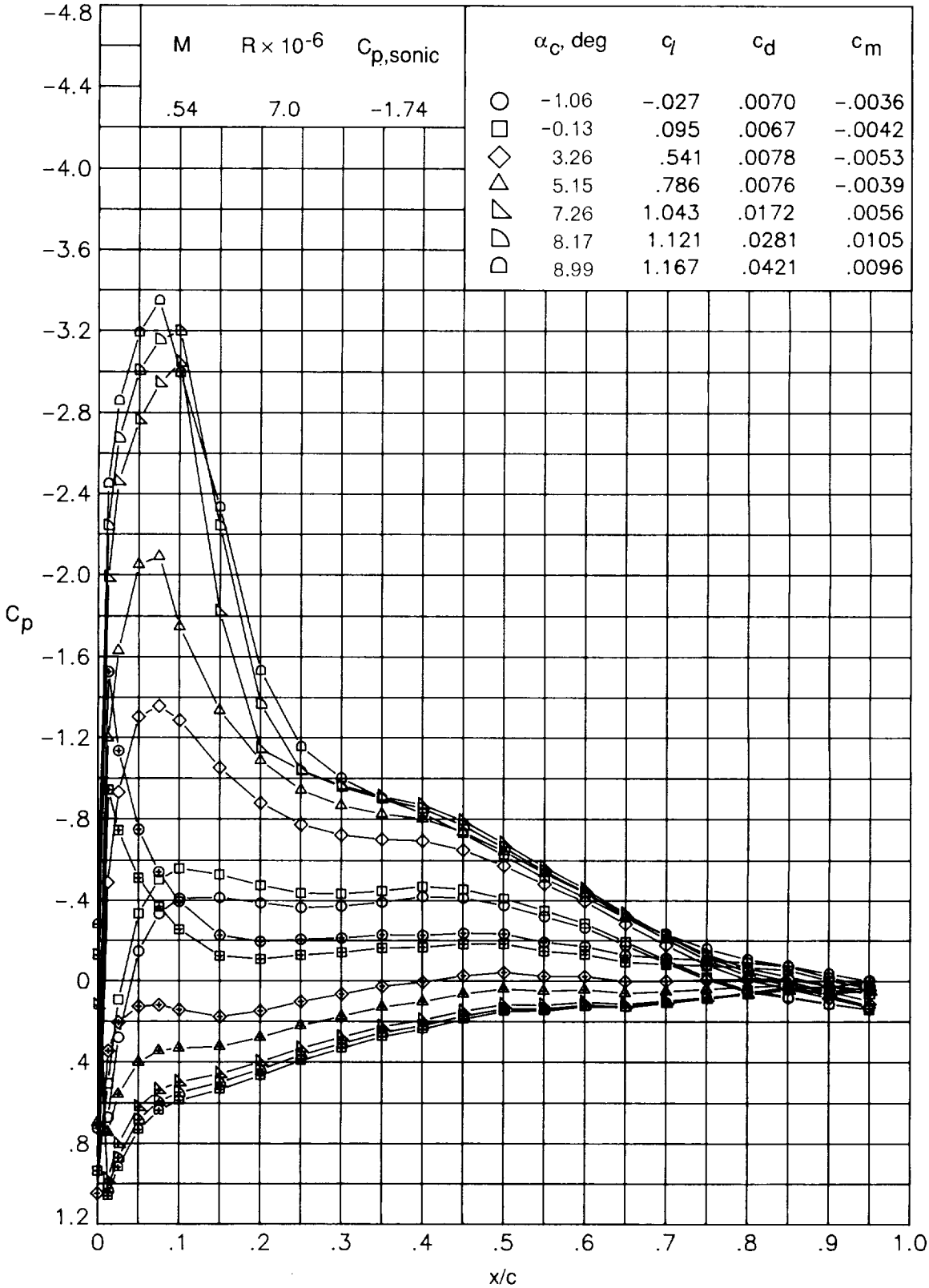

(e) $M = 0.54; R = 7.0 \times 10^6$.

Figure 25. Continued.

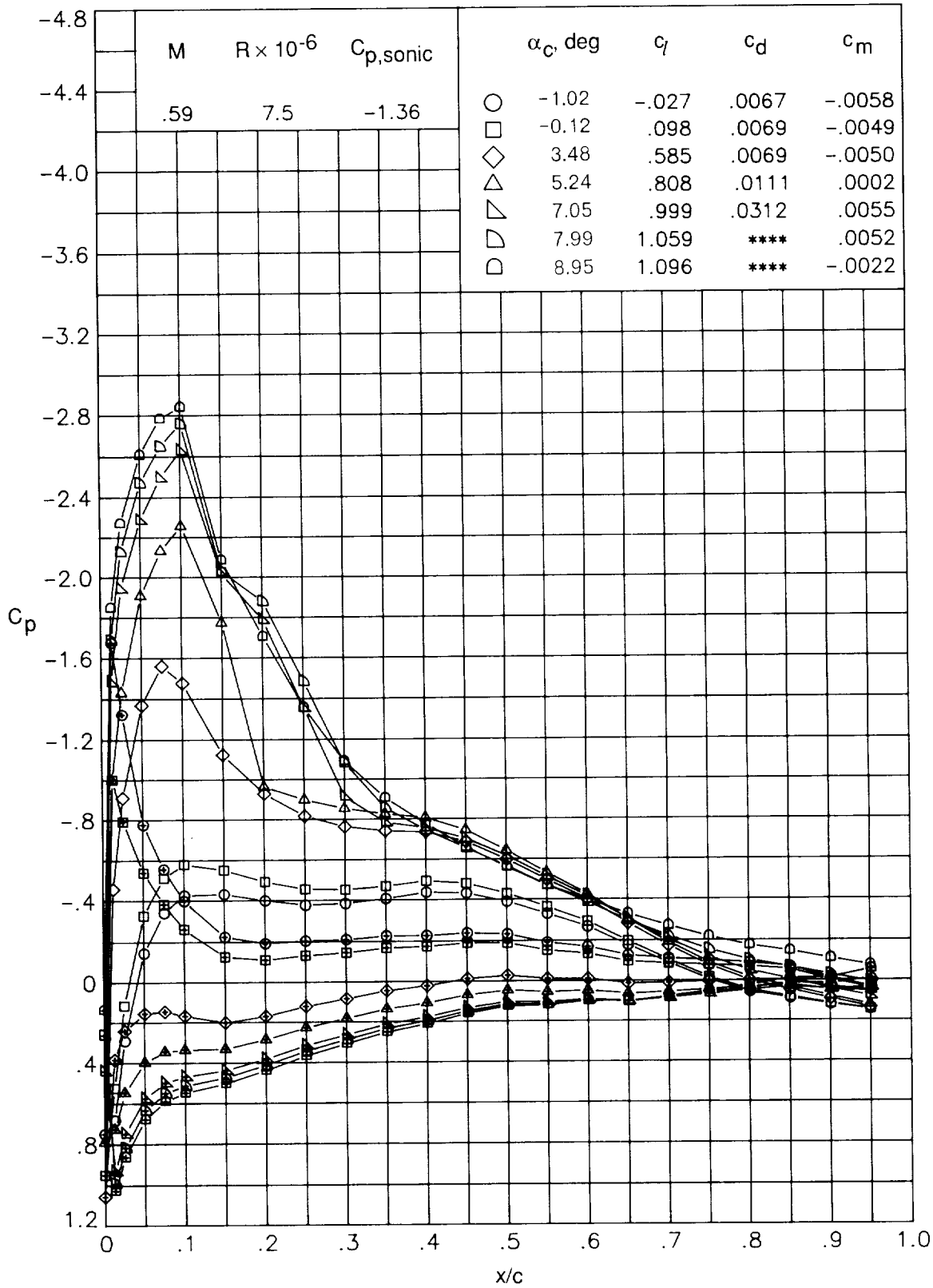

(f) $M = 0.59; R = 7.5 \times 10^6$.

Figure 25. Continued.

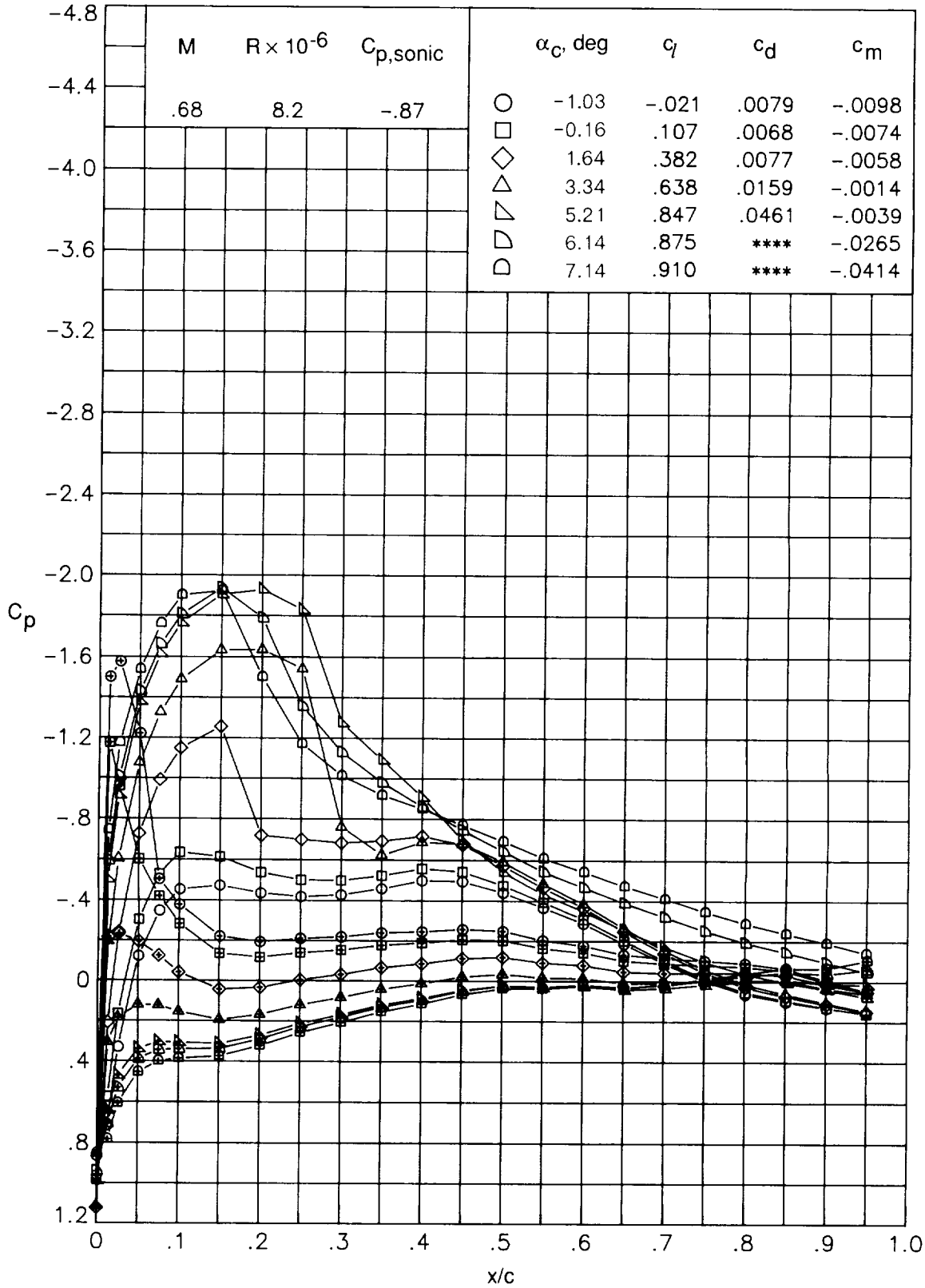

(g) $M = 0.68; R = 8.2 \times 10^6$.

Figure 25. Continued.

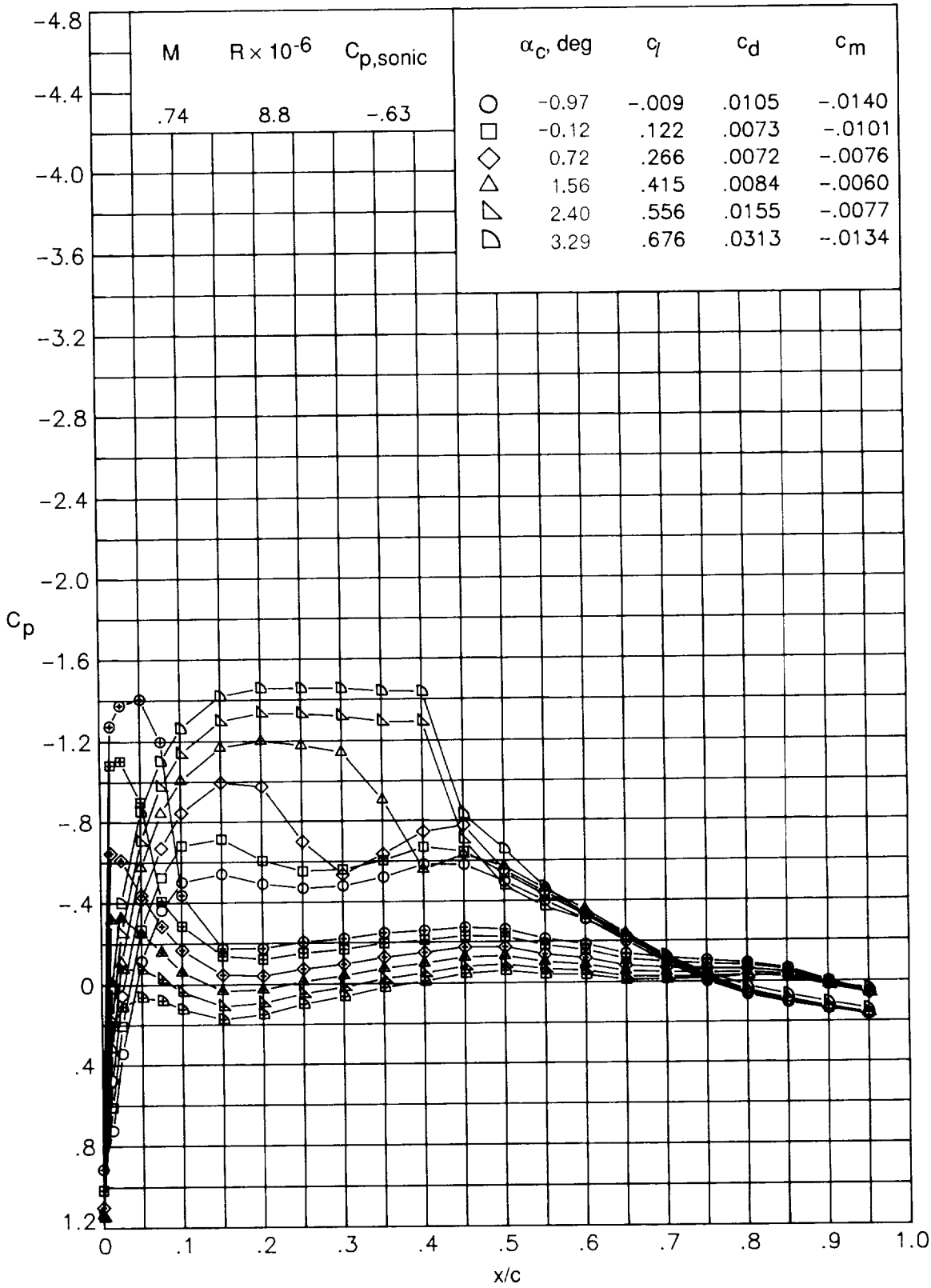

(h) $M = 0.74; R = 8.8 \times 10^6$.

Figure 25. Continued.

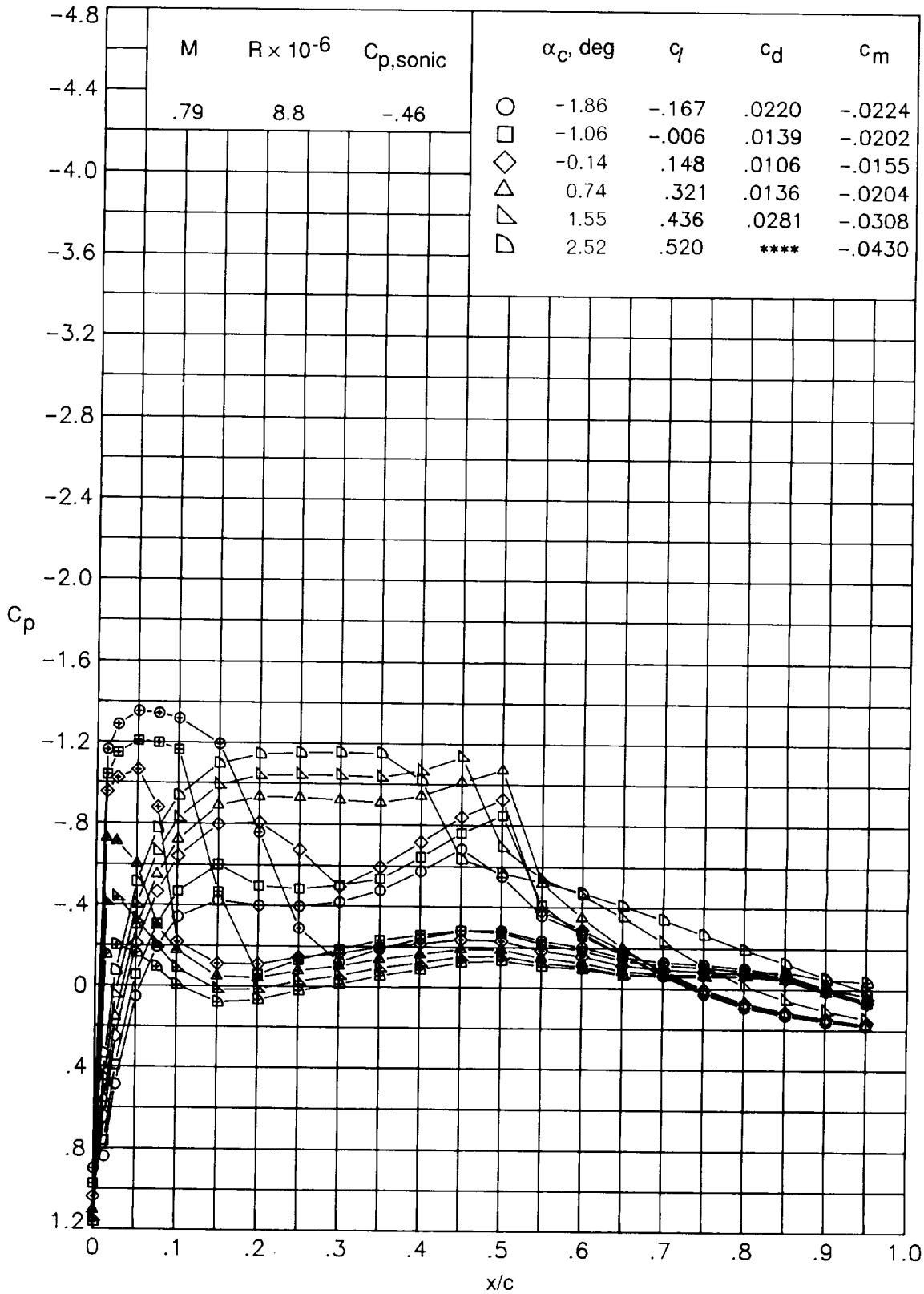

(i) $M = 0.79; R = 8.8 \times 10^6$.

Figure 25. Continued.

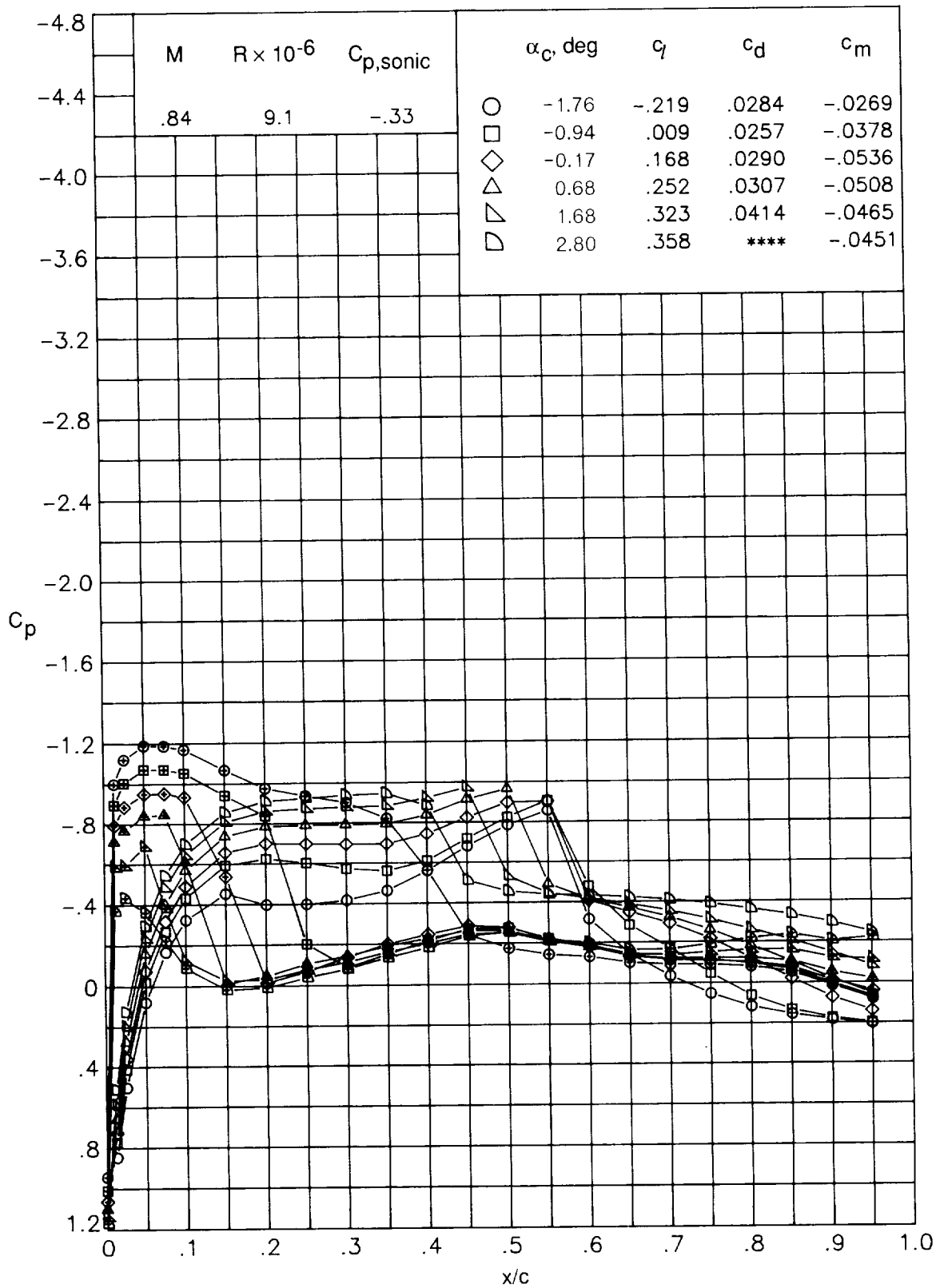

(j) $M = 0.84; R = 9.1 \times 10^6$.

Figure 25. Concluded.

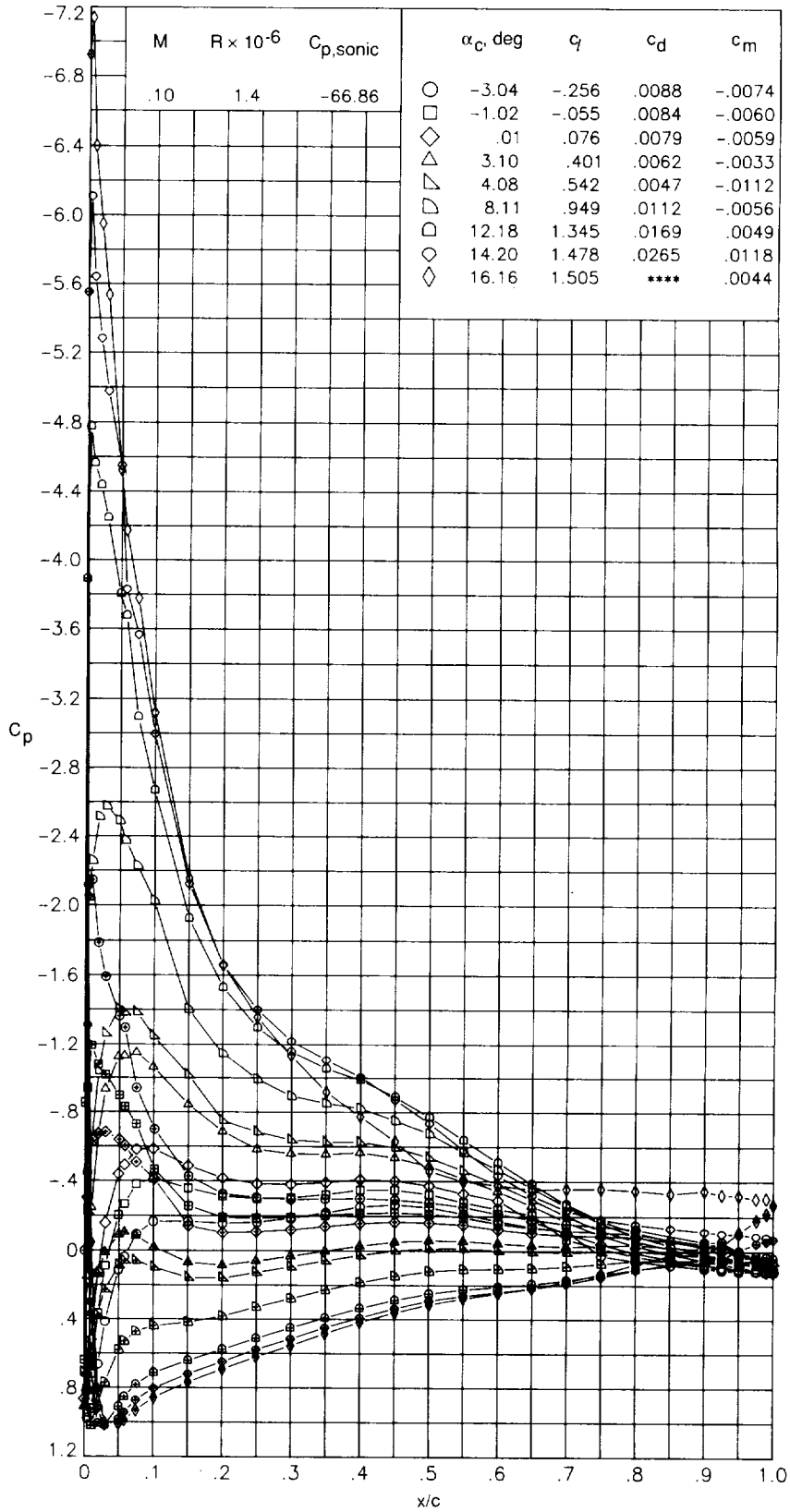

(a) $M = 0.10; R = 1.4 \times 10^6$.

Figure 26. Chordwise pressure distributions of RC(4)-10 airfoil measured in the Langley LTPT.

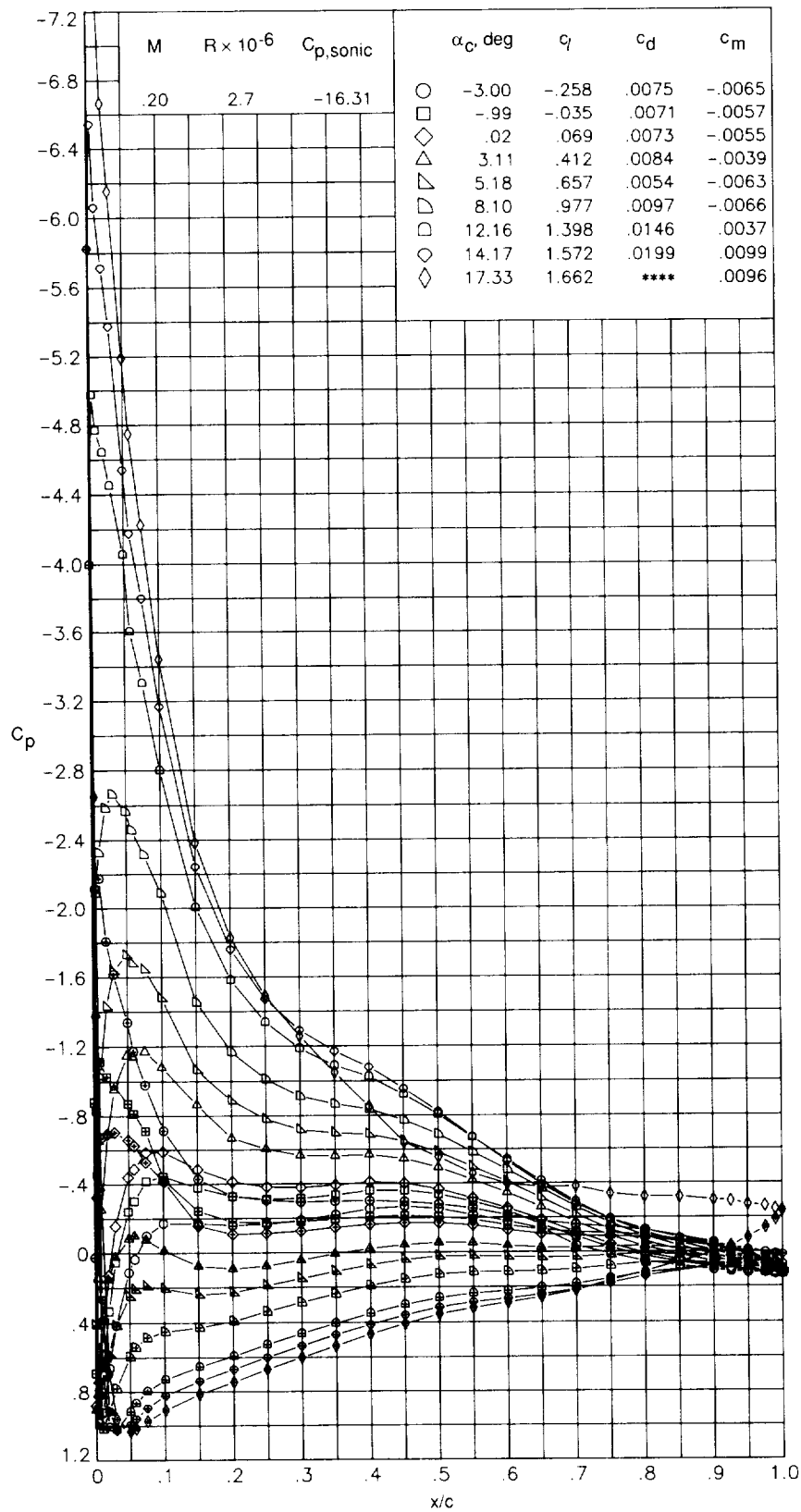

(b) $M = 0.20; R = 2.7 \times 10^6$.

Figure 26. Continued.

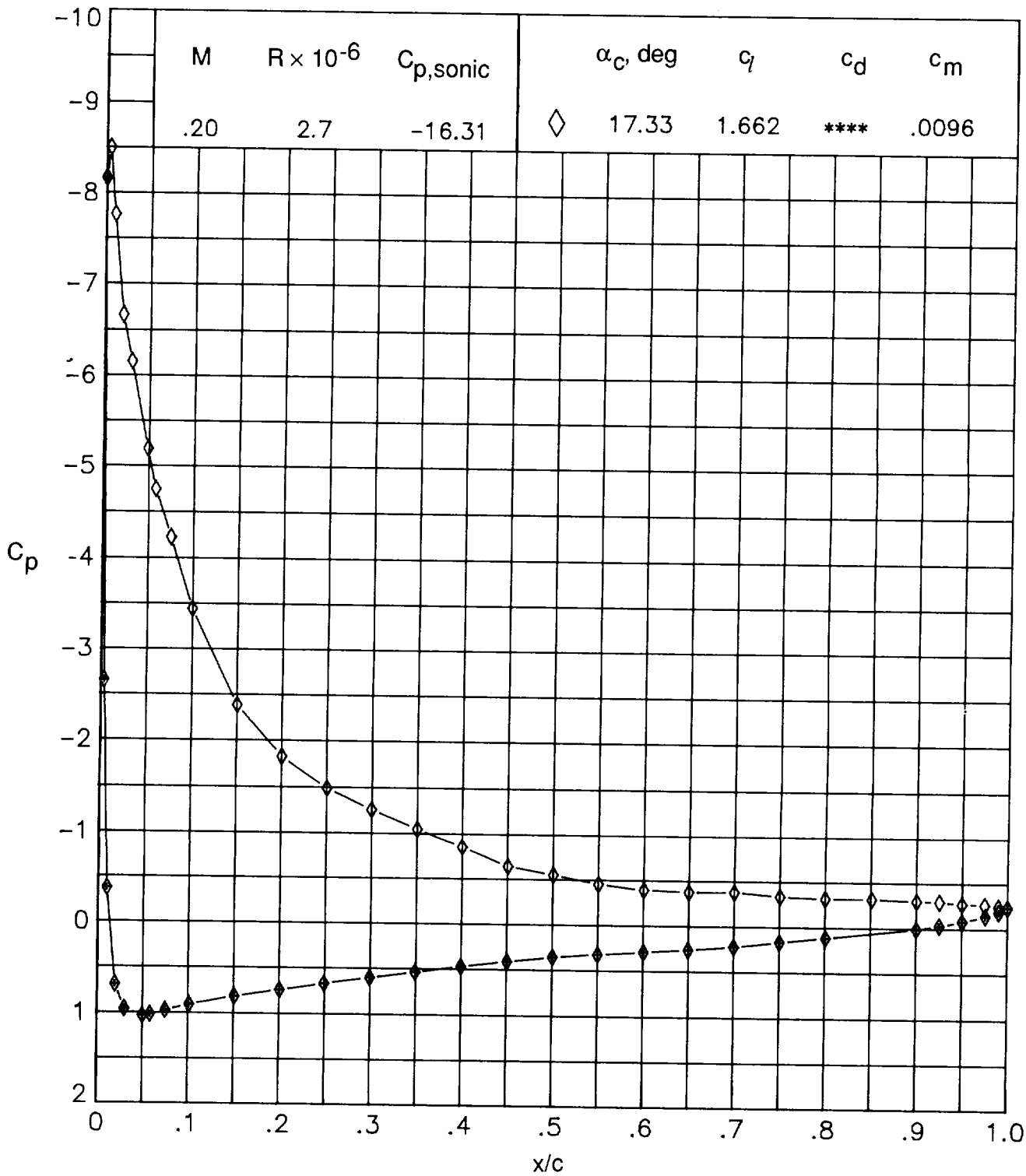

(b) Concluded.

Figure 26. Continued.

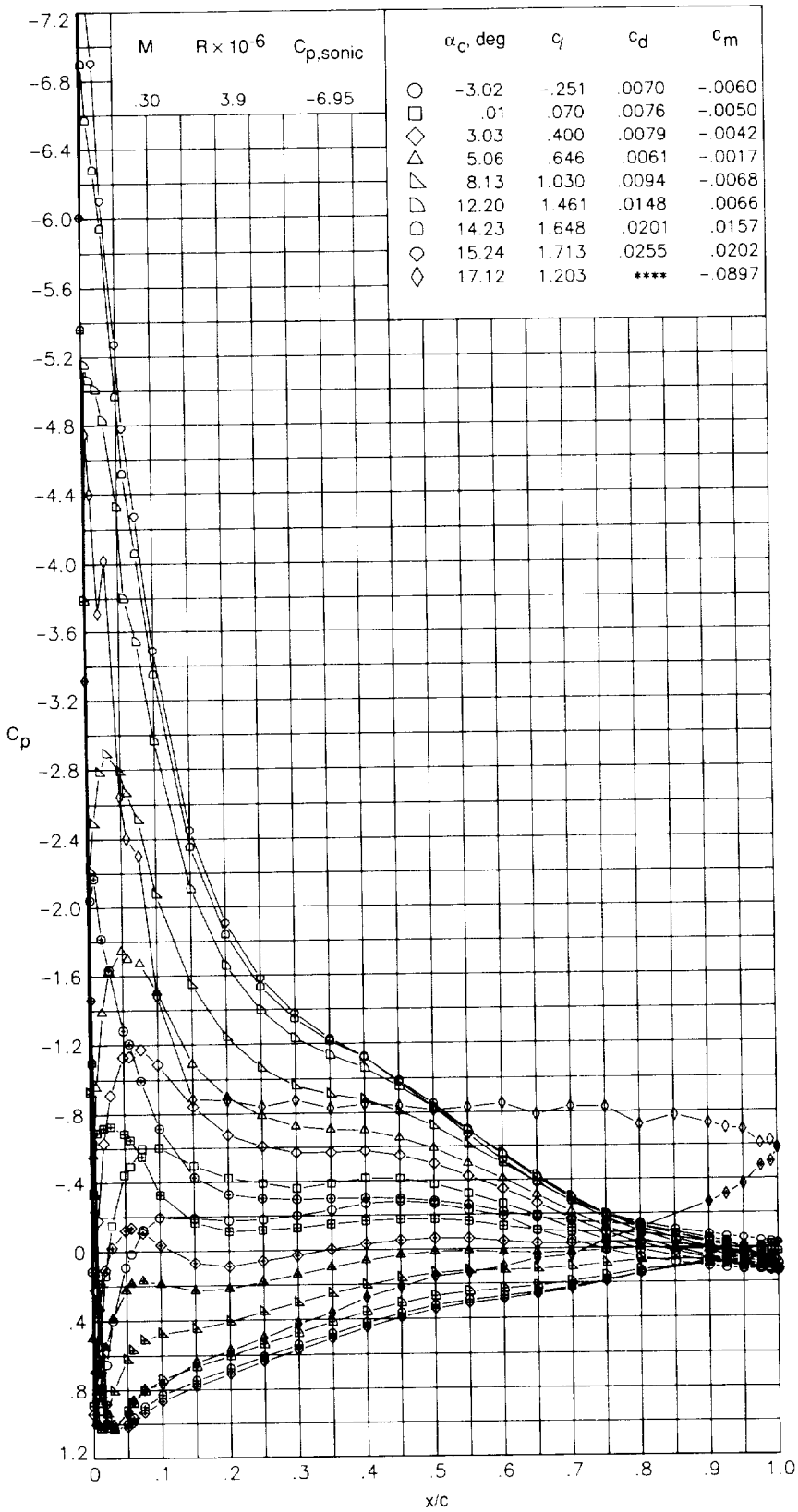

(c) $M = 0.30; R = 3.9 \times 10^6$.

Figure 26. Continued.

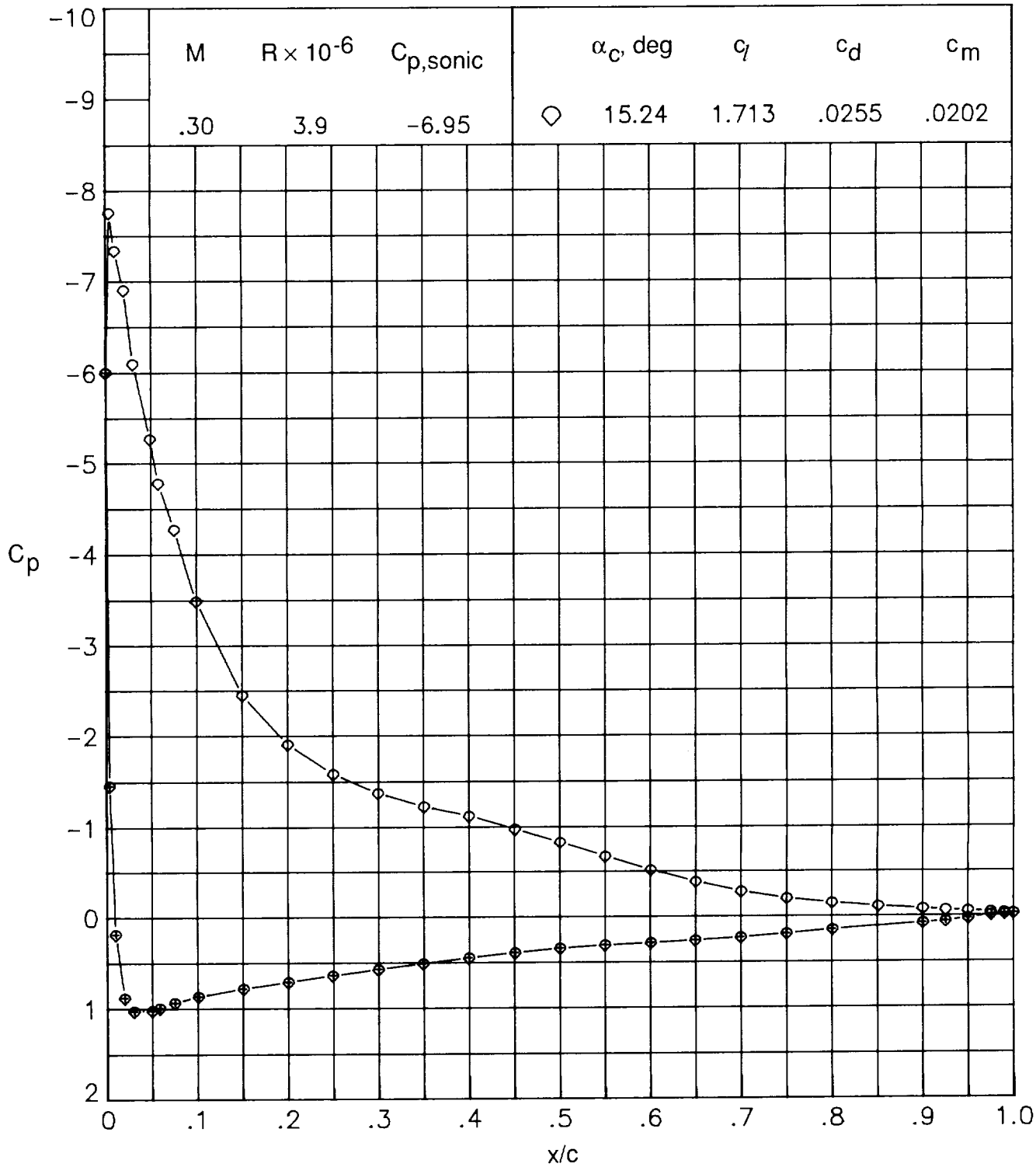

(c) Concluded.

Figure 26. Continued.

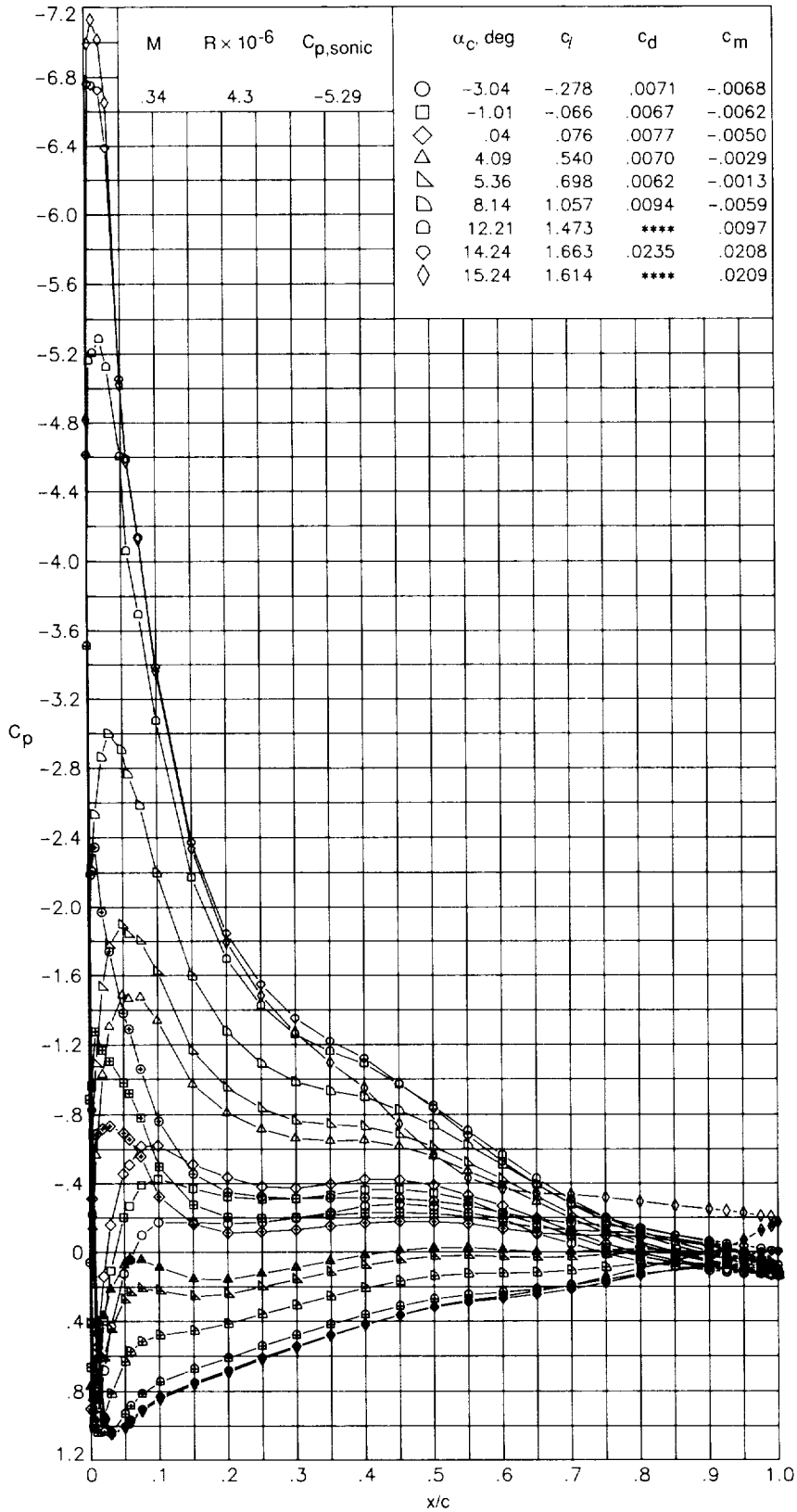

(d) $M = 0.34; R = 4.3 \times 10^6$.

Figure 26. Continued.

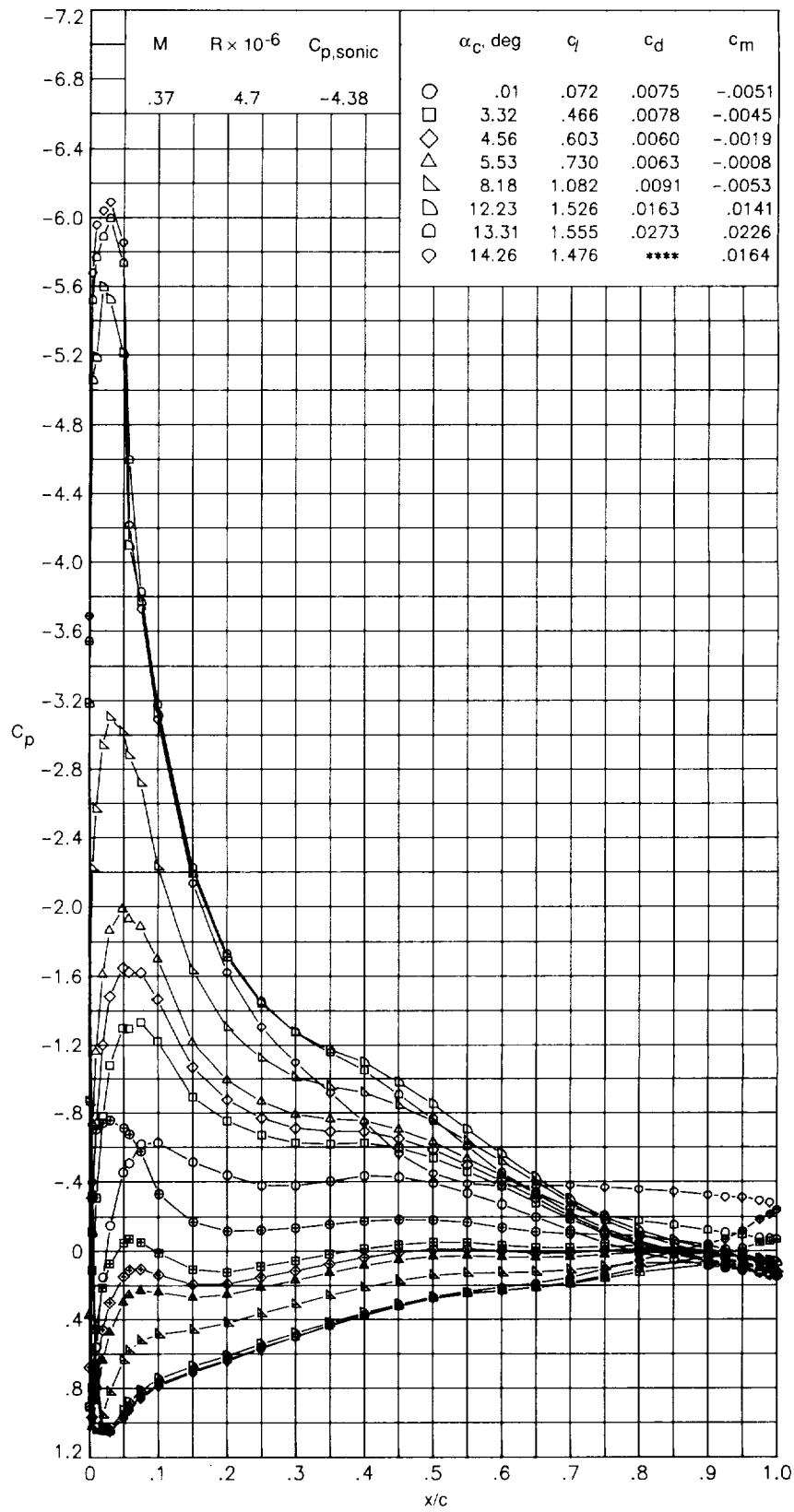

(e) $M = 0.37; R = 4.7 \times 10^6$.

Figure 26. Continued.

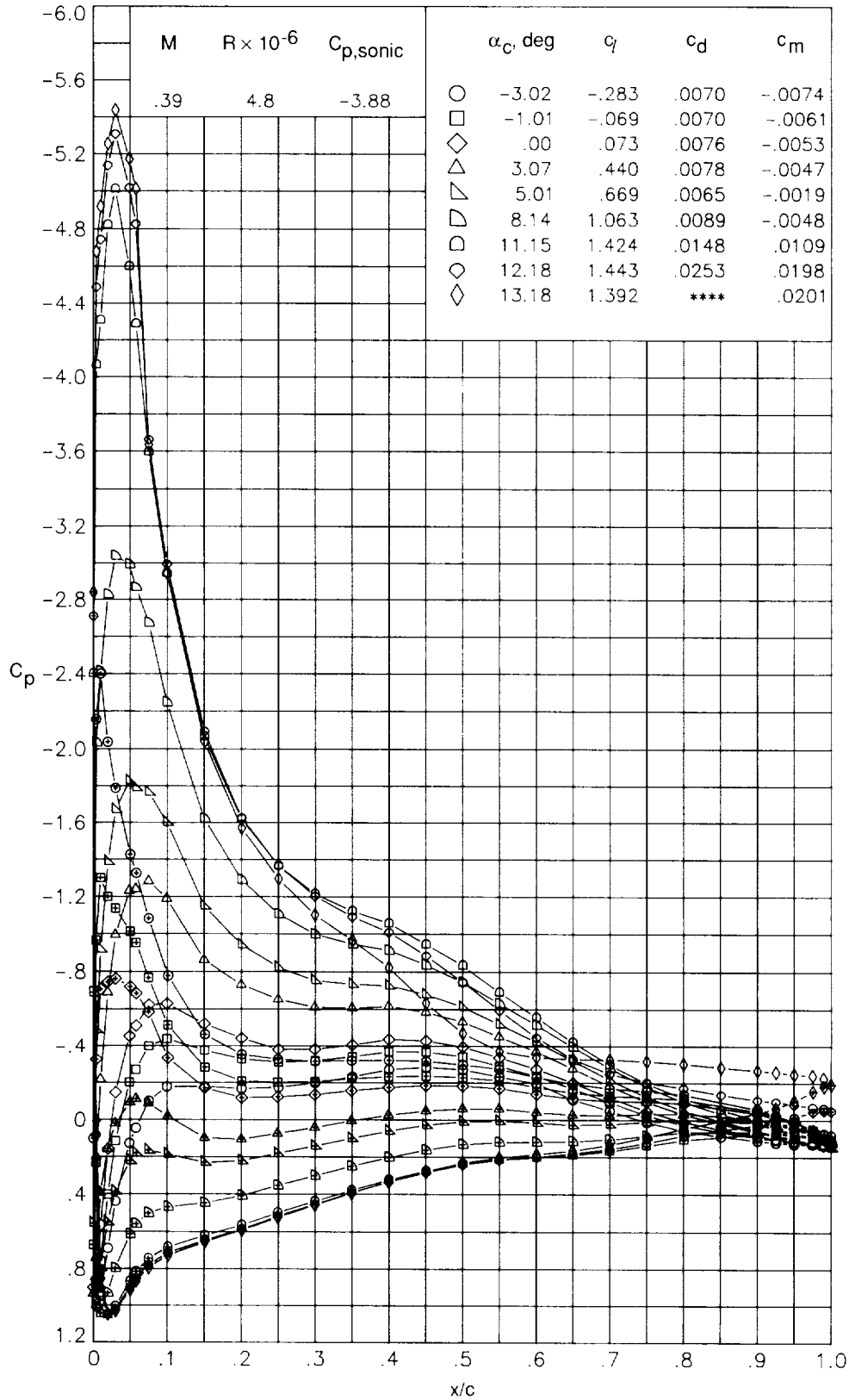

(f) $M = 0.39; R = 4.8 \times 10^6$.

Figure 26. Continued.

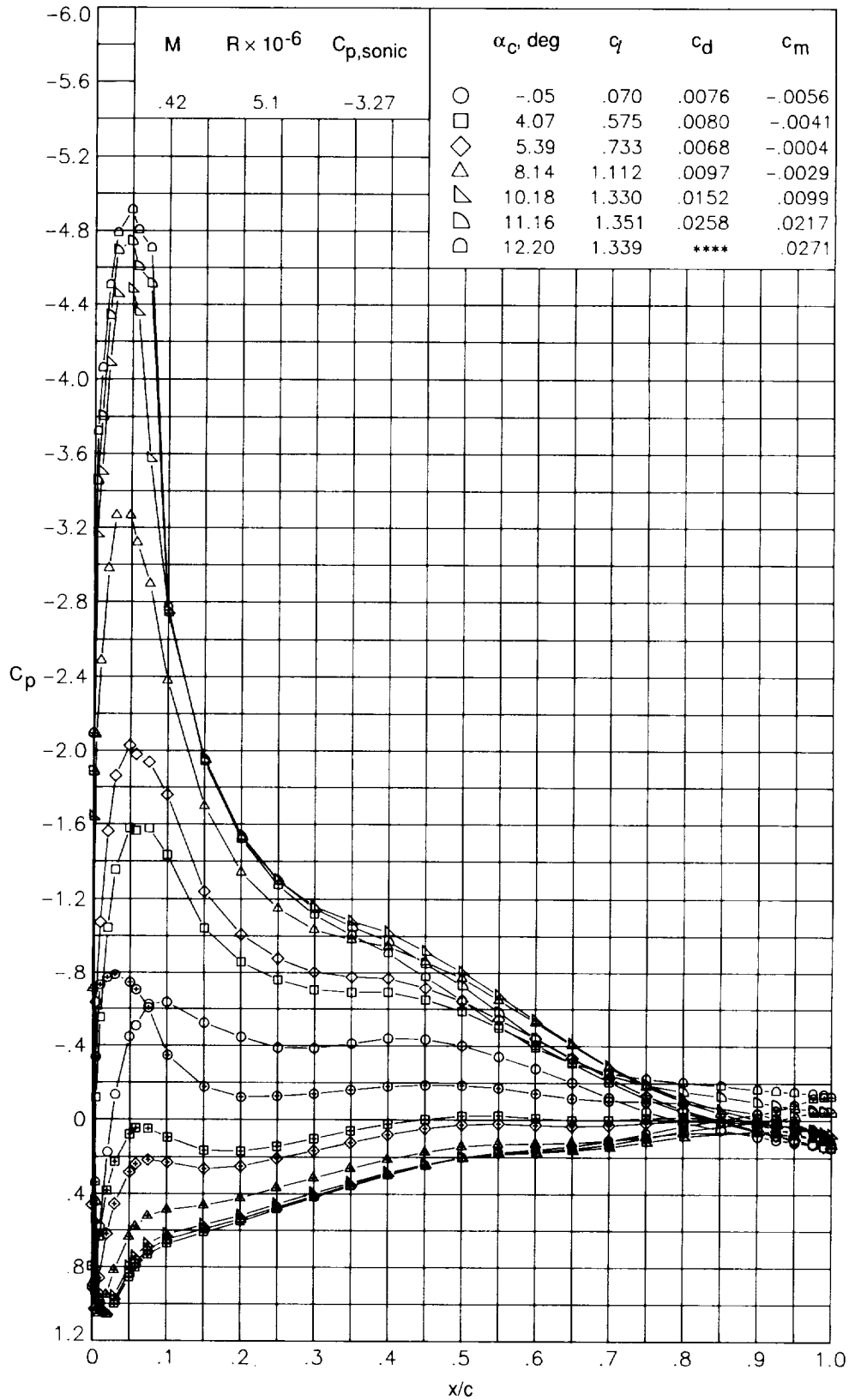

(g) $M = 0.42; R = 5.1 \times 10^6$.

Figure 26. Continued.

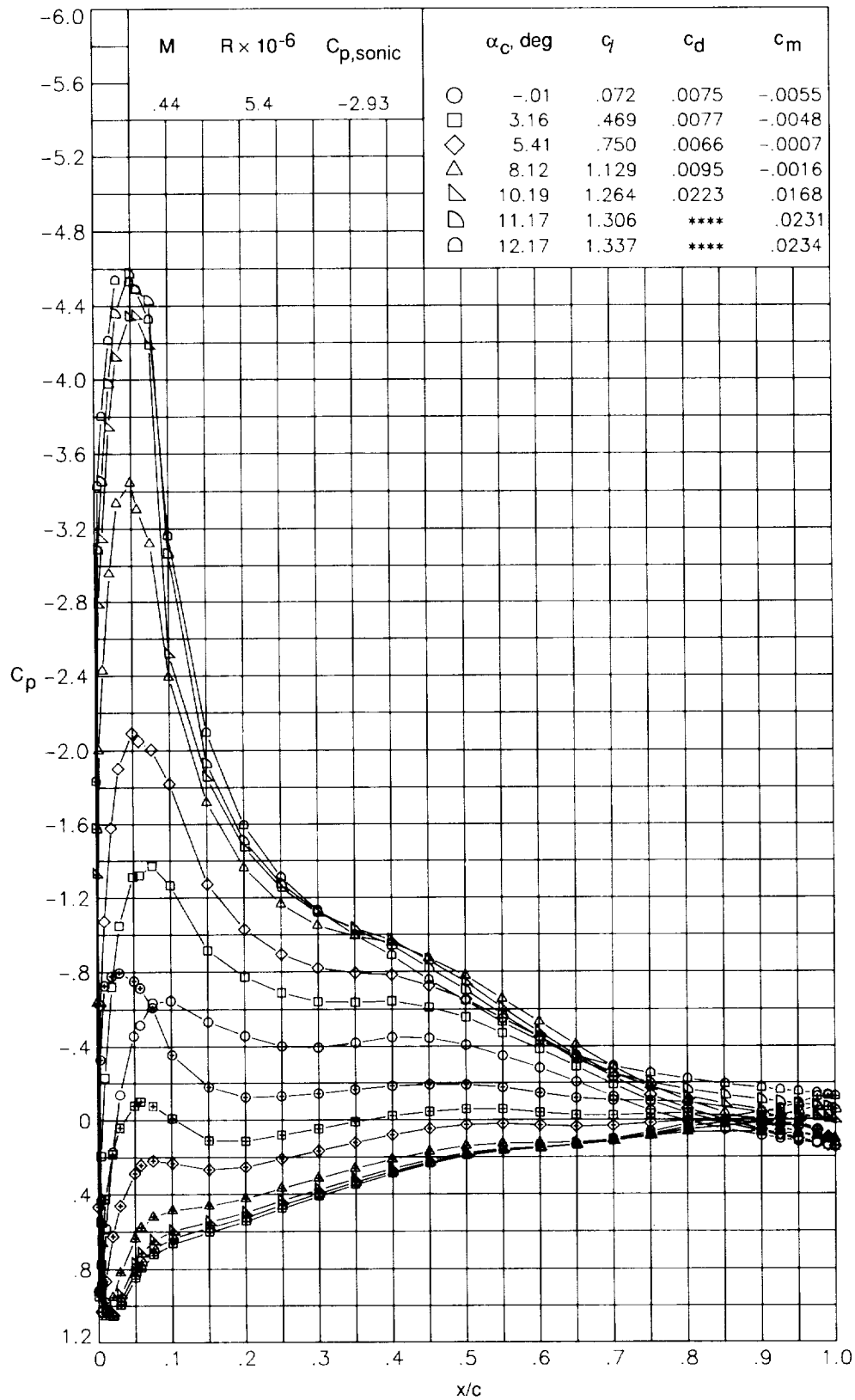

(h) $M = 0.44; R = 5.4 \times 10^6$.

Figure 26. Concluded.

NASA
National Aeronautics and Space Administration

Report Documentation Page

1. Report No. NASA TP-3009 AVSCOM TR-90-B-005	2. Government Accession No.	3. Recipient's Catalog No.
4. Title and Subtitle Aerodynamic Characteristics of Two Rotorcraft Airfoils Designed for Application to the Inboard Region of a Main Rotor Blade		5. Report Date July 1990
		6. Performing Organization Code
7. Author(s) Kevin W. Noonan		8. Performing Organization Report No. L-16737
9. Performing Organization Name and Address Aerostructures Directorate USAARTA-AVSCOM Langley Research Center Hampton, VA 23665-5225		10. Work Unit No. 505-61-59-76
		11. Contract or Grant No.
12. Sponsoring Agency Name and Address National Aeronautics and Space Administration Washington, DC 20546-0001 and U.S. Army Aviation Systems Command St. Louis, MO 63120-1798		13. Type of Report and Period Covered Technical Memorandum
		14. Army Project No. 1L162211A47AA

15. Supplementary Notes
Kevin W. Noonan: Aerostructures Directorate, USAARTA-AVSCOM.

16. Abstract

A wind-tunnel investigation has been conducted to determine the two-dimensional aerodynamic characteristics of two new rotorcraft airfoils designed specifically for application to the inboard region (stations $\leq$85 percent radius) of a helicopter main rotor blade. The two new airfoils, the RC(4)-10 and RC(5)-10, and a baseline airfoil, the VR-7 which is currently in use, were all investigated in the Langley 6- by 28-Inch Transonic Tunnel at Mach numbers from about 0.34 to 0.84 and at respective chord Reynolds numbers from about 4.7×10^6 to 9.3×10^6. The VR-7 airfoil had a trailing-edge tab that is deflected upward 4.6°. In addition, the RC(4)-10 airfoil was investigated in the Langley Low-Turbulence Pressure Tunnel at Mach numbers from 0.10 to 0.44 and at Reynolds numbers from 1.4×10^6 to 5.4×10^6, respectively. Some of the experimental data for the two new airfoils were compared with two different theories. The results of this investigation indicate that both of the new airfoils offer advantages over the baseline airfoil. Of the three airfoils investigated in the 6- by 28-Inch Transonic Tunnel, the RC(4)-10 airfoil had the highest maximum lift coefficients at Mach numbers M from 0.34 to about 0.42. The maximum lift coefficients of the RC(4)-10 were 1.57 at $M = 0.34$ and 1.42 at $M = 0.42$, whereas those of the baseline airfoil were 1.47 at $M = 0.34$ and 1.38 at $M = 0.42$. The highest maximum lift coefficient measured for the RC(4)-10 in the Low-Turbulence Pressure Tunnel was 1.74 at $M = 0.20$. The drag-divergence Mach number of the RC(5)-10 airfoil was higher than that of the baseline airfoil for lift coefficients from 0 to 0.3, whereas the drag-divergence Mach number of the RC(4)-10 airfoil was higher than that of the baseline airfoil for lift coefficients from 0.1 to 0.3. The drag-divergence Mach number at zero lift coefficient was 0.79 for the RC(5)-10, 0.74 for the RC(4)-10, and 0.75 for the baseline airfoil. In general, both new airfoils had lower drag coefficients and pitching-moment coefficients (nearly zero) than the baseline airfoil for Mach numbers up to 0.63.

17. Key Words (Suggested by Authors(s)) Rotor airfoils Airfoils Rotor Helicopter	18. Distribution Statement Unclassified—Unlimited Subject Category 02

19. Security Classif. (of this report) Unclassified	20. Security Classif. (of this page) Unclassified	21. No. of Pages 87	22. Price A05

NASA FORM 1626 OCT 86

NASA-Langley, 1990

For sale by the National Technical Information Service, Springfield, Virginia 22161-2171